UNIVERSITY OF NAIROBI

COMPARATIVE SORPTION OF ORGANIC DYES USING *Xylocarpus moluccensis* AND *Rhizophora mucronata* MANGROVE SPECIES FROM KENYAN COASTAL REGION

BY

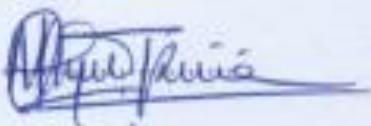**CHRISPINE MOSES ODERA OLOO**

I56/80706/2015

A Thesis Submitted for Examination in Partial Fulfilment of the Requirements for Award of the Degree of Master of Science in Chemistry of the University of Nairobi

MAY 2020

DECLARATION

I declare that this thesis is my original work and has not been submitted elsewhere for examination, award of a degree or publication. Where other people's work or my own work has been used, this has properly been acknowledged and referenced in accordance with the University of Nairobi's requirements.

Signature.. Date..18/6/2020

Chrispine Moses Odera Oloo

I56/80706/2015.

This thesis is submitted for examination with our approval as research supervisors.

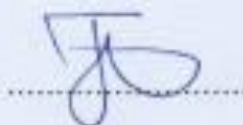|	Signature	Date
1. Prof. John Mmari Onyari. Department of Chemistry University of Nairobi P.O Box 30197-0010 Nairobi Kenya. Email, jonyari@uonbi.ac.ke.		22/6/2020
2. Dr. John Namakwa Wabomba Department of Chemistry University of Nairobi P.O Box 30197-00100 Nairobi Kenya. Email. jwabomba@uonbi.ac.ke.		22/06/2020
3. Dr. Wycliffe Chisutia Wanyonyi Department of Physical Science University of Kabianga P.O Box 2030-20200, Kericho Kenya. Email; wwanyonyi@kabianga.ac.ke.		22/06/2020

DEDICATION

To elite who prayed for my fitness, soundness and success.

ACKNOWLEDGEMENT

ABSTRACT

Bark and stem samples from two mangrove species, *Rhizophora mucronata* (RM) and *Xylocarpus moluccensis* (XM); obtained from Kenyan coastal region, were investigated as potential low-cost adsorbents for the removal of toxic Crystal Violet (CV) and Malachite Green (MG) from wastewater mixtures. Adsorption efficacies of these adsorbents were compared for the two dyes and with literature values of recommended adsorbents. *X. moluccenisis* stem and stem-bark dye removal rate within the first 5 to 20 minutes increased from $75.9 \pm 0.15\%$ to 97.1 ± 0.15, and from $85.2 \pm 0.16\%$ to $96.7 \pm 0.11\%$ respectively while uptake increase from $85.2 \pm 0.16\%$ to $95.3 \pm 0.20\%$ and from $85.2 \pm 0.47\%$ to $95.3 \pm 0.05\%$ capacity was observed for *R. mucronata* stem and stem-bark. The optimum pH for the adsorption of CV and MG dye-was at pH 8 and pH 7 respectively. Significant equilibrium adsorption capacities, Q_e (mg/g), with the stem-bark of the species giving highest capacities of 407.7 ± 0.03 mg/g for the adsorption of CV and 366.4 ± 0.07 mg/g, for MG dyes which translates up to $99.4 \pm 0.15\%$ dye removal. Equilibrium adsorption capacity increased with contact time, adsorbent dose and initial dye concentration but decreased with particle size, Ionic Strength and pH of the solution. Large correlation coefficient R^2 values ranging from 0.7885 to 1.0000 noted implies adsorption occurred through monolayer formation for both species fitting Langmuir model while very low Freundlich constant, K_f, values of the range of 0.5000 to 2.2000 were observed. Kinetics studies showed that the equilibrium adsorption follow pseudo-second order kinetics with the corresponding regression coefficient, R^2, in the range of 0.8788 to 1.0000 and interparticle diffusion was a factor that controlled adsorption process onto the two species. The results displayed in this study have demonstrated the effectiveness of *R. mucronata* (RM) and *X. moluccensis* (XM), in removing organic dyes from their aqueous wastewater mixtures.

TABLE OF CONTENTS

LIST OF TABLES

LIST OF FIGURES

LIST OF ABBREVIATIONS

AGOA   Africa Growth and Opportunity Act

AFM   Atomic Force Microscopy

CAA   Contact Angle Analysis

CV   Crystal Violet

EPZ   Export Processing Zone

EU   European Union

FTIR   Fourier Transform and Infra-Red

KMFRI   Kenya Marine and Fisheries Research Institute

MG   Malachite Green

MVGB   Mangrove Vegetation of Gazi Bay

NMEMP   National Mangrove Ecosystem Management Plan

ppm   parts per million

RM   *Rhizophora mucronata*

SEM   Scanning Electron Microscopy

SPM   Scanning Probe Microscopy

TEM   Transmission Electron Microscopy

UN   United Nations

UV/VIS   Ultraviolet Visible

UNEP   United Nations Environment Programme

UNESCO   United Nations Educational, Scientific and Cultural Organization

XPS   X-ray Photoelectron Spectroscopy

XRF   X-Ray Fluorescence

XR   *Xylocarpus moluccensis*

λ_{max} Maximum wavelength of absorption

CHAPTER ONE

1.0 INTRODUCTION

1.1 Background of the study

The amount of water usefully consumed per year is approximately 44% (1,716 km³) of the 3,928 km³ of water withdrawn worldwide while the other 56% (2,212 km³ per year) is released as agricultural drainage, wastewater and industrial effluents. The degradation of urban environments of most industrialised cities and towns poses health hazards as a result of the discharge of toxic chemicals into wastewater (UNESCO, 2017). It is estimated that by 2025, the volumes of industrial wastewater in most African Countries, Kenya included; will have doubled but currently, only a proportion of water is treated before discharge making the industry a major polluter (Andersson & Stockholm Environment Institute, 2016).

Most of the world's textile finishing companies and dye manufacturing industries consume the largest amount of water for dyeing and printing (Tan *et al*., 2012). In Kenya, apparel, clothing and textile industries use large quantities of reactive dyes due to the high demand of their products (Chanzu *et al*., 2012). The high demand of textile products implies large consumption of water and reactive organic dyes and therefore constant flow of dye contaminated effluents into the immediate ecosystem. Large companies like Rivatex East Africa rely on very expensive reactive dyes that are imported in large quantities annually. The number of textile enterprises within the Kenya Export Processing Zones, EPZ, is at the peak due to the increasing marketing relations with global markets in the United States of America (USA), United Kingdom, European Union and currently China (Ali *et al*., 2014). In fact, in 2013 alone, Kenya earned $543m from EPZ's textile export to USA and have now overtaken Lesotho under the preferential trade agreement of Africa Growth and Opportunity Act (AGOA). The Kenya National Bureau of Statistics (KNBS) data shows that the growth of Kenya's exports to USA had risen by 7% to

1

Sh35.3 billion in 2016, within the first 10 months; as exports to Britain tumbled by a similar margin to Sh30.9 billion. The aftermath is the growth and development of dye manufacturing companies reflecting increased investments in Kenya's vision 2030 projects. However, not adequate attention has been given to the need to provide proper disposal of the contaminated wastewater generated and ensuring that contaminants comply with effluent discharge standards. In fact, inadequate technical expertise, infrastructure and other important but less sophisticated management systems for the high volume of wastewater being produced, is at the point of wastewater crisis as nearly all wastewater treatment techniques are either very expensive or require very costly secondary technologies in both developing and developed countries (Jebrail *et al.*, 2016). Nitrogen and/ or phosphorous contained in industrial effluents and agricultural run-off are among other elements that increase the level of nutrients in water bodies and consequently influences eutrophication in rivers and lakes. These effluents containing synthetic dyes when discharged into water bodies, reduce photosynthesis activity thus affecting the stability of aquatic ecosystems (Muinde *et al.*, 2017).

1.2 Statement of the Problem

Industrial dye-contaminated aqueous mixture constantly released into the environment; usually nearby farm soil, rivers, lakes and to a larger extent into an ocean, have shown adverse effects to our immediate ecosystem. The EU-Directive, 2012, demonstrates that even minute(less than 1 ppm) quantities of dyes in water have lethal effects on exposed organisms in the immediate environment and depending on exposure time and dye concentration, the impacts of untreated wastewater to our immediate ecosystem range from chronic ecosystems damage given continuous oxygen depletion due to eutrophication and biodegradation, to pollution of domestic waters used for recreational activities like canoeing and swimming. Human health and coexistence are put at risk due to carcinogenic and mutagenic toxicity tendency implications that result from the dye contaminated textile wastewater. Dye-contaminated effluents discharged into

2

water bodies reduce photosynthesis activity thereby affecting the stability of aquatic ecosystems. Textile dyes cause allergies such as contact dermatitis and respiratory diseases, allergic reaction in eyes, skin irritation, and irritation to mucous membrane and the upper respiratory tract.

Bodies mandated with environmental legislation have enacted laws and regulations to ensure that industries and firms dealing with dyes and dye products dispose their effluents properly but even those observing these measures have consistently released the waste materials into rivers, lakes, oceans and other water body systems. Both untreated and treated textile dye wastewater have negative impacts even at very low concentrations due to their high toxicity level. The techniques so far employed in wastewater treatment, including chemical treatment using oxidizing agents like chlorine (chlorination), Ultraviolet (UV) sterilization method, biological treatment technique (aerobic and anaerobic methods), filtration, use of membranes, and thermal evaporation technologies; often used in the treatment of polluted wastewater discharge, are cost expensive in terms of material and applicable technological expertise and are not implementable on large scale. Treatment such as reverse osmosis, membrane filtration and coagulation/ flocculation are not economically feasible. Significant studies on adsorptive technique using agricultural, domestic or plant biomass waste, such as coconut husks, mangrove and polylactide blended films, grapefruit peel, jackfruit leaf powder, ginger waste, water hyacinth, etc, have been done but these materials cannot be applied on large scale since their adsorption capacity is low and the cost of setting up farms is way too high. While adsorption using activated carbon is efficient and recommendable technique, it is very expensive and this has called for scientific research into the use of adsorbents that are cost effective mainly from agricultural waste matter.

Mangroves are facing human attack for both domestic and economic use. In this study the exploitation of mangrove species from the mangrove vegetation of Gazi Bay is for the sole purpose of providing adsorbents, which if effective, can lead to the removal of dyes in contaminated water that flows into the ocean waters from industries that border the shoreline and

3

this justifies the need to plant more of these mangrove plants and explore other species to determine their effectiveness in dye removal.

1.3   Objectives

1.3.1 General Objective

The general objective of this study is to assess the efficacy of two mangrove species in removal of organic dyes in aqueous solutions.

1.3.2 Specific Objective

1. To determine the surface characteristics of *X. moluccensis* and *R. mucronata*'s stem and stem-bark by use of FTIR and compare the Adsorption Capacities of Crystal Violet (CV) and Malachite Green (MG).

2. To study the effect of contact time, particle sizes of the adsorbent, adsorbent dose, initial dyes concentrations, pH and ionic strength on the removal of the CV and MG dyes from aqueous solutions.

3. To determine the kinetics of dye adsorption using Pseudo-First order and Pseudo-Second order models.

4. To investigate the equilibrium removal conditions of a specific adsorbate in terms of adsorption isotherms and apply Langmuir and Freundlich adsorption isotherm models to fit the experimental data obtained.

1.4 Justification and Significance

The colour of water used by the public dictate its taste and quality; hence removing colour and any other soluble colourless organic matter in effluents that flow into water bodies is not only vital but also critical for the survival of the organisms in their various ecosystems. The textile industry worldwide consumes approximately 10^7 kg of dye per year, and about 90% is used in

the fabrics industry. About 2.5% of the dyes used in fabric industry, goes into effluents as a wastewater pollutant (Tan *et al*., 2012).

Despite high costs associated with textile wastewater dye removal, the development of wastewater treatment schemes and plants have been stimulated by stringent environmental legislation. The stability and fastness of a dye is a desirable property by textile manufacturers and consumers however the resultant dyestuffs are resistant to biodegradation and consequently very expensive technologies are required to ensure that the discharges are safe enough to release to the environment (Muinde *et al*., 2017).

Dye-adsorption using locally available agricultural waste materials is a promising alternative of a better effluent cleansing adsorbent. This is not only due to the fact that these materials are locally available and can be easily recycled, but also the fact that if their adsorptive behaviour is well established, they can be modified for industrial applications. Elsewhere mangroves have been reported to have adsorptive aspects hence there is an increased interest in their study and possible use as easily accessible adsorbents of low-cost for organic dye cleansing off aqueous mixtures; (Astuti *et al*., 2017; Ngugi *et al*., 2016; Santhi *et al*., 2010; Tan *et al*., 2012) and others, have demonstrated that aerial parts of the general mangrove plantation can be used for water purification without in effect identifying which particular species is responsible for the observed adsorption characteristics. Such studies having been inspired by the need to develop an eco-friendly and economical materials for dye removal from contaminated wastewaters have necessitated more associates in research work towards producing alternatives of low cost in preference to very expensive and sophisticated techniques currently enforced. Mangroves are unique woody plants that have the ability to concentrate most pollutants including toxic metal ions, herbicides, colourants, pesticides and are also used for phytoremediation of pollution caused by heavy metal (Ngugi *et al*., 2016).

CHAPTER TWO

2.0 LITERATURE REVIEW

2.1 Textile Wastewater Treatment

Dye contaminants are not easy to remove by conventional sewage treatment techniques and this is due to their complex structure that makes them stable (Aljeboree *et al*., 2016). These dye colorants concentrating industrial wastewater are mainly from textile industries, (Zolgharnein *et al*., 2015). Dye-textile retention by textile industries are always at low levels, forcing these industries to generate large quantities of wastewater polluted with dyes of different kinds at very high concentrations, (Boukhemkhem & Rida, 2017). Direct discharge of dye contaminated wastewater, especially into aquatic environment have several adverse effects, (Anirudhan *et al*., 2011). They become sources of eutrophication and aesthetic pollution and have a negative impact to the public health (Muinde *et al*., 2017). As a result, industrial textile discharge is a major environmental concern and several techniques tested and evaluated for their efficacy in dye removal include solar photo-fenton treatment, photocatalytic degradation, micellar enhanced ultra-filtrate, sonochemical degradation, electrochemical degradation, coagulation, cationic exchange membrane and adsorption among others, (Kharub, 2012). One of the most popular and currently being explored technique in dye and colorants removal in general is adsorption using agricultural wastes both in their unmodified and modified forms, (Jedynak & Repelewicz, 2017). Adsorption using activated carbon is very effective but is expensive and cannot be applied in large scale industrial wastewater treatment and also requires regeneration for re-use (Muinde *et al*., 2017). Recently more studies have focused on making low-cost agricultural wastes available for large scale application to clean industrial discharge which can be attributed to their availability at very low cost and also their excellent performance in removing dyes and pigments from wastewater mixtures (El-Sayed, 2011). Aerial parts of various Agricultural waste materials

6

have been investigated and shown that they are not only cost effective but have a higher adsorptive dye removal efficiency (Jain &Jayaram, 2010).

2.2 Mangroves

The word 'mangrove' refers to several species of plants which inhabit intertidal zone of tropical and subtropical coastlines. Ecological habitats inhabited by mangroves are a unique ecosystem exemplified by numerous stress conditions such as water logging, high salinity, low nutrition condition, light stress and low oxygen condition, normally found in abundant along the coastal regions of East Africa, India, South East Asia and Australia (Hendy *et al*., 2014). Mangroves form a vital coastal ecosystem. They are essential for communities inhabiting along the extensive world's major coastlines and most of these communities rely on mangrove forests for wood to build boats, furniture, houses and for firewood. Along the Kenyan-coastline, mangrove forests spread from approximately 54,000 ha, most of which are in Lamu and Tana River districts. Figure 2.1 show the map of Kenya showing major towns dominated by mangrove vegetation; the typical pattern of mangrove spread in East Africa and major coastlines around the world is such that the seaward side is occupied by *Sonneratia-Rhizophora*-giant *Avicennia* community. The trend is followed by *Rhizophora-Bruguiera-Ceriops* in the mid zone and dwarf *Avicennia-Lumnitzera-Xylocarpus* complex on the landward side (Lang'at & Kairo, 2008).
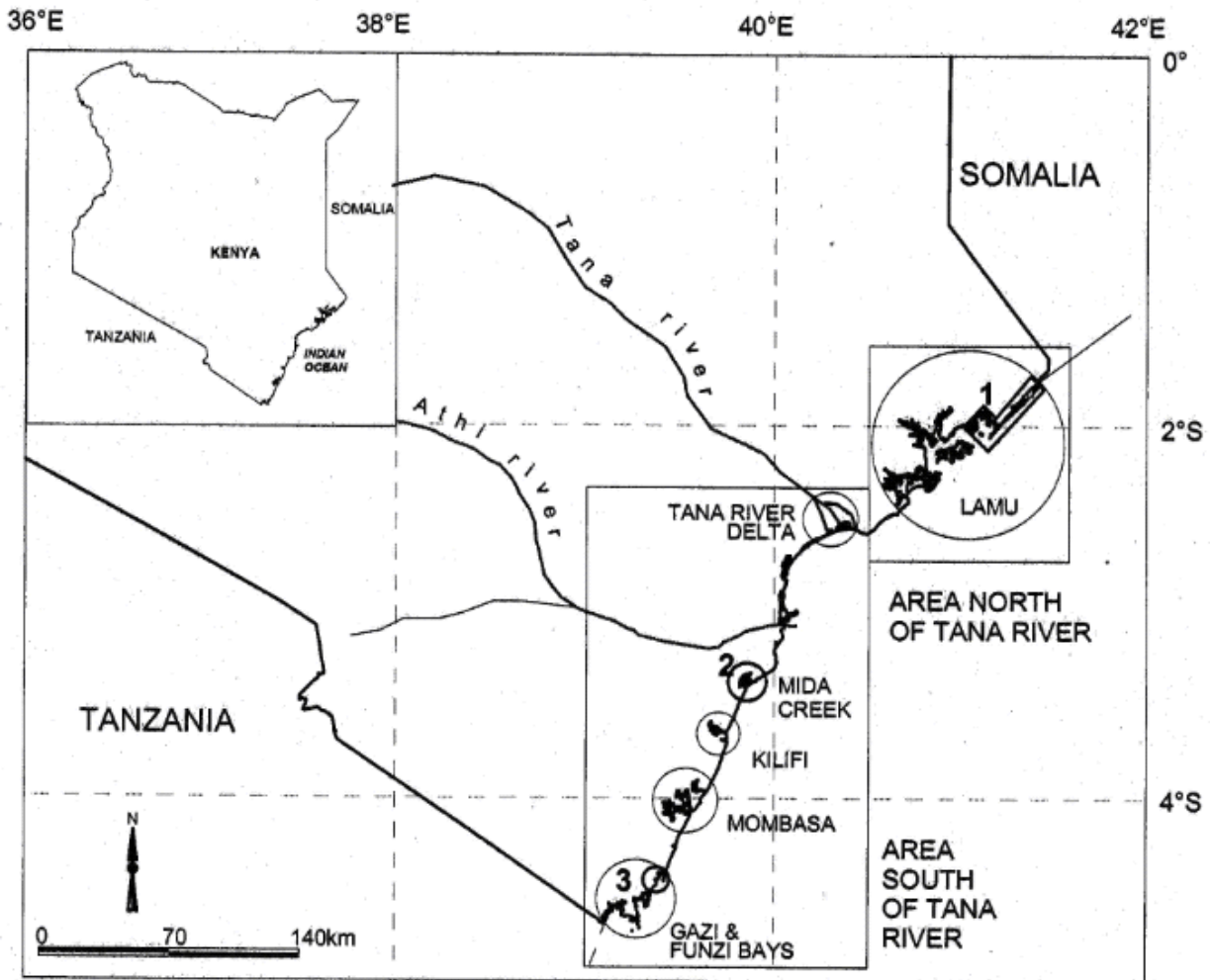
Figure 2.1: Coastal towns dominated by mangrove vegetation (*source: NMEMP*)

Communities along the Kenyan coastline about 30 miles South of Mombasa-Kenya's main coastal city are essentially the mangrove benefactors as they rely on the mangrove forests for both economic, environmental and ecological importance (Lang'at & Kairo, 2008).

The South Coast of Mombasa, Gazi region, centres major projects like the Mikoko Pamoja project, a community-based project that advocates on the benefits of planting the vast mangrove species and discourages deforestation along the coastline and mangrove vegetation of Gazi Bay (MVGB) (Ruwa, 1993). The study aims at increasing the awareness on the adsorptive nature of mangrove plant for the South Coast based projects and narrows down to specific species and their chemistry applications. Note that apart from shoreline protection, waste assimilation and carbon sequestration among other importance of the mangrove plant; fishes, some amphibians

8

and other fauna also inhabit these forests as breeding grounds and habitat; these have greatly influenced the mangrove plants adaptations and this further supports their study. Amongst the 9 mangrove species in Kenya, *R. mucronata* and *C. tagal* are the dominant species constituting approximately 70% of the 54000 *ha* mangrove forests formation (Romañach *et al*., 2018).

The mangrove species under investigation; *X. moluccensis* of the mahogany family, and *R. mucronata*, are fast growing plants and are used in the restoration of mangrove habitats. These are classified as true mangrove species because they are part of the major constituents of the mangrove ecosystem (*Mangrove Conservation, Kenyan Style*). The land-sea interface mangrove zonation is such that *R. mucronata* and *X. moluccensis* are inshore and offshore respectively along the wide mangrove forests.

R. mucronata is a member of *Bruguiera* a species of mangroves just like *R. stylosa* (RS), which was found to be capable of filtrating metal ions mainly Na^+ ions present in saline environment; biophysically through their root which possesses a hierarchical, triple layered pore structure with high surface potential area that block most of the Na^+ ions (Kim *et al*., 2016). Studies have also shown the potency of *R. mucronata* roots to adsorb Lead II ions present in aqueous mixtures (Ngugi *et al*., 2016); and is a viable alternative source of many biological and chemically active compounds which are already known to be of great economic and pharmaceutical importance (Basyuni *et al*., 2017). Chemical pigment extracts from *X. moluccensis* of the mahogany (meliaceae) family have been used in the manufacture of marine drugs. The two species' efficiency in dye stuffs removal from aqueous mixtures have however not been tested.

2.3 Textile Organic Dyes

The textile organic dyes classification can be in terms of its application characteristics or its chemical structure. The application characteristics refer to the Cl-generic common name like reactive, direct, disperse, acid or basic; while the chemical structure refers to Cl- constitution numbering like carotenoid, nitro-diphenylmethane or quinolone; among others (Crini *et al*., 2007). Chromophores present in dyes are groups of atoms that brings about the colouring property of the dyes. Diverse functional groups like azo, nitro, carbonyl, aril-methane, methane, anthraquinone and others, define these chromophores (Chequer *et al*., 2013). Most of organic dyes used for textile printing and dying are azo dyes with intense colorant and very toxic (Carmen *et al*., 2014). Figures 2.2 and 2.3 show the structures of the two dyes, CV and MG.
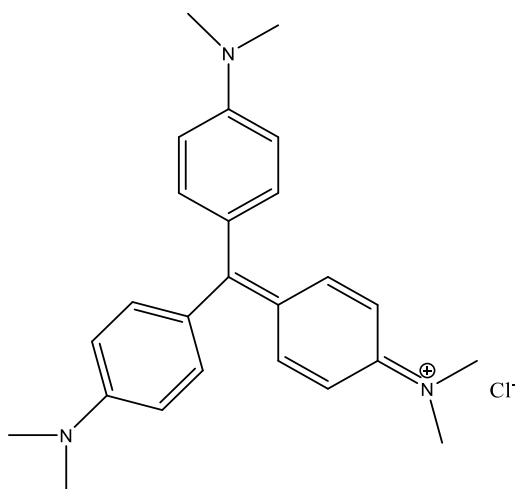
Figure 2.2: Structure of CV dye (*Source: Author*)
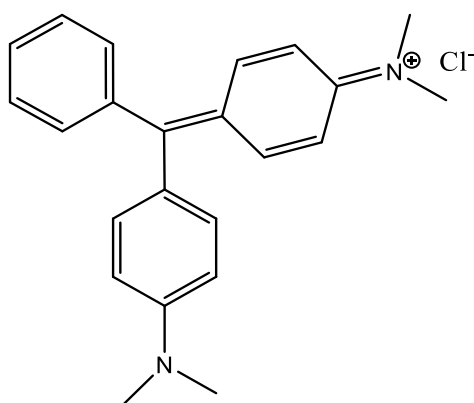
Figure 2.3: Structure of MG dye (*Source: Author*)

CV dye (Basic Violet-3) is a synthesized cationic dye prone to transmit violet colour in aqueous mixture. This triaryl methane dye is extensively useful in the textile plants dying silk, cotton, nylon, wool and also in veterinary medicine. It is a very toxic substance that is severely harmful on ingestion and or inhalation and it is easily absorbed through the skin and causes irritation (Bertolini *et al*., 2013).

MG is greenish blue in aqueous solutions and is used for colouring silk, leather and cotton paper among others and it is also used as a fungicide, parasiticide, anti-protozoan and anti-bacterial agent, (Kushwaha *et al*., 2014). These cationic dyes are hazardous and carcinogenic (Salahshoor *et al*., 2014). They both decrease growth, damages the heart, brain, kidney, spleen, lungs, liver and increase infertility rates (Chanzu *et al*., 2012). Their presence is not only catastrophic to the living organisms but also can lead to long term degradation and lower the quality level of the aspects of our immediate ecosystem hence careful disposal of these dyes is critical move to save our society.

2.4 Techniques for Surface Characterisation and Analysis

The surface layer is often considered as the layer from which important information is obtained using a specific analytical technique. The importance of the properties of solid surfaces is crucial in many areas of science and technology which are contributing to our daily well-being. These include, microelectronics, catalysis, metallurgy, microscopy, adhesion, science environment, corrosion, tribology and adsorption. Microscopy is a technique of characterization in which a material's surface and sub-surface structures are probed and mapped. Some of the methods used in microscopy include; Contact Angle Analysis (CAA), Scanning Probe/Atomic Force Microscopy (SPM, AFM), Fourier-Transform Infrared Spectroscopy (FT-IR), Transmission Electron Microscopy, Scanning Electron Microscopy – TEM and SEM, X-Ray Fluorescence (XRF) and X-ray Photoelectron Spectroscopy (XPS). FT-IR spectroscopy is a potent tool for the study of the functional groups present in these adsorptive sites in the material at molecular level,

11

that could be responsible for adsorption process and it offers a high molecular resolution and experimental flexibility (Alawam *et al*., 2014). In this study, the FT-IR spectroscopy was made use of as a tool to determine and help explain the major functional groups enhancing the sorption process observed during the experiments. FT-IR spectrometer passes IR radiation through a material sample and measures its wavelengths at which absorption occurs. Molecular vibrations (stretching, bending and twisting) that absorb varying amounts of energy at a given frequency, enables FT-IR to provide chemical and structural information that is useful in determining the reactive sites of the molecule (Coates *et al*., 2000).

2.5 Techniques of Dye Removal

Textile waste water treatment have attracted quite a number of scientific and technological innovations in recent past. Some of the commonly exploited methods for dye removal include biological, chemical, and physicochemical techniques such as fungal decolorization flocculation and electrochemical, respectively (Bertolini *et al*., 2013). However, since effluents contain dye mixtures of complex structures, most industries have found it tricky to apply these conventional methods in treating the aqueous discharge from their firms (Bajpai & Jain, 2012).

Adsorption is a surface occurrence whereby solutes in a multicomponent fluid are attracted to the surface of a solid adsorbent by physical and chemical means; forming attachments and become part of the system (Zhang & Ou, 2013). Since the major part of industrial effluents are in the solution form, adsorption is an applicable technique in removing tiny chemical contaminants from the solution (Saeed *et al*., 2010). The development of industrial-large scale treatment methodology for the dye extraction depends on an in-depth study and optimisation of the above adsorptive parameters (Upadhye *et al*., 2018). As various adsorbents differ in the structure, chemical composition and affinity for the adsorbate, this study will investigate the adsorptive capacities for two mangrove species from different geographical regions along the Kenyan coastline.

2.6 Adsorption Isotherms

Adsorption at molecular level may mechanistically be controlled by the formation of a monolayer or multilayer. An adsorption isotherm is a model for a given data, experimentally obtained from adsorption processes and it predicts the mechanisms involved in various adsorption systems. For a proper understanding of an adsorption process, the adsorption equilibrium criteria is vital. If understood and interpreted properly, an adsorption isotherm becomes the backbone to the overall improvement of the design and pathways of adsorption system and mechanism respectively (Ayawei *et al*., 2017). Linear regression analysis is used as a tool for quantifying adsorbate distribution and verify the consistency of the theoretical assumptions with the adsorption isotherm model (Mittal *et al*., 2007). The two most useful adsorption isotherms in the current study are the Langmuir isotherm and the Freundlich isotherm. This study correlates ideas by Langmuir's isotherm which describes the monolayer adsorption and those by Freundlich isotherm which describes multilayer (Hameed & El-Khaiary, 2008).

2.6.1 Langmuir Isotherm

In Langmuir adsorption isotherm the adsorbent material has one adsorptive layer with each active site interacting with only one molecule and these active sites are energetically equivalent (Chen *et al*., 2012). The affinity between adsorbate and adsorbent is measured by the Langmuir constant K_L, however the reciprocal value of K_L is a measure of the concentration at which adsorbent material attains half its maximum adsorption capacity (Önal *et al*., 2007). Equation 1 below gives the Langmuir isotherm on a linear form;

$$\frac{C_e}{Q_e} = \frac{1}{K_l}\frac{1}{Q_{max}} + \frac{C_e}{Q_{max}}$$
<div align="right">Equation (1)</div>

where Q_e- the amount of adsorbate at equilibrium (mg/g).

Q_{max}- maximum monolayer adsorption capacity of the adsorbent (mg/g).

C_e- equilibrium concentration of adsorbate (mg/L).

K_l- Langmuir adsorption constant related to the free energy adsorption (L/mg).

The Langmuir constant Q_{max} and K_l values are calculated from the slope and intercept respectively, of linear plot of C_e/Q_e verses C_e. A separation factor of equilibrium parameter, R_L, illustrates important features of Langmuir isotherm model and is worked out by the Equation;

$$R_L = \frac{1}{q_m K_L} \qquad \text{Equation (2)}$$

where q_m is the maximum monolayer adsorption capacity of the adsorbent (mg/g).

The type of biosorption isotherm is indicated R_L values and is interpreted as;

Linear (R = 1)

Favourable ($0 < R_L < 1$)

Unfavourable ($R_L > 1$) (Irving Langmuir, 1916)

2.6.2 Freundlich Isotherm

The empirical isotherm equation proposed by Freundlich is given as ;

$$Q_e = K_f \, C_e^{\frac{1}{n}} \qquad \text{Equation (3)}$$

The assumption in equation 3 outlines energetically variable, active sites on a heterogeneous adsorption surface (Mittal *et al*., 2007). In linear form, Freundlich isotherm relation can be given in as shown in Equation 4;

$$\text{Log } Q_e = \text{Log } K_f + \frac{1}{n} \log C_e. \qquad \text{Equation (4)}$$

where C_e = equilibrium concentration of solution (mg/L).

Q_e = amount of dye adsorbed per unit mass of adsorbent (mg/g).

n = number of layers.

K_f = Freundlich constant.

In this equation, the adsorption capacity of materials under investigation is measured by K_f value while the change in adsorbate molecular affinity with time as adsorption proceeds is determined by the 'n' quantity and the isotherm constant K_f is the intercept.

2.7 Kinetics of Adsorption

Adsorption process can further be illustrated by the use of kinetic models that fit in experimentally obtained data. Pseudo-first order, -second order models are in this study to evaluate the kinetics of CV and MG adsorption processes and these were further modelled by intraparticle diffusion.

2.7.1 Pseudo-First Order Kinetics

A pseudo first order reaction is one which is literally a second order but the concentration of one of the reactants is in excess rendering the overall order a first order reaction. Lagergrens pseudo-first order kinetics equation (Ho & McKay, 1998) given as:

$$\log (q_e - q_t) = \log q_e + \frac{k_1}{2.303} t \qquad\qquad \text{Equation (5)}$$

where q_e = equilibrium amount of dye adsorbed per unit mass of adsorbent (mg/g).

q_t = amount of dye adsorbed per unit mass of adsorbent at time t (mg/g).

k_l = pseudo-first order adsorption rate constant (min^{-1}).

t = time (min).

2.7.2 Pseudo- Second Order Kinetics

The (Ho and McKay, 1999) kinetics equation is given as:

$$\frac{t}{q_t} = \frac{1}{k_2 q_e^2} + \frac{t}{q_e} \qquad\qquad \text{Equation (6)}$$

15

where q_e = equilibrium amount of dye adsorbed per unit mass of adsorbent (mg/g).

q_t = amount of dye adsorbed per unit mass of adsorbent at time t (mg/g).

K_2 = pseudo-second order adsorption rate constant $(g min^{-1}mg^{-1})$.

t = time (min).

The equilibrium adsorption capacity, q_e (mg/g) and the pseudo-second order rate constant K_2 are described by the gradient and the intercept respectively, of the linear plot t/q_t (gmin/mg) against time, t. The values of the parameters of this second order kinetics must agree with high values for R^2.

2.7.3 Intraparticle Diffusion

The sorption mechanism during sorbate-adsorbent interaction occurs by either particle diffusion or film diffusion process. In this case, the sorbate diffuses through the solution bulk towards the film surrounding the adsorbent and then into the macrospores and micro pores of the adsorbent. Expressed as the square root of time, the intraparticle model equation is given by (Weber & Morris, 1963) is;

$$q_t = K_{diff.} \, t^{\frac{1}{2}} + C \hspace{4cm} \text{Equation (7)}$$

where q_t = amount of dye adsorbed per unit mass of adsorbent at time t (mg/g).

$K_{diff.}$ = intraparticle diffusion rate constant $(mg \, g^{-1}min^{-1})$.

t = time (min).

C = intercept.

CHAPTER THREE

3.0 Materials and Methods

3.1 Adsorbent Collection and Preparation

The mangrove samples were collected from Gazi Bay, Ukunda Kwale county, Kenya. *X. moluccenisis* and *R. mucronata,* the two mangrove species were botanically identified at KMFRI laboratories-Gazi Branch, Kwale county. Figures 3.1 and 3.4 show the two species; *R. mucronata* and *X. moluccensis* from mangrove forests along Gazi Bay.
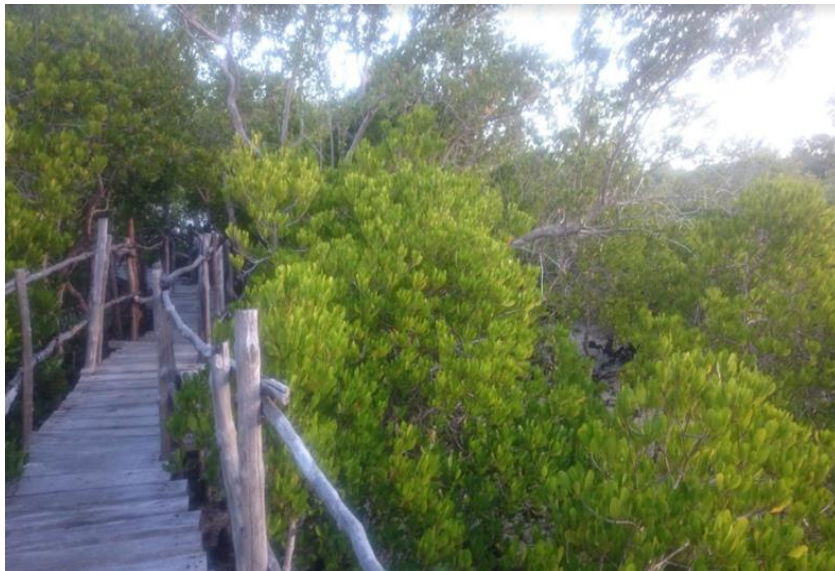
Figure 3.1: *R. mucronata* from Gazi bay, Kenya (*Source: Author*)

Figure 3.2: *X. moluccensis* from Gazi bay, Kenya (*Source: Author*)

17

The materials were then transported to the University of Nairobi for batch adsorption experiment to determine efficacy of each species on the adsorption of organic dyes. The materials were then dried and ground into powder form. The stem and stem-bark powder for each species were then soaked in water for 3 days after which they were filtered and put into fresh water to remove colorants. This procedure was repeated for a period of two months to dissolve and remove the plant pigments and the clean materials were further washed in double distilled. The clean materials were then dried in at a temperature of 25^0C and 1 atmosphere pressure (1atm) to preserve their important structures and functional groups. The powdered Mangrove samples were then sieved into various particle sizes namely parts less than 300 µm, parts greater than 300 but less than 425 µm and those greater than 425 µm by gradation technique. The sieved particles were then stored, at room temperature and pressure 25^0C and 1atm respectively, in medium sized self-sealing plastic bags and containers shown in Figures 3.3 and 3.4;
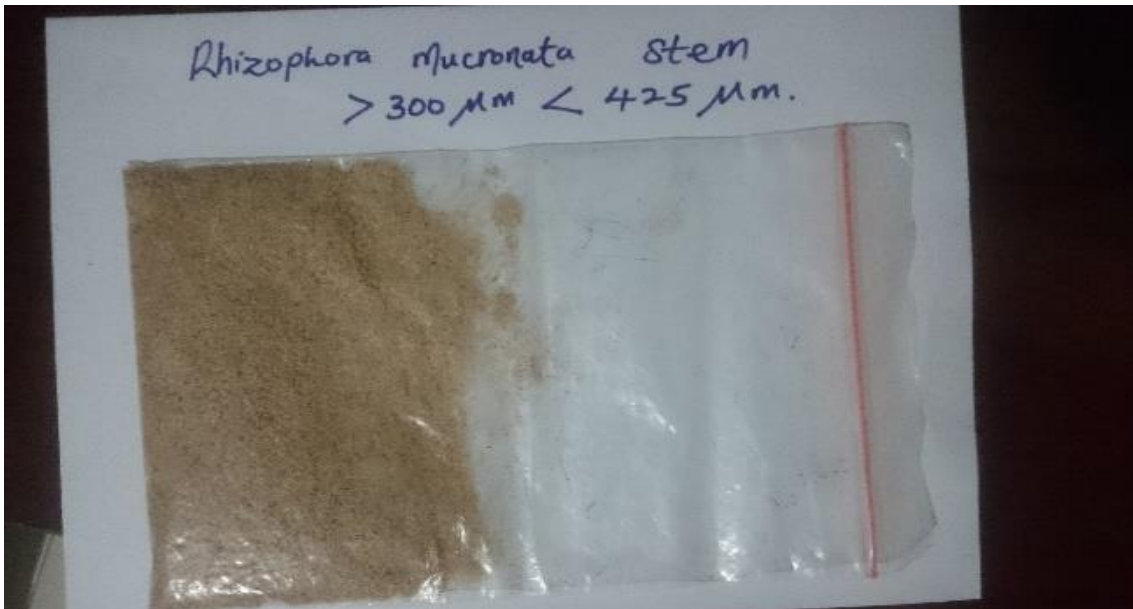
Figure 3.3: Prepared *R. mucronata* adsorbent stem of particle size, > 300µm < 425µm.

Figure 3.4: Prepared *R. mucronata* adsorbent stem-bark of particle size, $> 300\mu m < 425\mu m$.

Under various experimental conditions, these were then subjected to batch adsorption experiments as reported in section 3.4; sub-section 3.4.2; for CV adsorption experiments and section 3.5 for MG adsorption experiments.

3.2 Surface Characterisation

The fine powder of each mangrove was cleaned using double distilled water and the raw samples were mixed with potassium bromide (KBr) powder, triturated and then made into a 1 mm pellets for Fourier-transform infrared (FT-IR) analysis at frequency range of $4000 - 400cm^{-1}$. The FT-IR analysis was performed on Shimadzu FT-IR Affinity-IF spectrometer and was run successfully. The graphical results were then interpreted to ascertain the key compounds present in the matrix of the materials.

3.3 Adsorbate Collection and Preparation

3.3.1 Preparation of CV and MG dyes.

The crystal violet dye was purchased from Manigate Agencies LTD, analysed and subjected to adsorption experiments without any further purification. 0.0408 g of CV dye (99.99%pure) crystals was measured and used to prepare 40.8 mg/L stock solution.

Cationic Malachite Green dye, obtained from Kobian Scientific (Merck Manufactures), was also analysed and subjected to adsorption experiments without further purification. About 0.092903g of MG dye (99.98% pure) crystals was used to prepare 92.903 mg/L stock solution.

The stock solution was serially diluted to 2.50×10^{-5}, 1.25×10^{-5}, 1.00×10^{-5}, 5.00×10^{-6} and 2.50×10^{-6}M of CV and MG dyes using the formula shown below:

$$M_1V_1 = M_2V_2 \hspace{4cm} \text{Equation (8)}$$

Where; M_1 = Concentration of the stock solution, mol/dm^3.

M_2 = Concentration of dilute solution, mol/dm^3.

V_1 = Volume extracted from the stock solution, cm^3.

V_2 = Final volume of dilute solution, cm^3.

Various parameters were then investigated with a few adjustments as presented in the batch adsorption experimental procedures described in section 3.4.

3.4 CV Adsorption Experiments

3.4.1 Determining Calibration Curve

With the concentrations kept constant at room temperature and pressure, 40 ml of CV dye of concentration 2.50×10^{-5}M was measured using a measuring cylinder into three 250 ml Erlenmeyer flasks and the initial absorbance of each solution determined at $\lambda_{max} = 590$ nm using a UV/VIS spectrophotometer (Shimadzu UV 1700, Japan). Consecutive serial dilution was done and the experiment was repeated for concentrations; 2.50×10^{-5}, 1.25×10^{-5}, 1.00×10^{-5}, 5.00×10^{-6} and 2.50×10^{-6}M. A graph of absorbance against the concentrations was then plotted. For the following consecutive experiments, the initial absorbance of each solution was determined at $\lambda_{max} = 590$ nm using a UV/VIS spectrophotometer (Shimadzu UV 1700, Japan).

3.4.2 Effect of contact Time

To a set of three 250 ml Erlenmeyer flasks, 40 ml of CV dye of concentration 2.50×10^{-5}M was transferred. These measurements were done at a temperature of 25^{0}C and 1 atmosphere pressure (1atm). To each of the flasks, 0.25 g powdered *X. moluccenisis* stem-bark, particle size >300 µm to < 425 µm, was then added and the system set on an orbital shaker (Thermolyne-type 65800) preset at 350 rpm. Using a laboratory filtration syringe, aliquots were withdrawn every 5 minutes, filtered and their absorbance determined at λ_{max} = 590 nm, and returned into the solution. The experiment was done for 60 minutes and various parameters investigated and the procedures repeated for *X. moluccenisis* stem.

3.4.3 Effect of Particle Size

40 ml of 2.5×10^{-5}M of CV dye was placed in 250 ml Erlenmeyer flask. With a stop watch started simultaneously, 0.25 g of finely powdered *X. moluccenisis* stem-bark of particle size < 300 µm, was added and the system placed on an orbital shaker (Thermolyne-type 65800) preset at 350 rpm. Aliquots were then withdrawn, adsorbent filtered and absorbance measured at λ_{max} = 590 nm, every 5 minutes time intervals during the 60 minutes experiment duration, before being returned into the solution. The experiment was done three times and repeated for particle sizes >300 µm < 425 µm, and > 425 µm.

3.4.4 Effect of Adsorbent Dose

40 ml of 2.50×10^{-5}M of CV dye was placed in 250 ml Erlenmeyer flask at 25^{0}C and 1 atmosphere. With a stop watch started simultaneously, 0.125 g of finely powdered *X. moluccenisis* stem-bark of particle size >300 µm < 425 µm, was added and the system placed on an orbital shaker (Thermolyne-type 65800) preset at 350 rpm. Aliquots were then withdrawn, adsorbent filtered and absorbance measured at λ_{max} = 590 nm, every 5 minutes time intervals during the 60 minutes experiment duration, before being returned into the solution. The experiment was done three times and repeated for adsorbent doses 0.250 g, 0.375 g and 0.500 g.

3.4.5 Effect of Concentration

40 ml of 2.5×10^{-5}M of CV dye was placed in 250 ml Erlenmeyer flask at 25^0C and 1 atm. With a stop watch started simultaneously, 0.25 g of finely powdered *X. moluccenisis* stem-bark of particle size >300 µm < 425 µm, was added and the system placed on an orbital shaker (Thermolyne-type 65800) preset at 350 rpm. Aliquots were then withdrawn, filtered and absorbance measured at $\lambda_{max} = 590$ nm, every 5 minutes time intervals during the 60 minutes experiment duration, before being returned into the solution. The experiment was done three times and repeated for concentrations; 1.25×10^{-5}, 1.0×10^{-5}, 5.0×10^{-6} and 2.5×10^{-6}.

3.4.6 Effect of pH

40 ml of 2.50×10^{-5}M of CV dye was placed in 250 ml Erlenmeyer flask at 25 ^{0}C at 1 atmosphere. The pH was then adjusted to pH 2 using 1.00M HCl and 1.00M NaOH and double distilled water. With a stop watch started simultaneously, 0.25g of finely powdered *X. moluccenisis* stem-bark of particle size >300 µm < 425 µm, was added and the system placed on an orbital shaker (Thermolyne-type 65800) preset at 350 rpm. Aliquots were then withdrawn, filtered and absorbance measured at $\lambda_{max} = 590$ nm, every 5 minutes time intervals during the 60 minutes experiment duration, before being returned into the solution. The experiment was done three times and repeated for pH 3.0, 4.0, 5.0, 6.0, 7.0, 8.0, 9.0, 10.0, and 11.0.

3.4.7 Effect of Ionic Strength

30 ml of 2.50×10^{-5}M of CV dye was placed in six 250 ml Erlenmeyer flasks at room temperature and pressure. To each flask, specific amounts (ml) of 1M NaCl and distilled water were added as given in the Table 3.1 shown.

Table 3.1: Variation of Ionic Strength with Volume of the Aqueous Solution.

Flask	1	2	3	4	5	6
Volume of 1.0M NaCl (ml)	0	2	4	6	8	10
Volume of Distilled Water (ml)	10	8	6	4	2	0

With a stop watch started simultaneously, 0.25 g of finely powdered *X. moluccenisis* stem-bark of particle size >300 µm to < 425 µm, was added and the system placed on an orbital shaker (Thermolyne-type 65800) preset at 350 rpm. Aliquots were then withdrawn, filtered and absorbance measured at λ_{max} = 590 nm, every 5 minutes time intervals during the experiment duration, before being returned into the solution. The results were recorded and subsequently plotted to obtain graphs.

3.5 MG Adsorption Experiments

The parametric procedures in section 3.4 were carefully repeated for Malachite Green dye (λ_{max} = 617 nm) at a temperature of 25^0C and 1 atmosphere pressure. The results were compared and various constants determined for each species adsorptive nature and conclusions drawn as given in Chapter 5.0.

3.6 Determining the surface characteristics by use of FTIR

The attenuated total reflectance method was used to analyse the species samples. Fine powdered species samples (having a maximum length of about 5 µm) was selected from the unused materials (raw) and used materials. The samples were then mixed with potassium bromide (KBr) powder, triturated and then made into a 1 mm pellets for Fourier-transform infrared (FT-IR) analysis at frequency range of 4000 – 400 cm^{-1}. Below this value (5 µm), scattering losses can be ignored. The spectral results were then computer generated and presented for interpretation.

CHAPTER FOUR

4.0 Results and Discussions

4.1 Maximum Absorption Wavelength (λ_{max})

The maximum absorption wavelengths for CV was obtained by scanning from 300 nm to 700 nm while for MG, the scanning was in the range; 300 nm to 900 nm using UV/VIS spectrophotometer (Shimadzu UV 1700, Japan). The maximum wavelength, λ_{max}, for CV and MG dyes were found to be 590 nm and 617 nm respectively as shown in the figures 4.1 and 4.2. This was in line with the literature values which put the maximum adsorption wavelengths at 592 nm and 617 nm for CV and MG respectively, (Bulut *et al*., 2008; Sun *et al*., 2007).
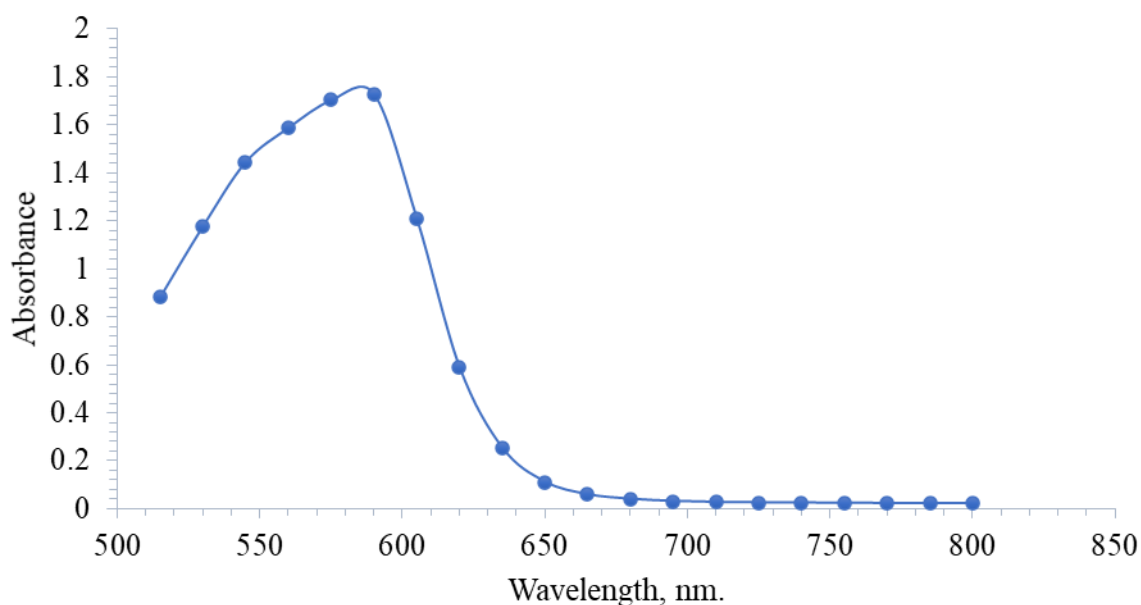
Figure 4.1: Maximum wavelength, λ_{max}, for CV dye.
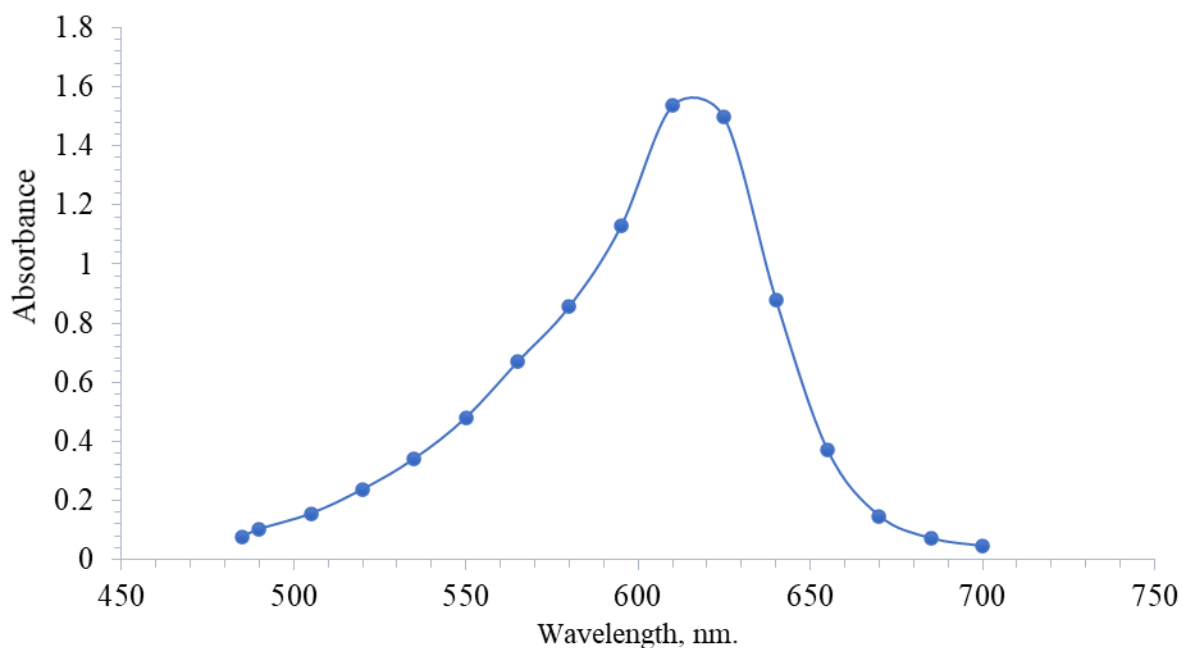
Figure 4.2: Maximum wavelength, λ_{max} , for MG dye.

4.2 Calibration Curves

A calibration curve is a standard curve that determines a substance's concentration in a given sample under investigation. It compares the concentration of unknown sample to a set of standard samples whose concentrations are known (Chieng *et al*., 2013). The calibration curves for CV and MG dyes were generated from dilute solutions prepared from the stock solutions. To compare the concentrations in this study, a calibration curve was developed for CV and MG dyes as given in figure 4.3 and 4.4 respectively;

Calibration Curve for CV

$y = 1.8876x - 0.1926$

$R^2 = 0.9897$
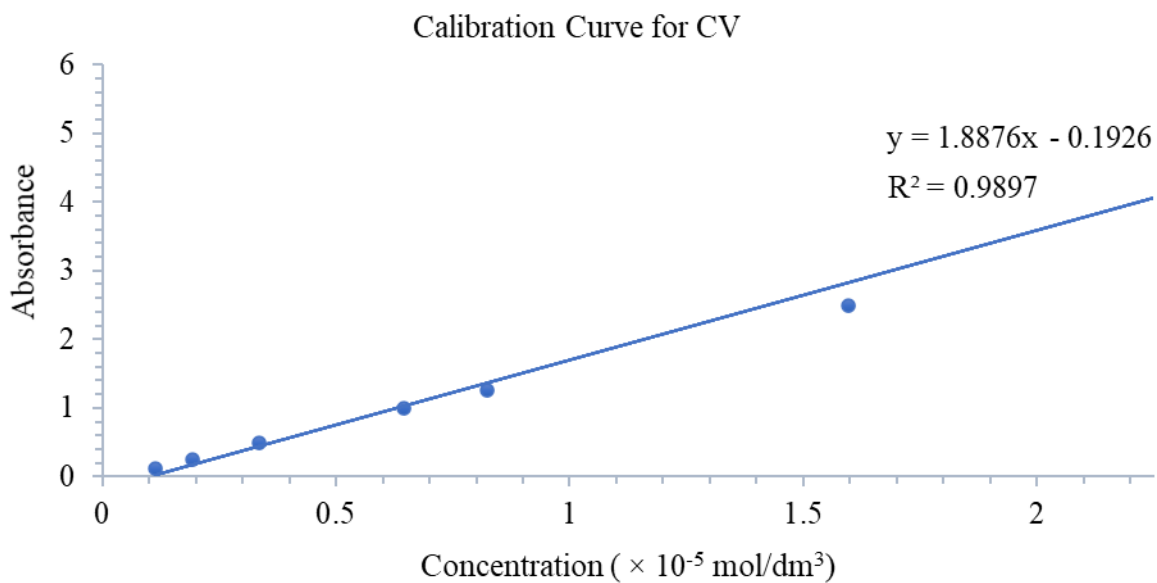
Figure 4.3: Calibration curve for CV dye.

Calibration Curve for MG

$y = 0.6198x + 0.0072$

$R^2 = 0.9934$
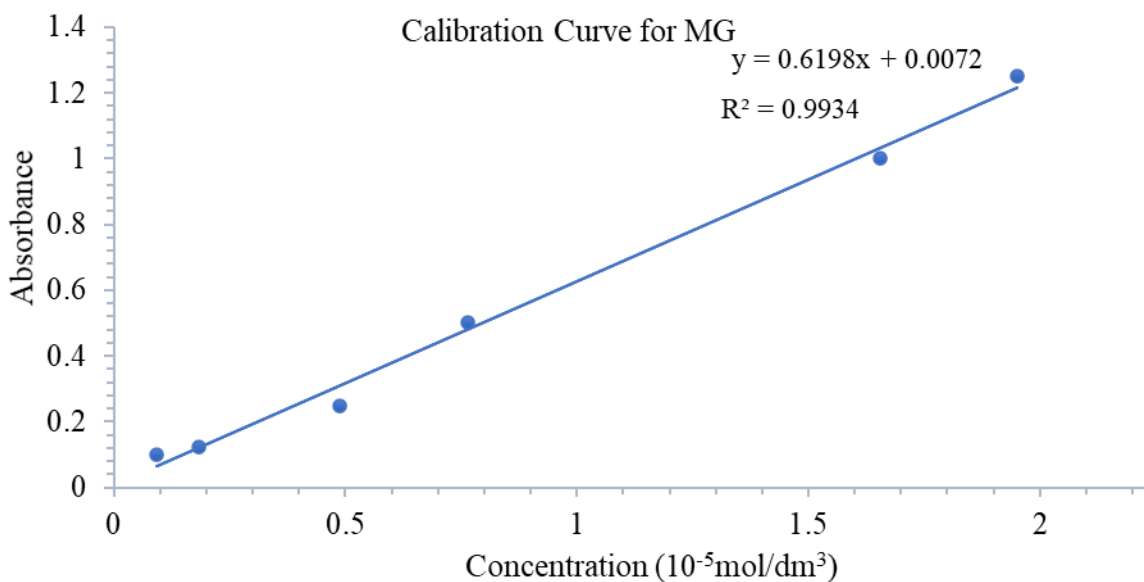
Figure 4.4: Calibration curve for MG dye.

The coefficient of determination, R^2, values in Figures 4.3 and 4.4 are high demonstrating good calibration curves. The standard curves presented show the correct concentrations that will be used in the batch experiments.

4.3 Batch CV Adsorption using Arial Parts of *X. moluccenisis* and *R. mucronata*

4.3.1 Effect of Contact Time

The efficiency of the adsorption process and its associated kinetics and equilibrium time, between dye molecules and the adsorbent materials, is determined by the contact time. CV dye adsorption onto the surface of *X. moluccenisis* stem-bark and *R. mucronata* stem-bark, was found to be higher than onto the species stem. In both cases, dye sorption rapidly increased with time but is slowed down as the system attains equilibrium. The following plots, Figures 4.5 and 4.6, illustrates the adsorption of CV dye with time onto species stem and stem-bark.

Figure 4.5: Effect of Contact Time on adsorption of CV onto *X. moluccenisis* stem and stem-bark.
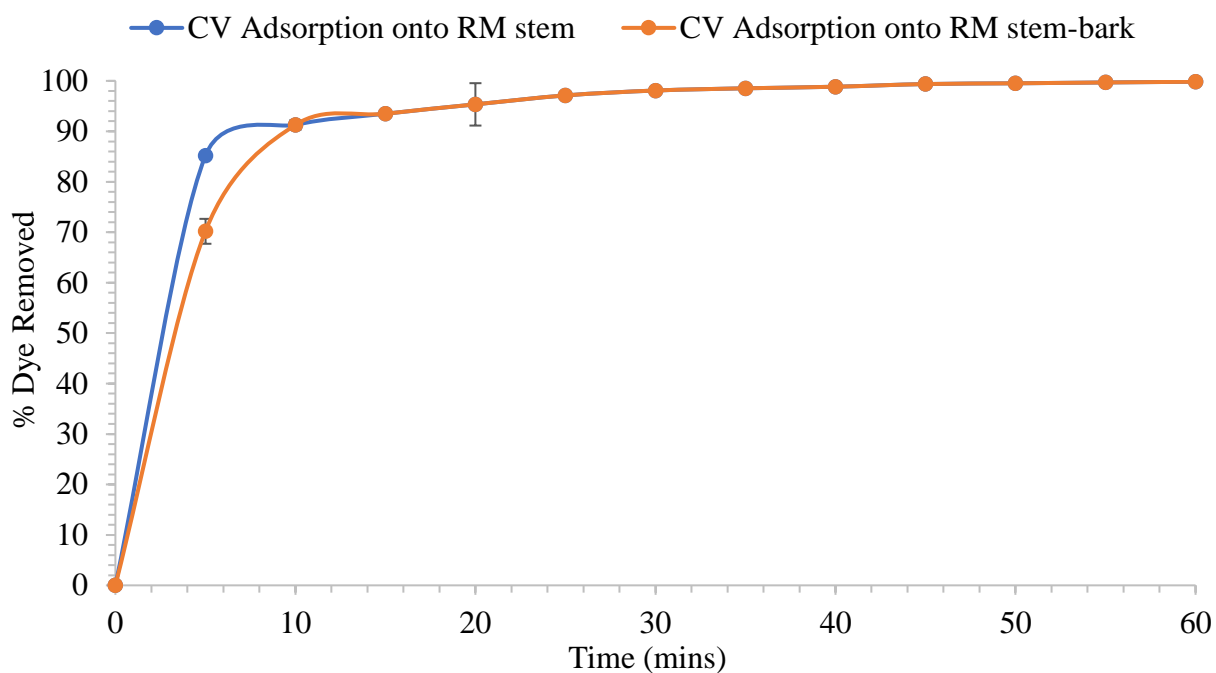
Figure 4.6: Effect of Contact Time on adsorption of CV onto *R. mucronata* stem and stem-bark.

From Figures 4.5 and 4.6, the trend of dye uptake by the stem and stem-bark of the two mangrove species is visibly contact-time dependant. The amount of dye adsorbed by *X. moluccenisis* stem and stem-bark within the first 5 to 20 minutes, increased from $75.9 \pm 0.15\%$ to 97.1 ± 0.15, and from $85.2 \pm 0.16\%$ to $96.7 \pm 0.11\%$ respectively. For *R. mucronata* stem, the uptake increased from $85.2 \pm 0.16\%$ to $95.3 \pm 0.20\%$ and from $85.2 \pm 0.47\%$ to $95.3 \pm 0.05\%$ capacity for *R. mucronata* stem-bark and thereafter becomes constant as the process reaches its equilibrium position. The results demonstrate that adsorption is time dependent and approximately 45 minutes was required by each adsorbent to attain equilibrium; with an adsorption capacity ranging between 98.1 to $99.8 \pm 0.16\%$. The time factor shows that the adsorption process onto these species parts is kinetically stable as compared with other adsorbents previously examined (Alshabanat *et al.*, 2013). In both Figure 4.5 and Figure 4.6, the stem-bark of the species was found to have a higher capacity than the stem with other factors remaining constant. At 45 minutes the performance of the bark was at about $99.5\% \pm 0.15\%$. capacity compared to the stem which was at $98.6\% \pm 0.16\%$ capacity.

4.3.2 Effect of Initial Concentration

Figures 4.7 and 4.8 shows how dye concentration affects adsorption of adsorbate molecules onto the species stem and stem-bark. In figure 4.7, adsorption of CV dye increased with concentration for both the stem and stem-bark of *X. moluccensis* adsorbent materials. The lowest and highest equilibrium adsorption capacity Q_e mg/g was 40.78 ± 0.002 mg/g and 407.98 ± 0.002 mg/g for the stem-bark showing an increase in Q_e mg/g with increase in adsorbate concentration. This trend was also observed in Figure 4.8 with *R. mucronata* adsorbent materials.
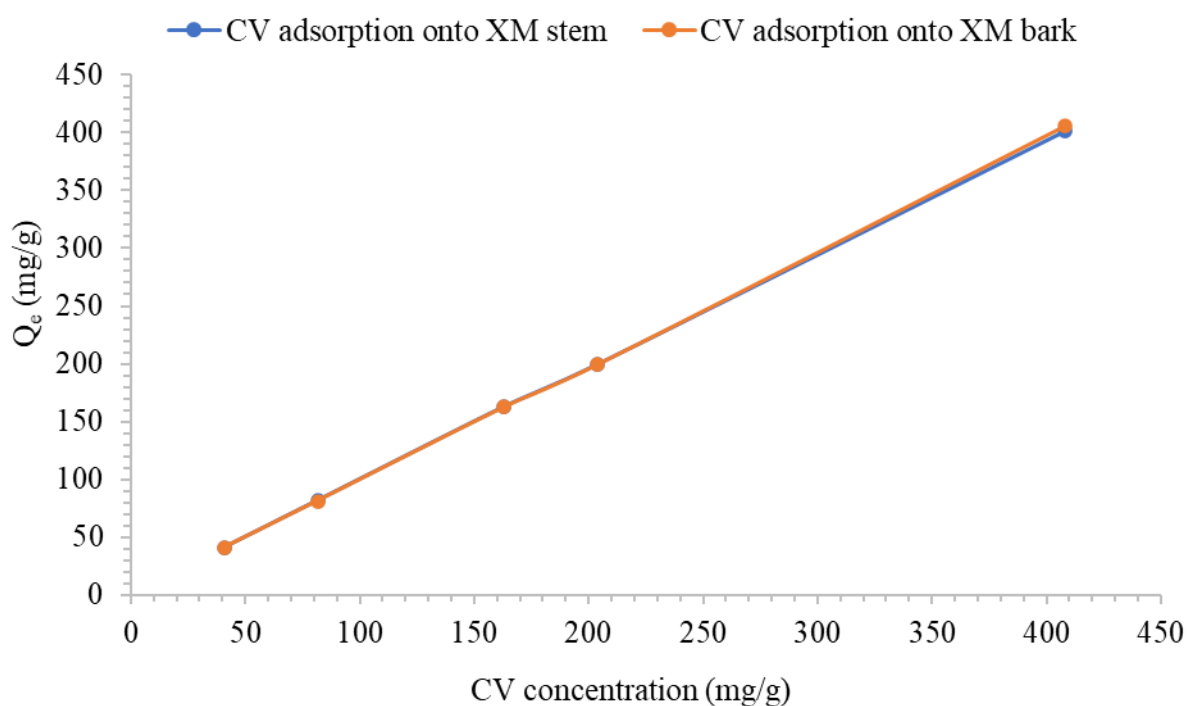
Figure 4.7: Effect of Initial CV Concentration for Adsorption onto *X. moluccenisis* stem and stem-bark.
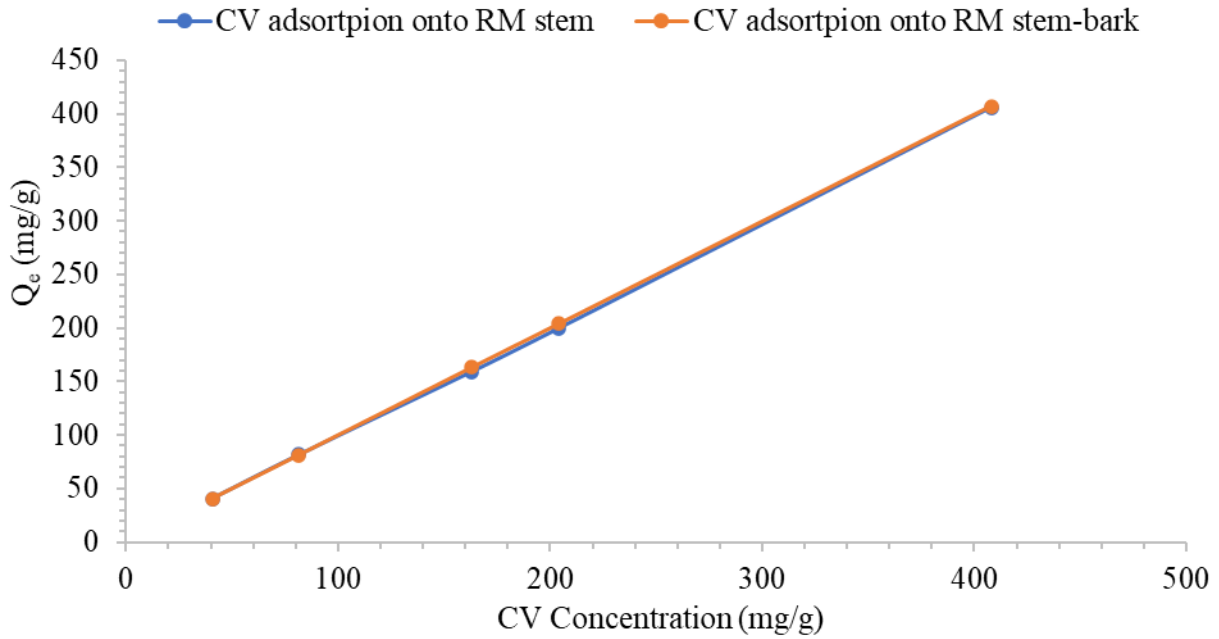
Figure 4.8: Effect of Initial CV Concentration for Adsorption onto *R. mucronata* stem and stem-bark

Figures 4.7 and 4.8 demonstrates that adsorption process depend on the concentration of the dyes and at very low CV dye concentration, fractional adsorption is low and the adsorption process is not dependent on the initial dye concentration. However larger fractional adsorption ratio is realized at higher concentrations (Chakraborty *et al*., 2012). The actual available sites for adsorption become fewer at higher concentrations since the dye molecules overlap over these sites. The quantity of dye being adsorbed becomes less and hence the adsorption capacity is low (Arivoli *et al*., 2009).

4.3.3 Effect of the Particle Size

The surface area is a factor affecting adsorption and this can be assessed by characterisation of the particle sizes of the adsorbent materials (Joseph *et al*., 2013). Smaller particle sizes of the adsorbent material provide large surface area and ensures a high amount adsorbed per unit area (Wanyonyi *et al*., 2014). The effect of the particle sizes is shown in Figures 4.9 and 4.10; in the graphs, the percentage dye removed at equilibrium have been used as a measure of the species materials performance at different particle sizes.
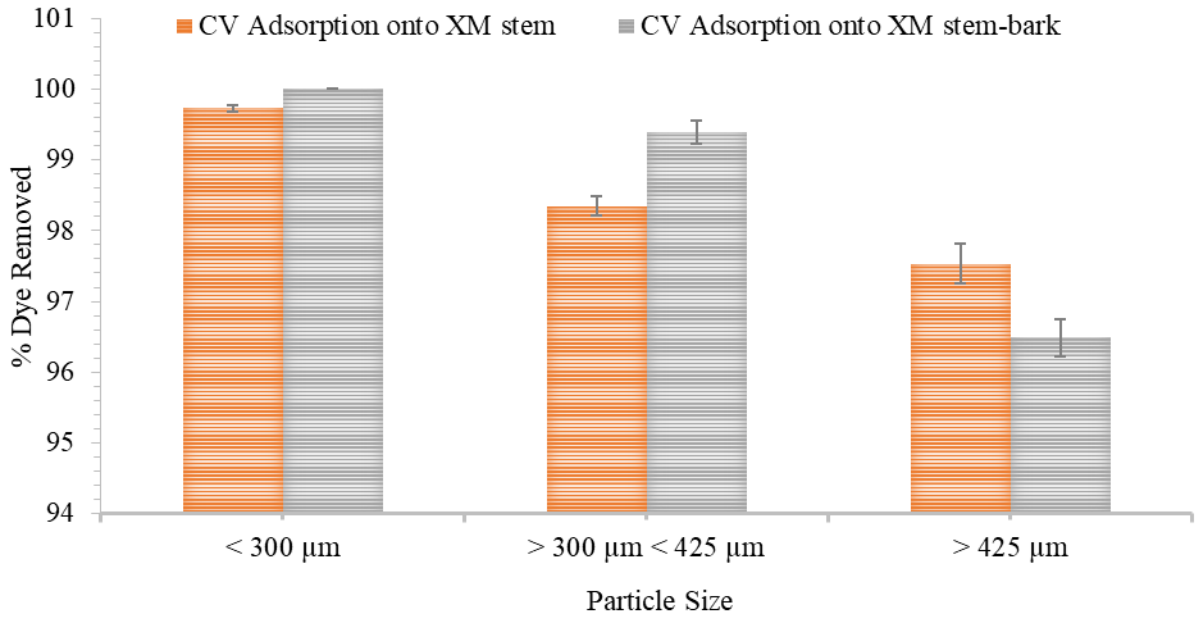
Figure 4.9: Effect of Particle size on Adsorption of CV onto *X. moluccenisis* stem and stem-bark.
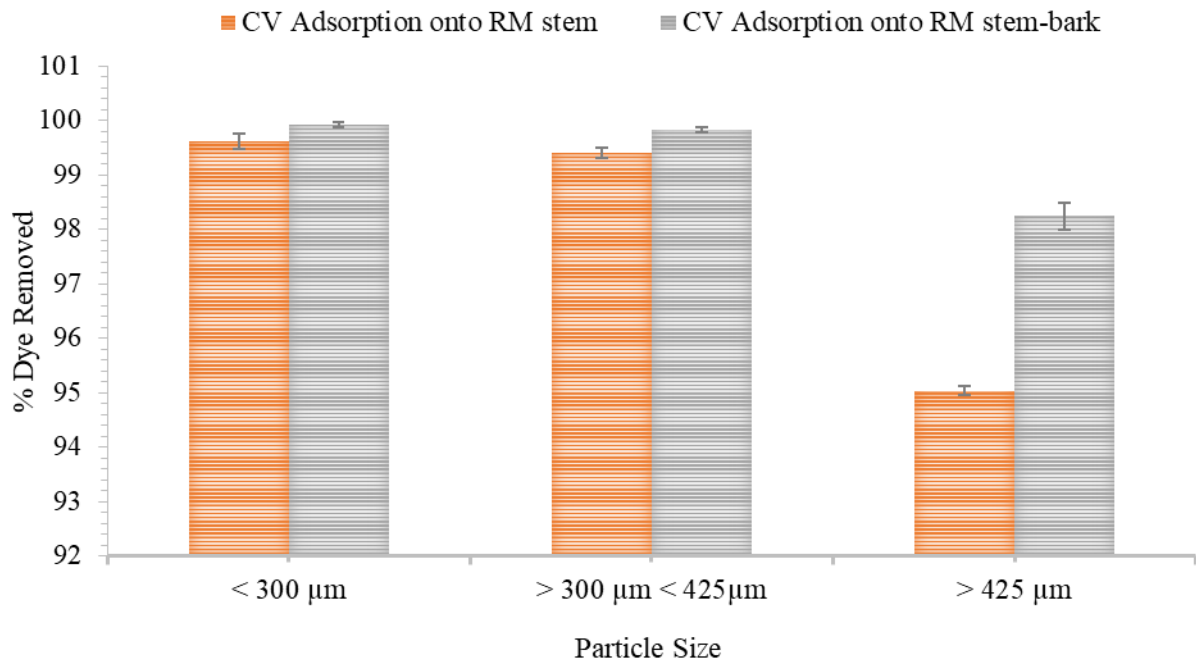
Figure 4.10: Effect of Particle size on Adsorption of CV onto *R. mucronata* stem and stem-bark.

Minute particle sizes means large surface area implying an increased number of surface active sites that can adsorb the dye molecules (Wanyonyi *et al*., 2014). The bar graphs in Figures 4.9 and 4.10 clearly show that as the particle size decreases, the CV dye sorption at equilibrium also increases. At equilibrium the CV dye adsorbed increased from 397.9 ± 1.05 mg/g to 406.9 ± 1.07

mg/g and 391.5 ± 0.2 mg/g to 408.0 ± 0.2 mg/g for the stem and stem-bark of *X. moluccensis* respectively as particle sizes decreased from > 425 µm to < 300 µm. The dye adsorption onto the stem-bark surface was superior to that of the stem. For *R. mucronata*, the adsorbed dye at equilibrium as particle size decreases from > 425 µm to < 300 µm increased from 387.7 mg/g to 406.4 ± 1.07 mg/g and 400.8 ± 0.95mg/g to 407.6 ± 1.07 mg/g for the stem and stem-bark respectively. The equilibrium adsorption capacities show that the stem-bark performed better than the stem of the species with other factors held constant, demonstrating that external environmental factors such as adaptations to harsh climatic conditions affect surface adsorption. The exposure of the stem-bark of the species to harsh saline conditions increased its sorption abilities hence the slight difference. A decrease in the equilibrium time as the particle size decreases have also been observed by Mohammed *et al*., (2014). This reduction in the equilibrium time can be due to diffusion by the finer particles as the particle size decreases. Further breaking the particles into finer powder opens up some tiny sealed channels that are necessary for and increases dye sorption (Kumar & Gayathri, 2009). Hence finer particle sizes have better adsorption properties than granular particle size.

4.3.4 Effect of Adsorbent Dose

The quantized adsorbent material used on CV sorption process was evaluated and the results obtained are as in Figures 4.11 and 4.12;
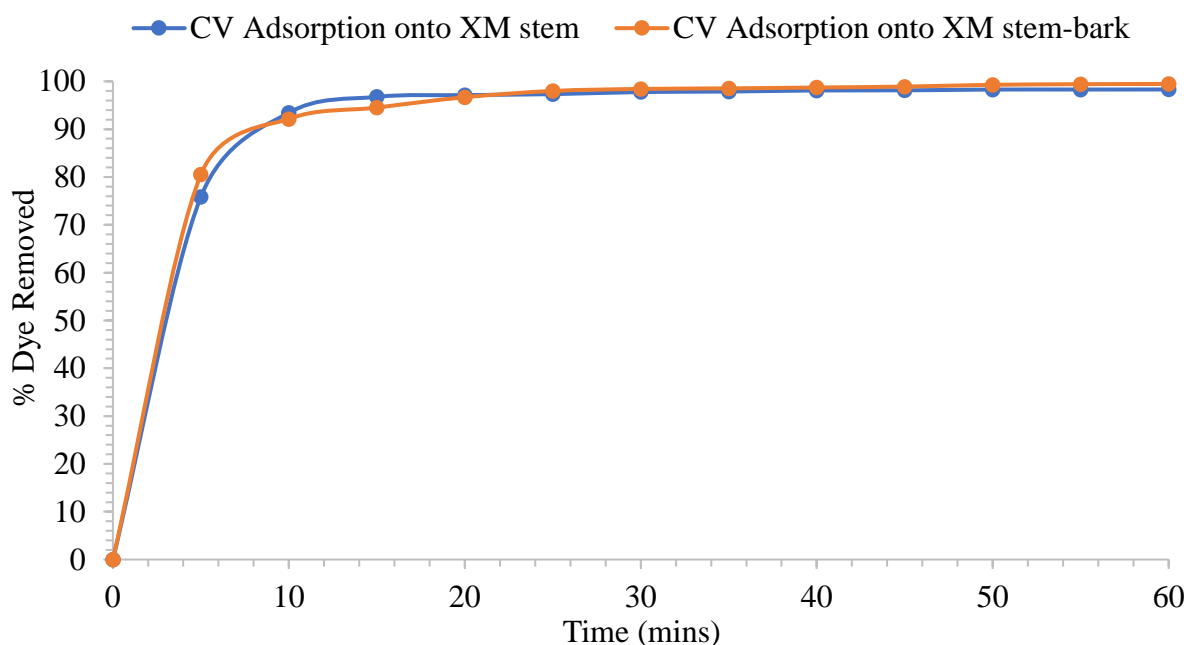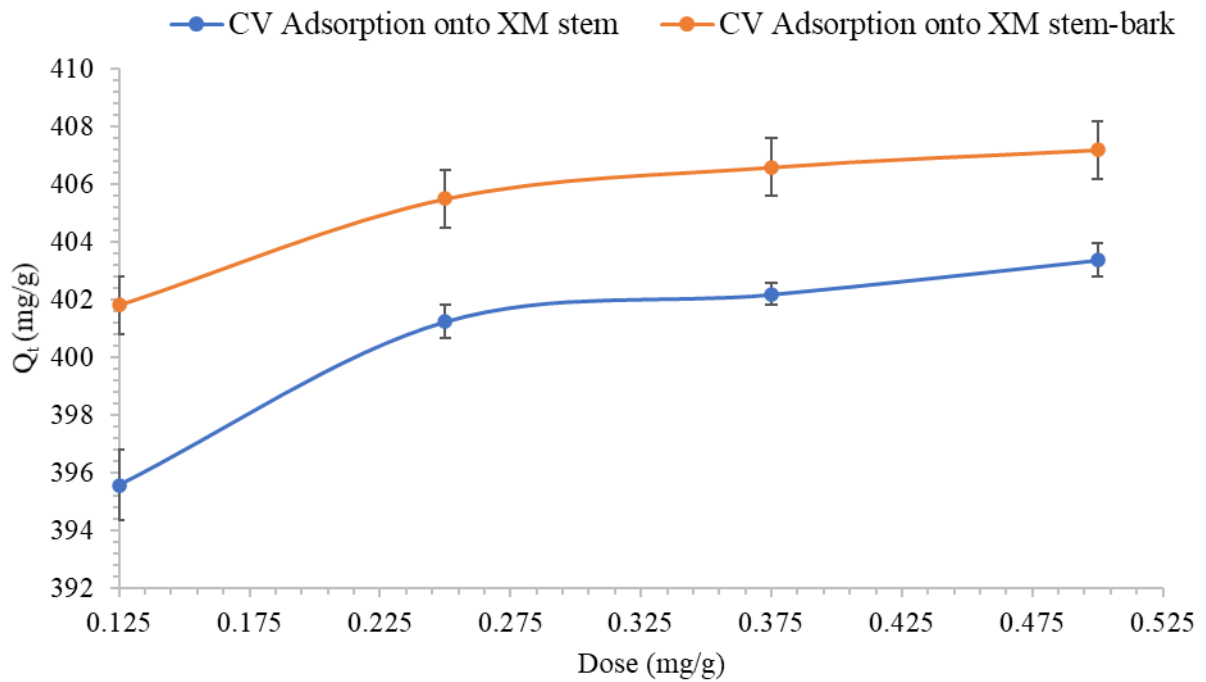
Figure 4.11: Effect of Adsorbent Dose on Adsorption of CV onto *X. moluccensis* stem and stem-bark.
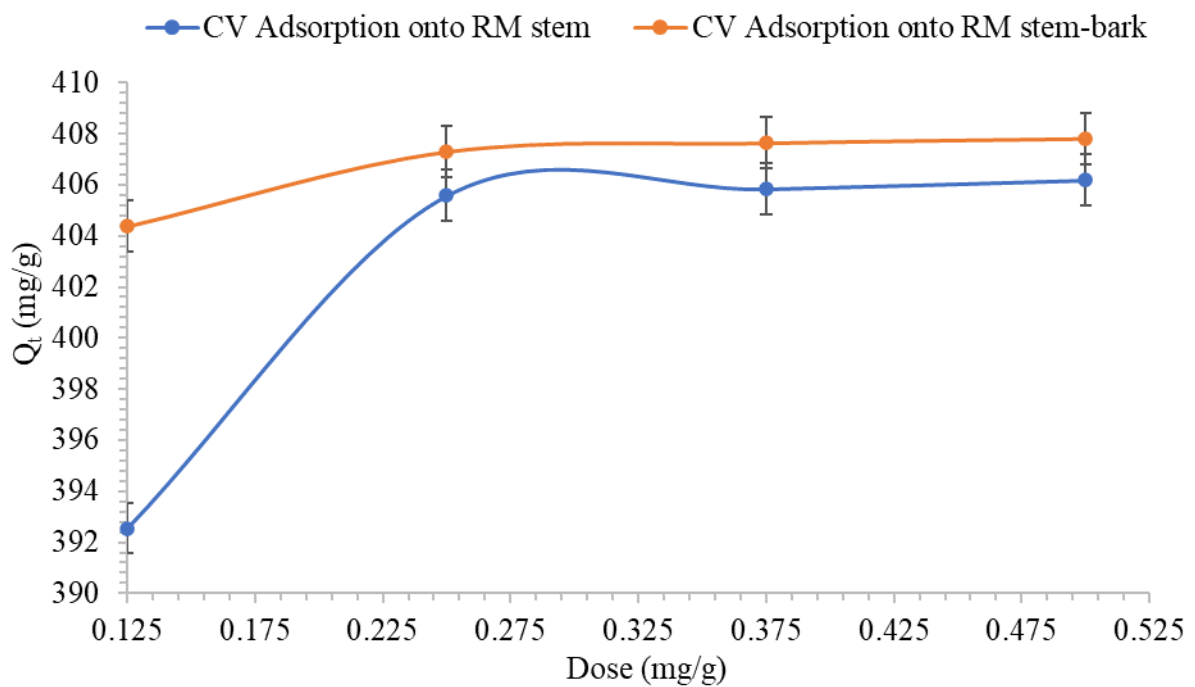
Figure 4.12: Effect of Adsorbent Dose on Adsorption of CV onto *R. mucronata* stem and stem-bark.

The figures 4.11 and 4.12 show that the stem-bark is a better dye remover and the larger the dose, the higher the adsorption capacity although overlapping particles of the adsorbent increases with time reducing the efficiency of the process (Jedynak & Repelewicz, 2017). An increase in

adsorbent dose increases the process of adsorption and can be associated to the fact that at constant dye concentration and volume, sorption sites become unsaturated as the adsorbent dose increases (Salleh *et al*., 2011), and an equilibrium will develop between the two media (Raval *et al*., 2017).

4.3.5 Effect of Ionic Strength

The cations and anions present in textile industrial effluents generally increase the ionic strength of aqueous mixture. By varying the volume of the 1.0M NaCl and distilled water, the concentrations of Na^+ and Cl^- were altered at various stages. Effects of ionic strength on Crystal Violet adsorption are illustrated on Figure 4.13 and 4.14.
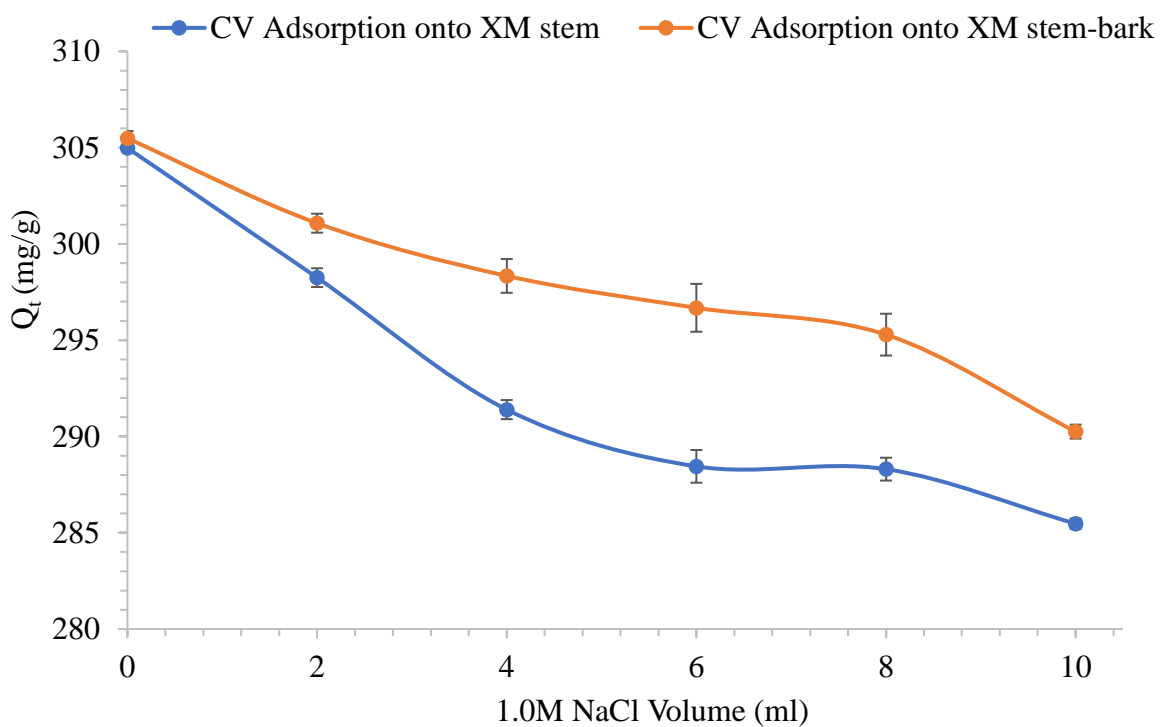
Figure 4.13: Effect of Ionic Strength on Adsorption of CV onto *X. moluccensis* stem and stem-bark.
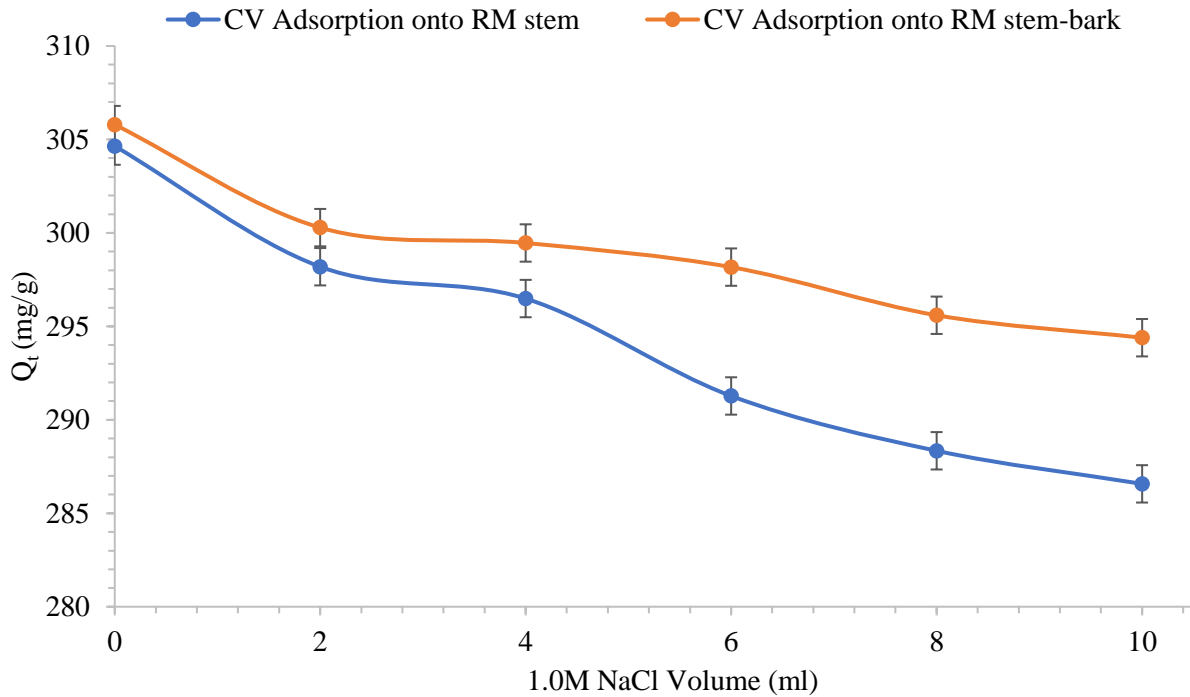
Figure 4.14: Effect of Ionic Strength on Adsorption of CV onto *R. mucronata* stem and stem-bark.

The sorption properties of the materials decreased as ionic strength increases and at higher concentrations of the Na^+ ions in the adsorbate solution for both dyes, a tremendous decrease in the amount adsorbed at equilibrium was witnessed with about 6.72 ± 0.003 % fall observed. Both the stem and stem-bark of the two Mangrove species, however, still showed over $93.28 \pm 0.015\%$ dye sorption at higher ionic strengths. The ionic strength determines the rate at which the cationic characters in the aqueous mixture compete for the available sites (Ali *et al*., 2014). A higher concentration of Na^+ would viciously compete for the available sites out numbering the cationic dyes particles at molecular level, leading to a sorption decrease. Further the Na^+ ions are smaller in size than the dye molecules (in which there are quite a number of groups causing screening effect); and will swiftly access the anionic sites still present on the adsorbent surface. Similar results on CV and MG removal reduction with increase in ionic strength have been reported; (Oladipo & Gazi, 2014) and (Samiey & Toosi, 2010).

4.3.6 Effect of pH

Figure 4.15 and 4.16 illustrates the pH factor on CV dye adsorption.
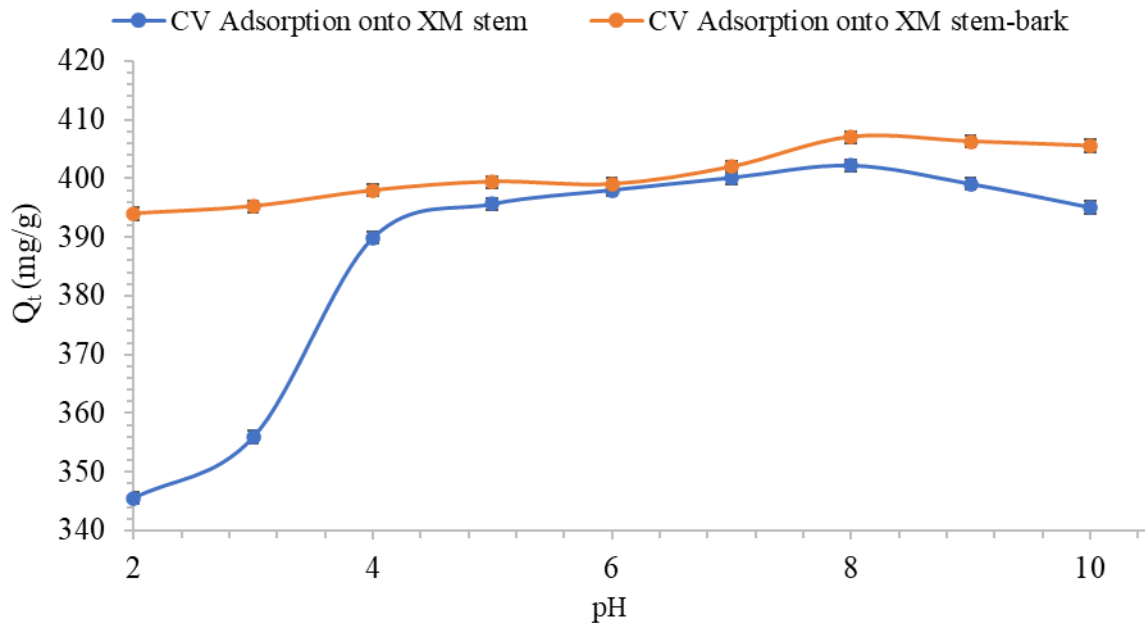
Figure 4.15: Effect of pH on Adsorption of CV onto *X. moluccensis* stem and stem-bark.
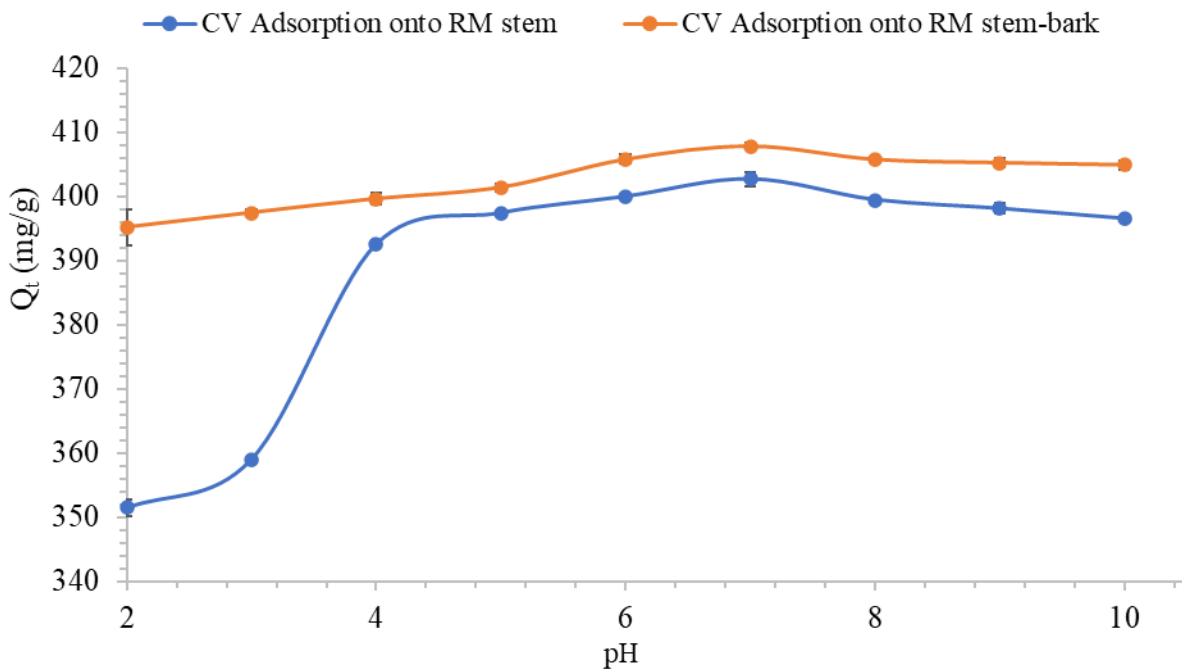
Figure 4.16: Effect of pH on Adsorption of CV onto *R. mucronata* stem and stem-bark.

The best pH at which maximum adsorption is observed for the stem and stem-bark are pH 8 and pH 7 for CV adsorption onto *X. moluccensis* and *R. mucronata* species respectively with the stem-bark showing a higher capacity at 407.1 ± 0.05 mg/g and 407.8 ± 0.05 mg/g. The pH of a

solution as observed, modifies the adsorbent surfaces depending on whether the solution is acidic, neutral or alkaline (Zolgharnein *et al*., 2015). Investigations in this study involved determination of the optimum pH at which maximum adsorption occurs. As shown in Figures 4.15 and 4.16, an increase in the pH beyond the neutral region, results to a slightly lower or constant adsorption process. A result that maybe due to characteristic observation that cationic dyes experience high affinity to anionic adsorbent sites at higher pH values (Pavan *et al*., 2014).

4.4 Batch MG Adsorption using Arial Parts of *X. moluccensis* and *R. mucronata*.

4.4.1 Effect of Contact Time

This study emphasised adsorptive properties of *X. moluccensis* and *R. mucronata.* The species stem-bark was found to have superior adsorptive properties than stem samples of the species. The equilibrium was found to set up within 10 minutes for both *X. moluccensis* stem and the stem-bark as demonstrated in Figure 4.17 and 4.18;

Figure 4.17: Effect of Contact Time on Adsorption of MG onto *X. moluccensis* stem and stem-bark.
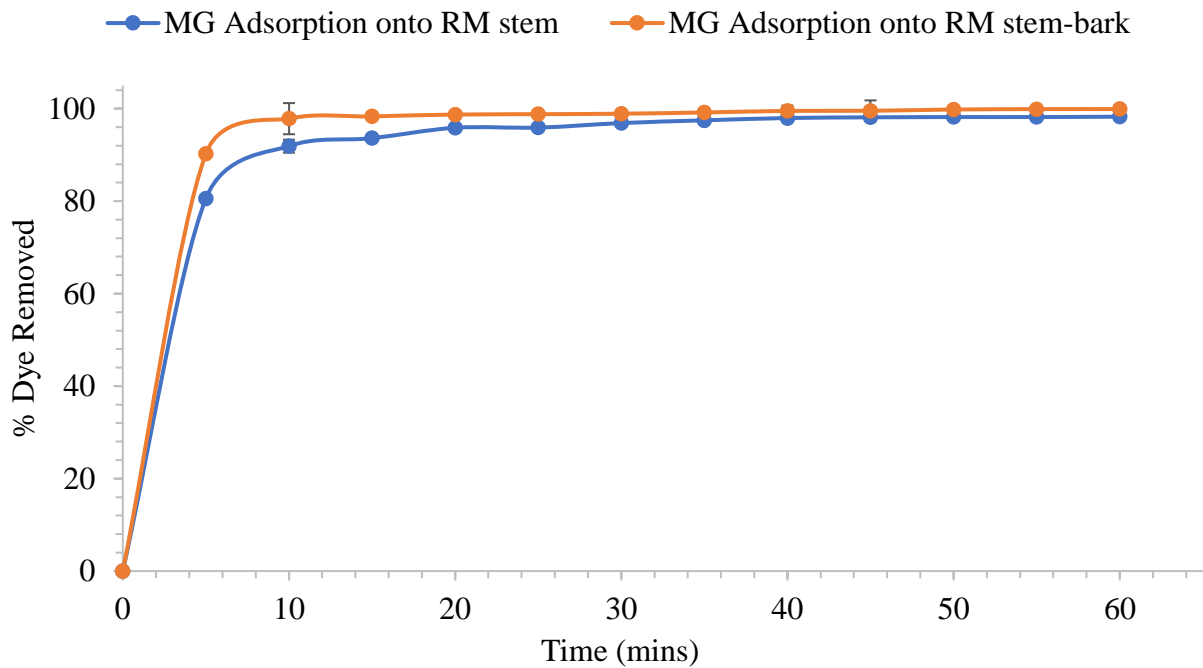
Figure 4.18: Effect of Contact time on Adsorption of MG onto *R. mucronata* stem and stem-bark.

The adsorption process was found to rapidly increase with time for the first 5 minutes but slowed down on attaining equilibrium. The rapid adsorption shown could be due to available surface empty sites (Veetil *et al*., 2012). After 50 minutes, both CV and MG dye adsorption was slower indicating that the equilibrium conditions have been attained (Bertolini *et al*., 2013).

4.4.2 Effect of Initial Concentration

Effect of concentration of MG dye is illustrated on Figure 4.19 and 4.20;

Figure 4.19: Effect of Concentration on Adsorption of MG onto *X. moluccensis* stem and stem-bark.
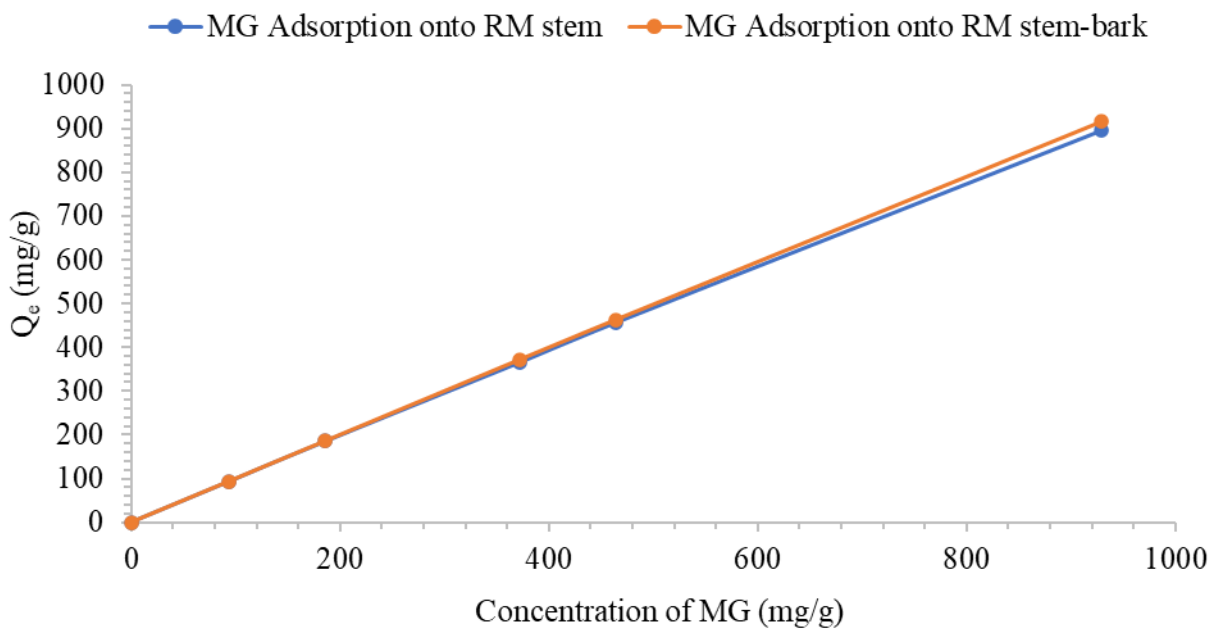
Figure 4.20: Effect of Concentration on Adsorption of MG onto *R. mucronata* stem and stem-bark.

Figures 4.19 and 4.20 characteristically compares to observed results in section 4.3; sub-section

4.3.2.

4.4.3 Effect of the Particle Size

The particle size as a parameter on the adsorption of MG dye are given in figures 4.21 and 4.22
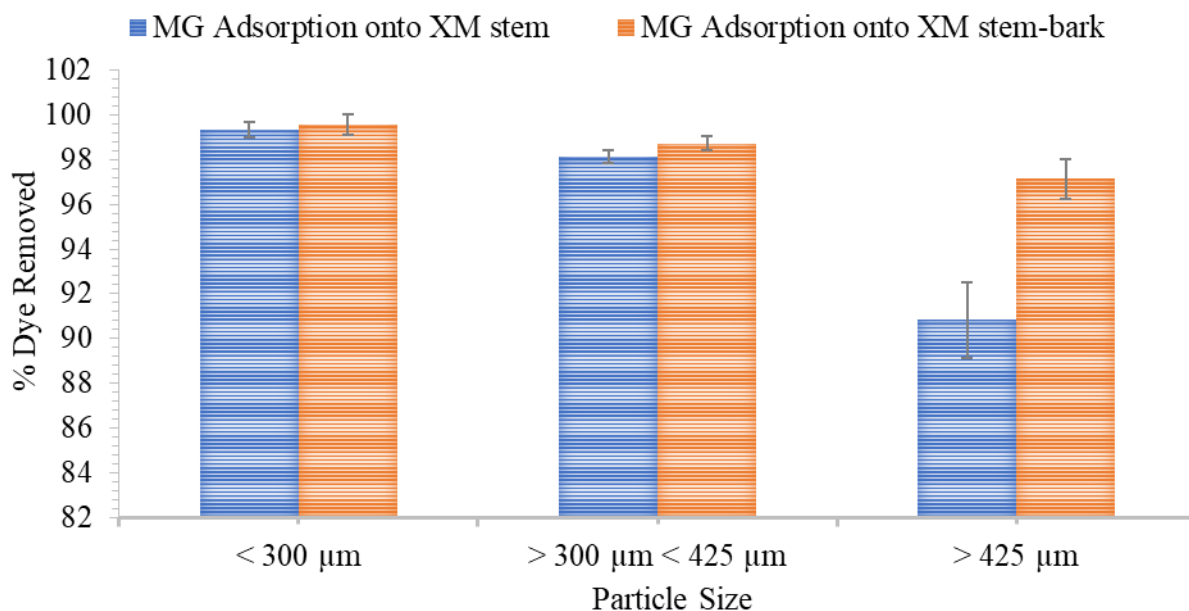
Figure 4.21: Effect of Particle size on Adsorption of MG onto *X. moluccensis* stem and stem-bark.
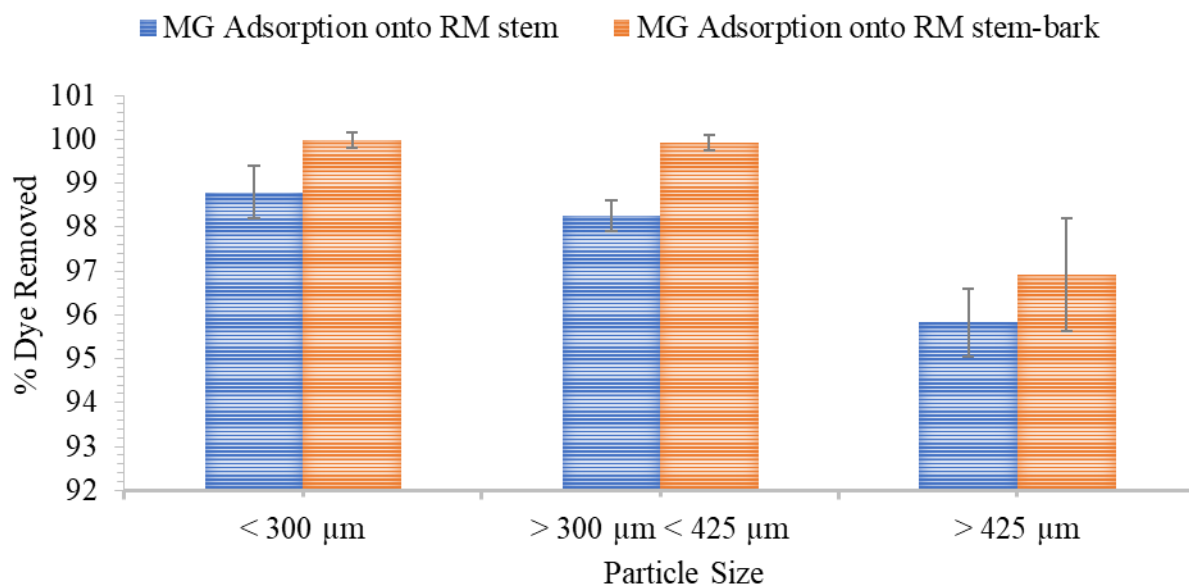
Figure 4.22: Effect of Particle Size on Adsorption of MG onto *R. mucronata* stem and stem-bark.

An inverse relation was found to exist between adsorption capacity and adsorbent particle sizes hence a direct influence on the equilibrium time of the adsorption for both dyes. This is evident in the higher adsorption capacities observed in the Figures 4.21 and 4.22. At equilibrium, the

MG dye adsorbed increased from 337.6 mg/g to 369.2 ± 0.07 mg/g and 361.0 mg/g to 370.0 ±

0.03 mg/g for the stem and stem-bark of *X. moluccensis* as the particle sizes decreased from >

425 µm to < 300 µm. respectively. With *R. mucronata*, there was respective increase from 356.1

mg/g to 367.1 ± 0.03mg/g and 360.1 mg/g to 371.5 mg/g for the stem and stem-bark respectively.

X. moluccensis and *R. mucronata* bark was found to have a higher adsorption capacity than stem

for both MG dye. The results support other findings in literature; that fine particle sized

adsorbents have higher affinity for dye contaminants compared to coarse particle for most

materials (Lim *et al*., 2015).

4.4.4 Effect of Adsorbent Dose

With other parameters kept constant, the adsorbent dose was studied and the final data evaluated

as shown in figures 4.23 and 4.24;
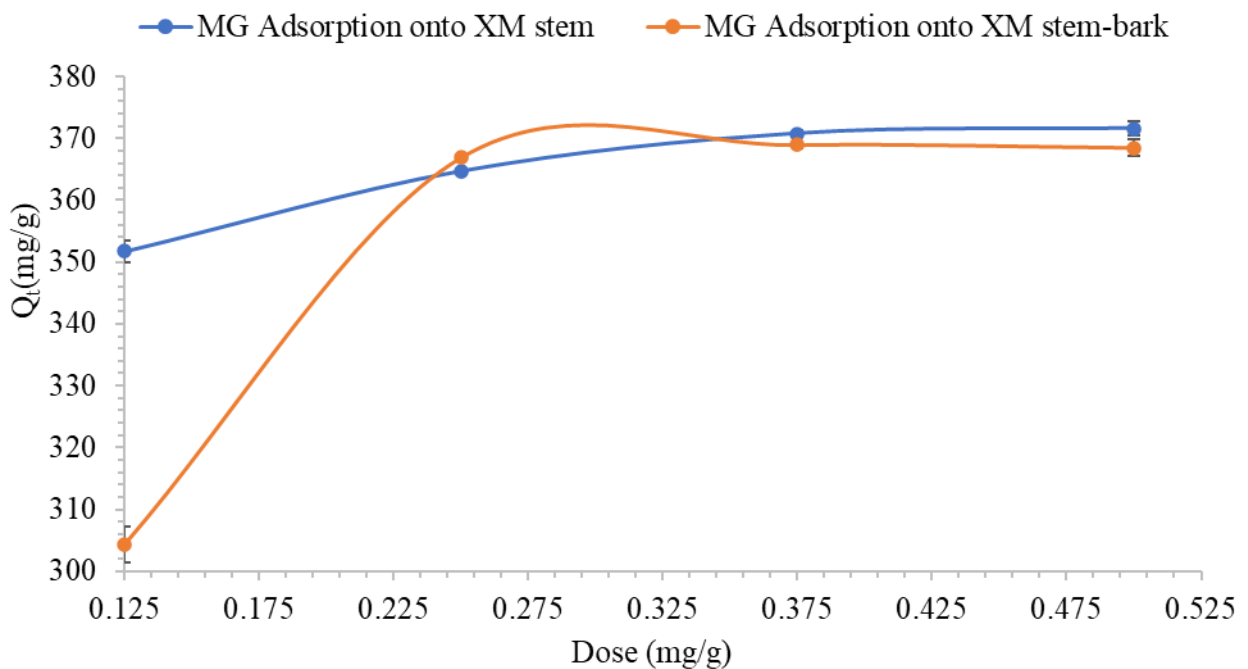
Figure 4.23: Effect of Adsorbent Dose on Adsorption of MG onto *X. moluccensis* stem
and stem-bark.
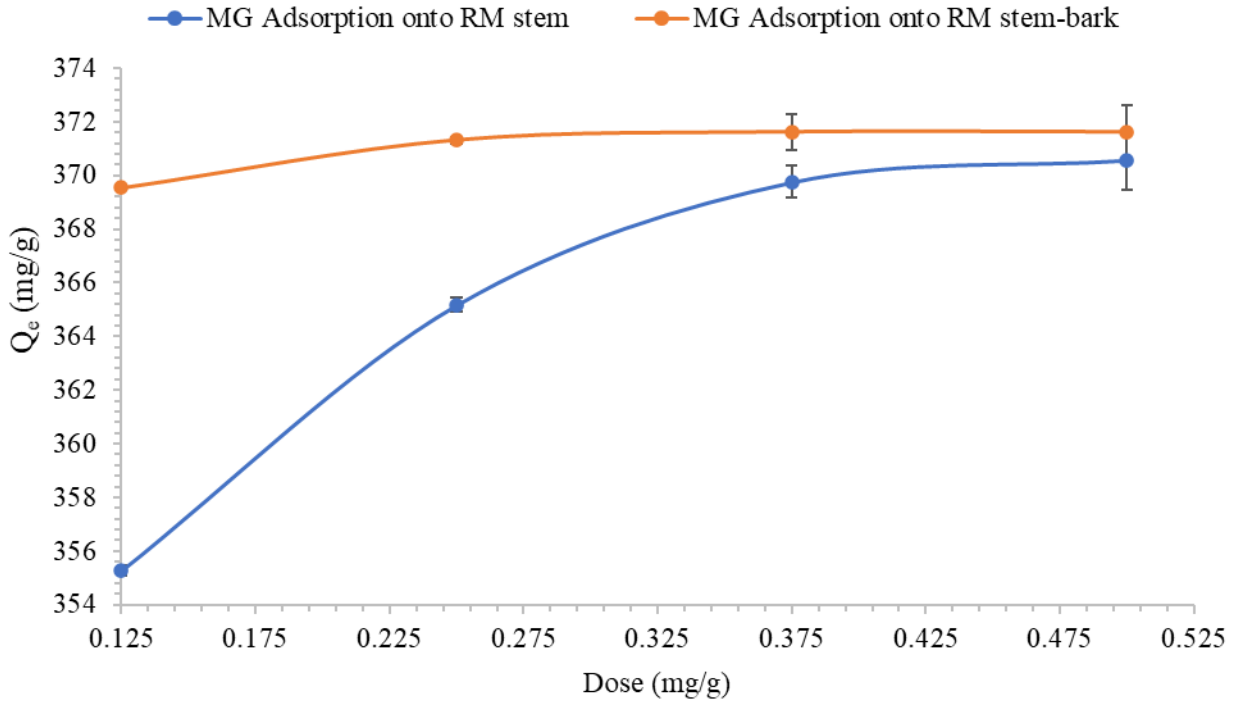
Figure 4.24: Effect of Adsorbent Dose on Adsorption of MG onto *R. mucronata* stem and stem-bark.

As shown in figures 4.23 and 4.24, the stem-bark of the species had greater performance at 371.6 ± 0.01 mg/g compared with the stem at 370.6 ± 0.02 mg/g. Increased adsorbent dose increases the available adsorption sites and at 350 rpm, the overlap of these sites are inhibited and more dye molecules are adsorbed thereby increasing the materials' adsorption capacity (Chowdhury *et al.*, 2013).

4.4.5 Effect of Ionic Strength

Metal cations present in textile industrial effluents generally increase the ionic strength of aqueous mixture as already discussed. Figures 4.25 to 4.26 gives the results obtained from these electrostatic effects on MG dye.
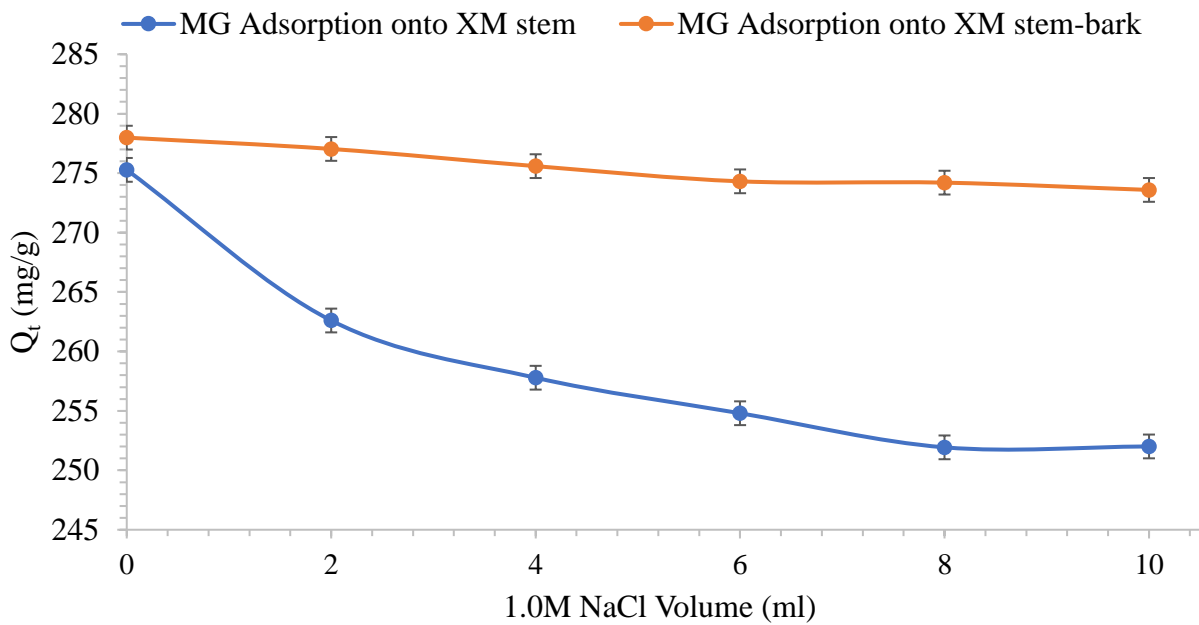
Figure 4.25: Effect of Ionic Strength on Adsorption of MG onto *X. moluccensis* stem and stem-bark.
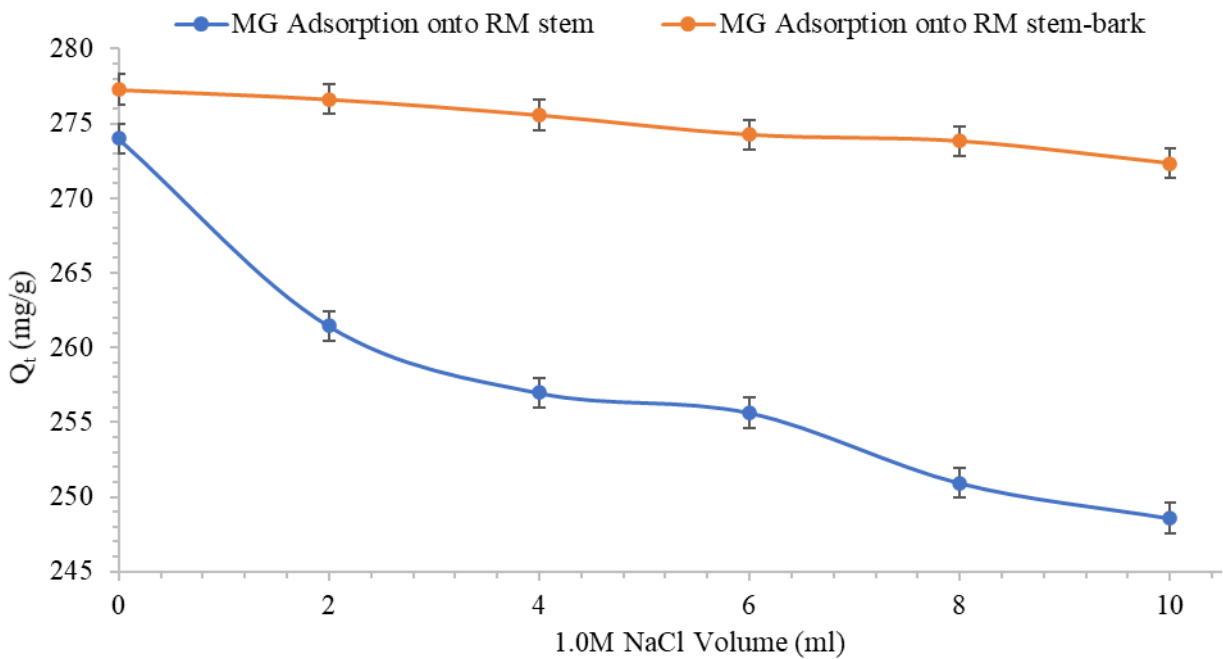
Figure 4.26: Effect of Ionic Strength on Adsorption of MG onto *R. mucronata* stem and stem-bark.

The sorption capacity of MG dye is inversely correlated to ionic strength and the latter was found to have an increased effect of MG dye ($66.9 \pm 0.08\%$ at 10 ml of 1.0M NaCl) compared with CV dye ($93.3 \pm 0.08\%$ at 10 ml of 1.0M NaCl). This can be related to the difference in the molecular structure with CV having two amino groups which have lone pairs of electrons and act as

nucleophilic attractive centres (Eren, *et al.*, 2010). MG dye has only one extra site of this kind hence the disadvantage in comparison to CV dye.

4.4.6 Effect of pH

Figure 4.27 and 4.28 below show the variation in MG dye adsorption with pH of the solution.
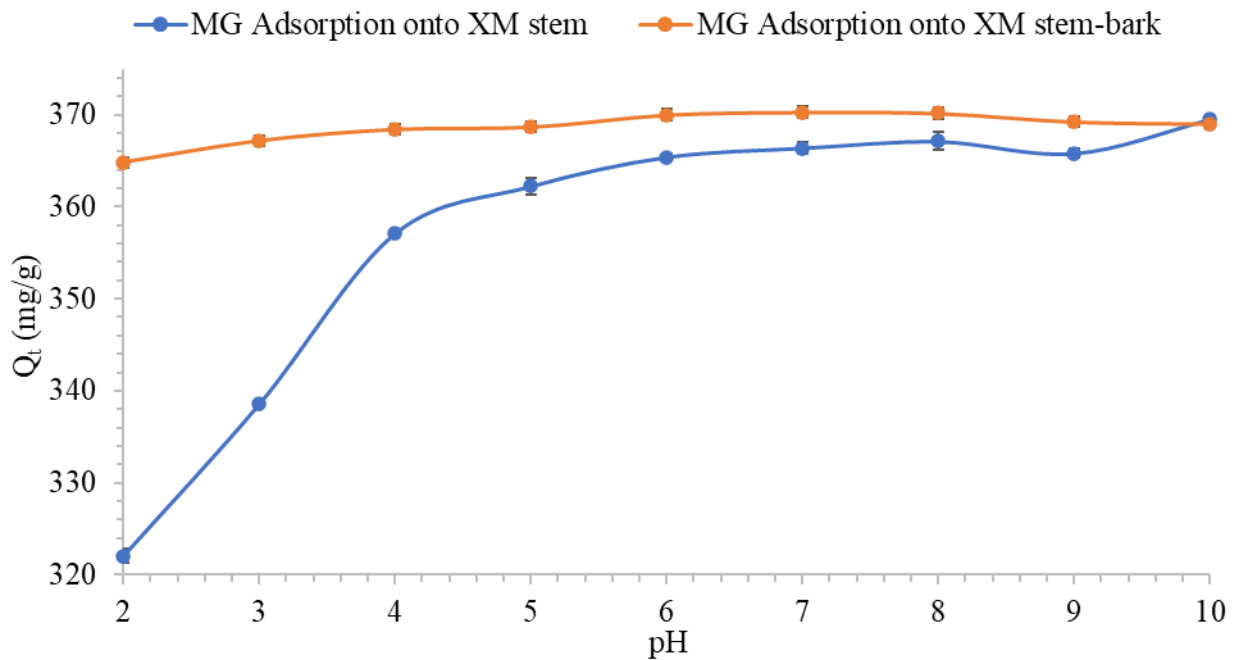
Figure 4.27: Effect of pH on Adsorption of MG onto *X. moluccensis* stem and stem-bark.

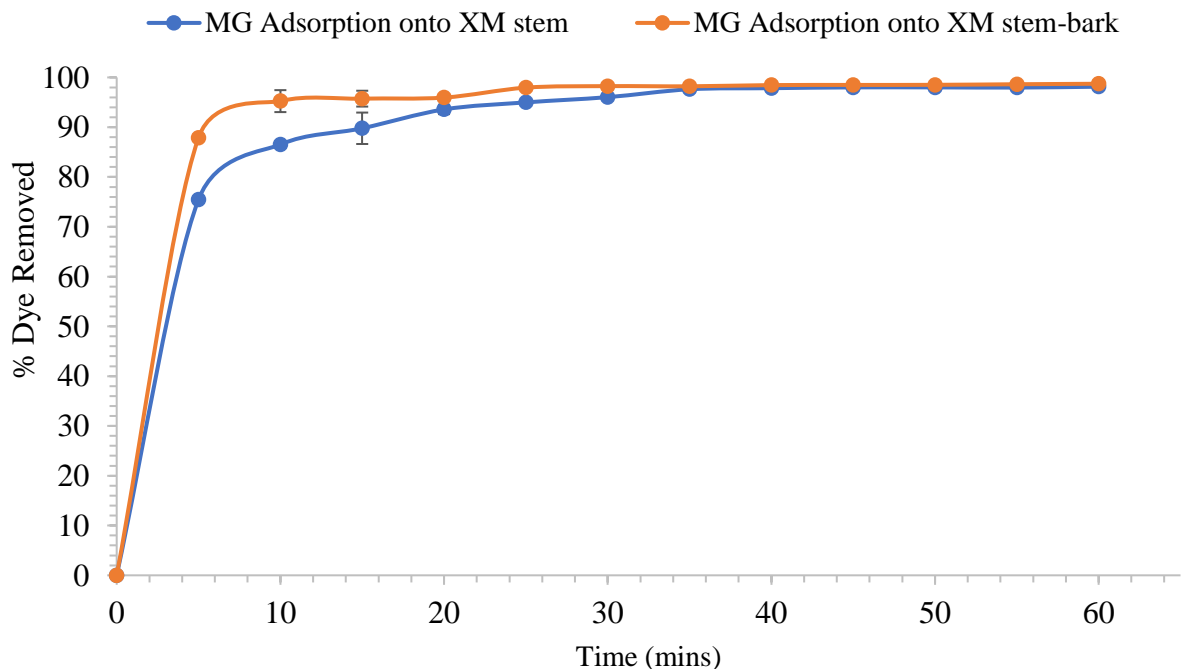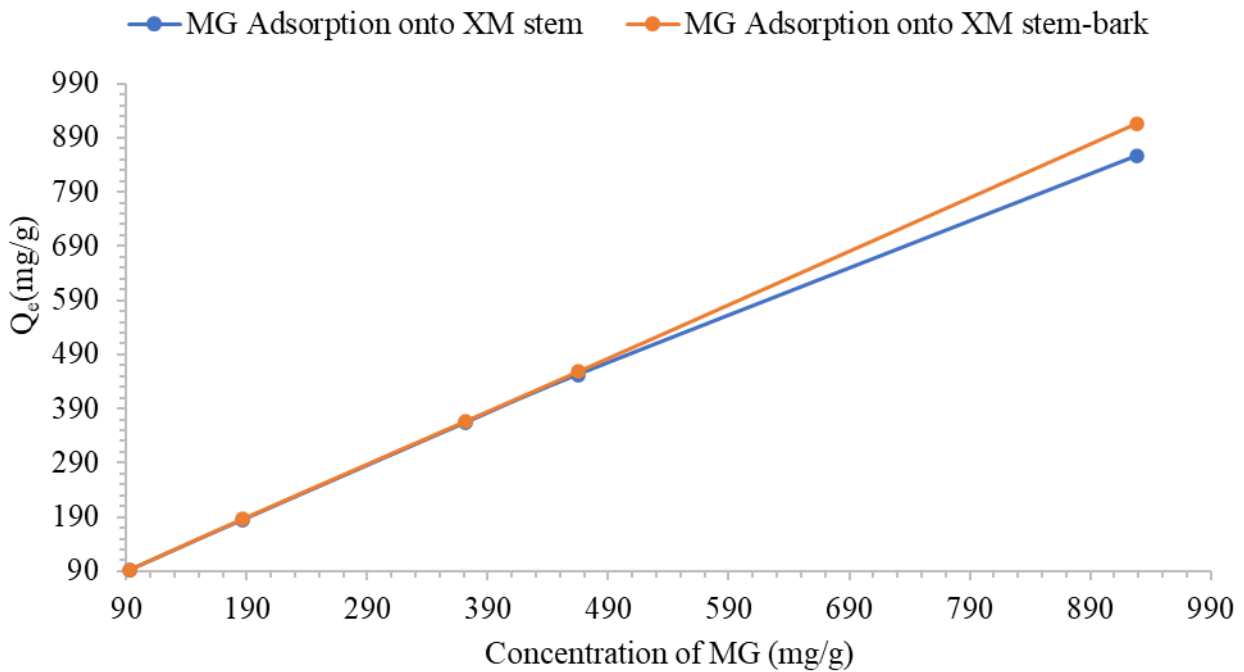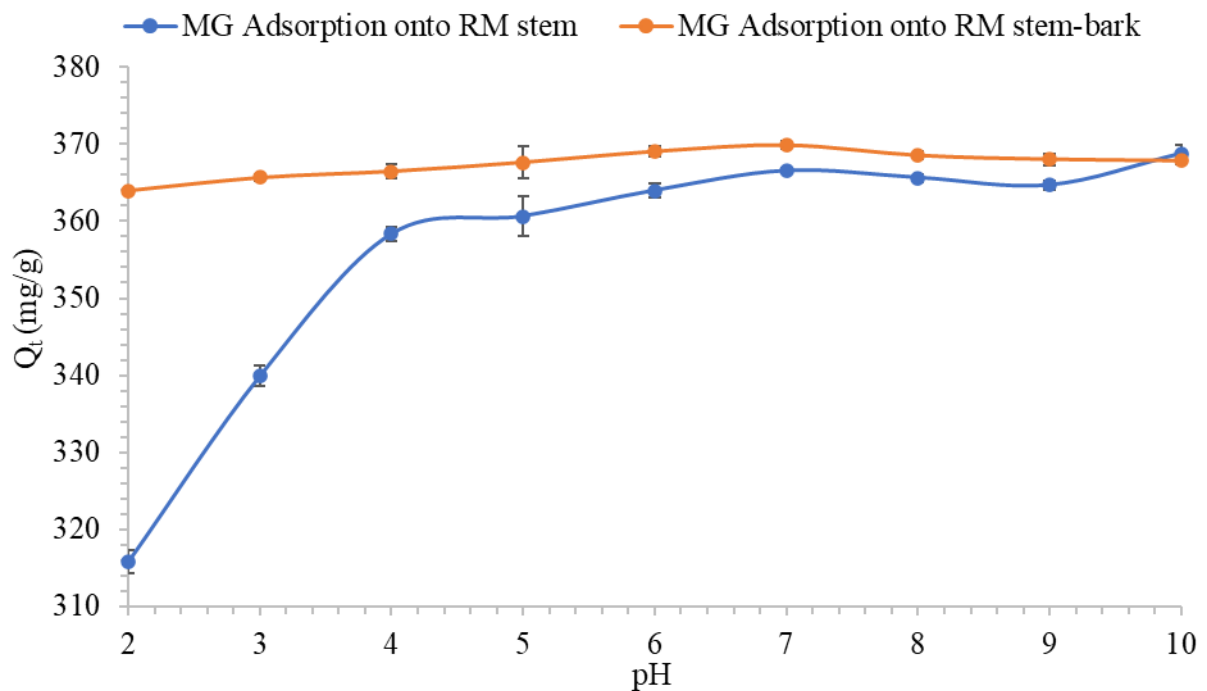Figure 4.28: Effect of pH on Adsorption of MG onto *R. mucronata* stem.

The value of optimum pH was between 6.5 to 8.5 and 6 to 8.5 for CV and MG dyes respectively. The characteristic affinity for bases observed for the two dyes shows that both dyes are cationic and the functional groups may include amino, hydroxyl, sulphonyl and carbonyl groups (Nandi *et al*., 2009). These functional groups become anionic at higher pH due to attractive tendency between the opposite charges on site. After pH 8.5, the observed colour change was negligible (Baek *et al*., 2010). These observations indicate protonation of CV and MG in acidic medium. At molecular level and as the pH range (pH< 6) rises, de-protonation of the dyes occurs and a positively charged surface which hinders effective adsorption of dye particles (Hameed & El-Khaiary, 2008).

4.5 Adsorption Equilibrium

The equilibrium characteristics of a given adsorption process can be evaluated using various isotherms including; Langmuir, Freundlich, Sips and Reddich-Peterson isotherms. These give equilibration curves which help optimise the design of the sorption process. To predict the sorption characteristics at equilibrium of these cationic, this study looked at the applications of Langmuir and Freundlich isotherms model to investigate the equilibrium characteristics of the adsorption process.

4.5.1 Langmuir Isotherm on CV and MG Adsorption

Equilibrium adsorption data for various initial CV concentrations was modelled using the Langmuir isotherm to determine whether the adsorption process occurs through monolayer covering of the adsorbent surface. The Langmuir Isotherm model (equation 1) is a linear plot of $\frac{c_e}{q_m}$ verses C_e with the slope giving q_m (mg/g) and intercept giving K_L. For adsorption process to follow the Langmuir model the regression coefficient R^2, must closely approach 1. Figure 4.29 to 4.36 below show the Langmuir Isotherm for CV and MG adsorption onto *X. moluccensis* and *R. mucronata* stem and stem-bark.
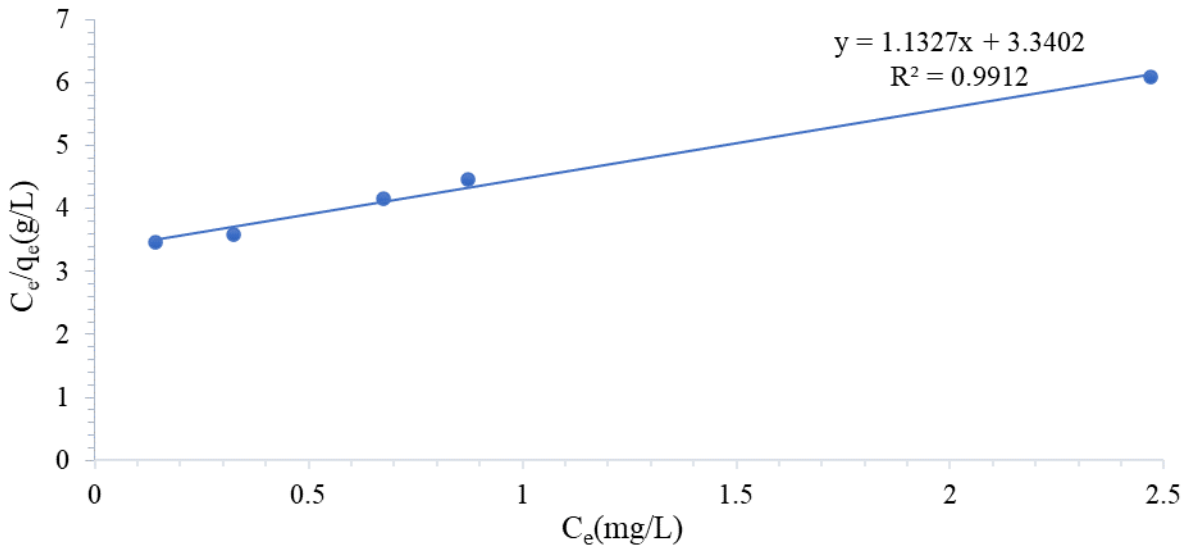
Figure 4.29: Langmuir Isotherm for CV Adsorption onto *X. moluccensis* stem-bark.
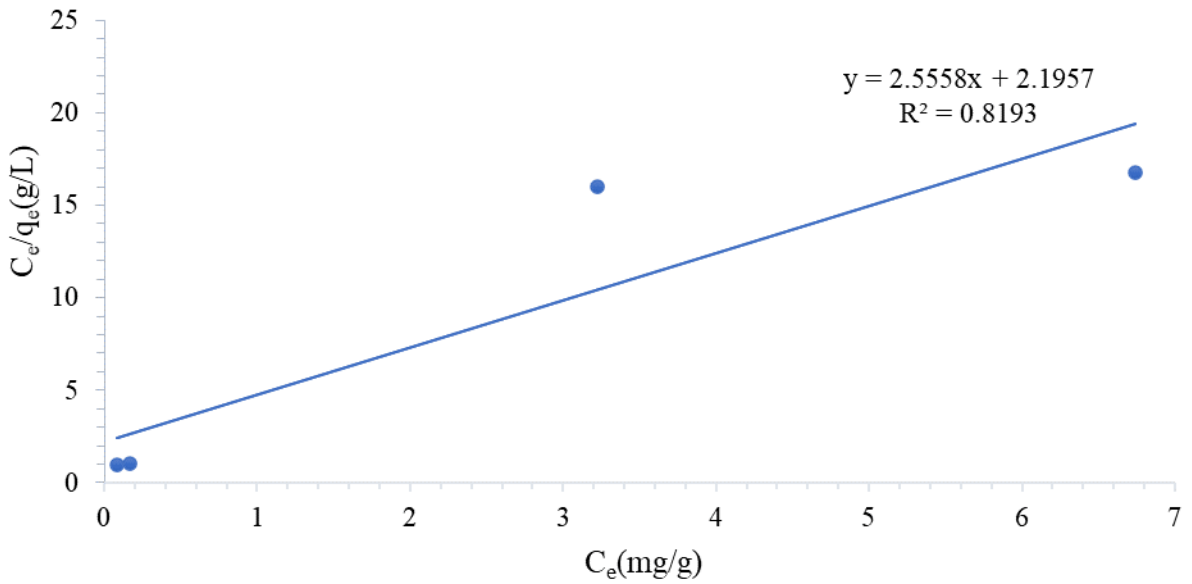
Figure 4.30: Langmuir Isotherm for CV Adsorption onto *X. moluccensis* stem.
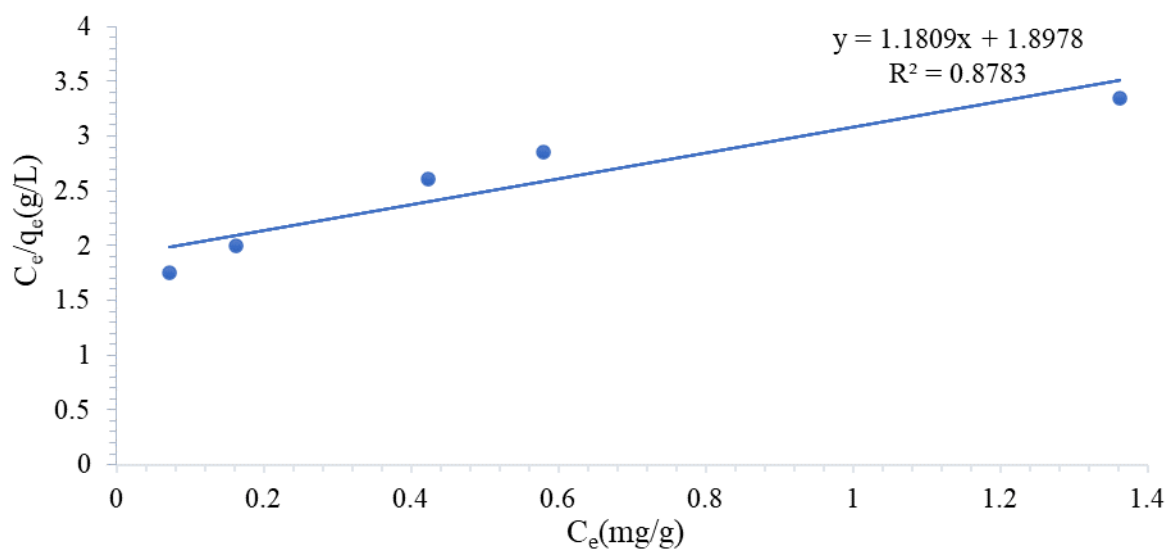
Figure 4.31: Langmuir Isotherm for CV Adsorption onto *R. mucronata* stem-bark.
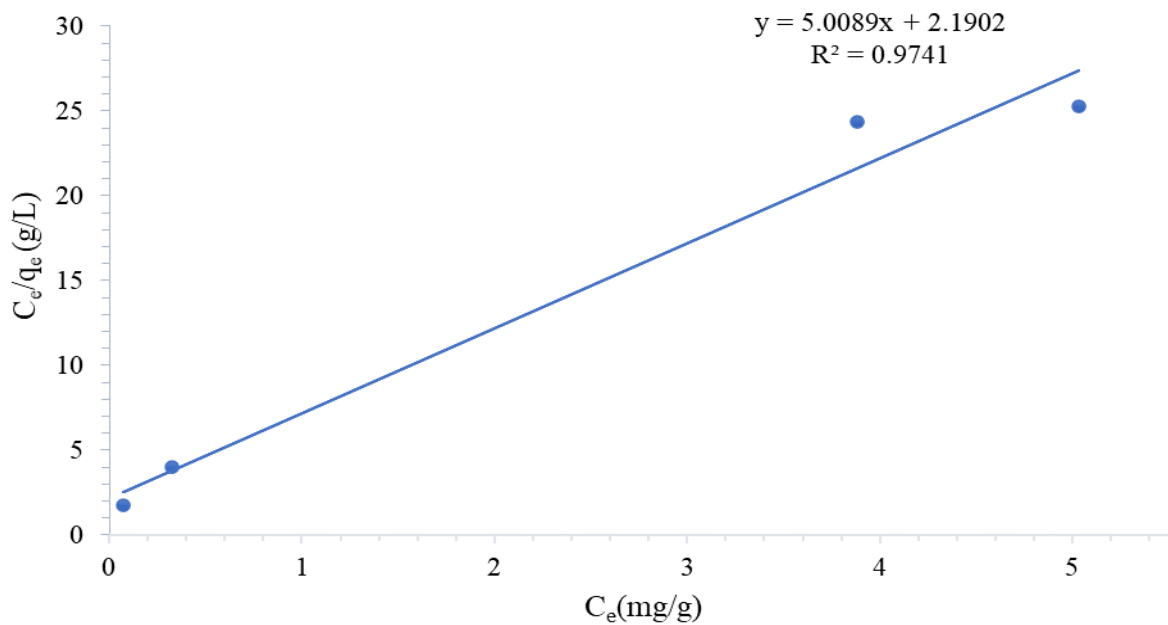
Figure 4.32: Langmuir Isotherm for CV Adsorption onto *R. mucronata* stem.
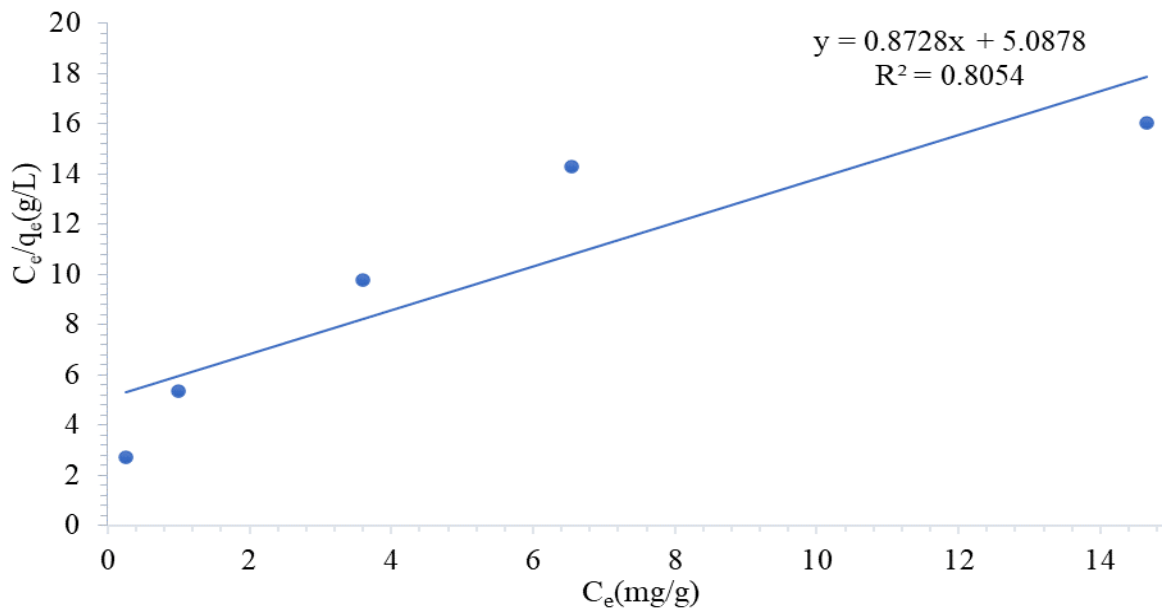
Figure 4.33: Langmuir Isotherm for MG Adsorption onto *X. moluccensis* stem-bark.
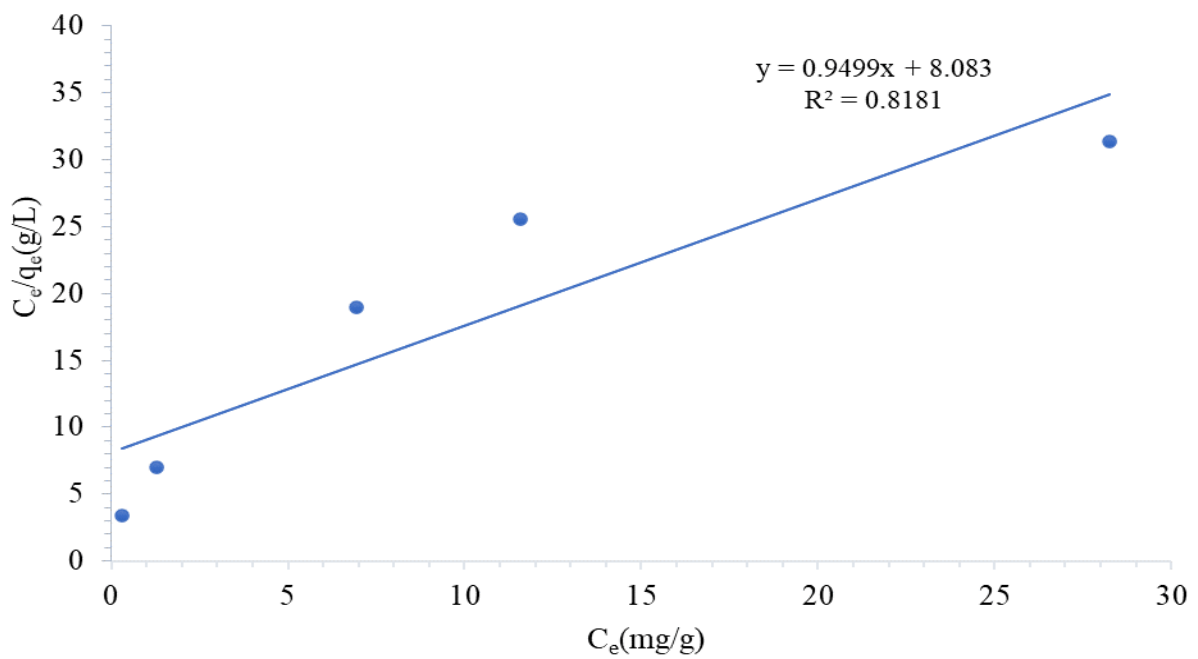
Figure 4.34: Langmuir Isotherm for MG Adsorption onto *X. moluccensis* stem.

$$y = 1.6652x + 0.5547$$
$$R^2 = 0.9945$$
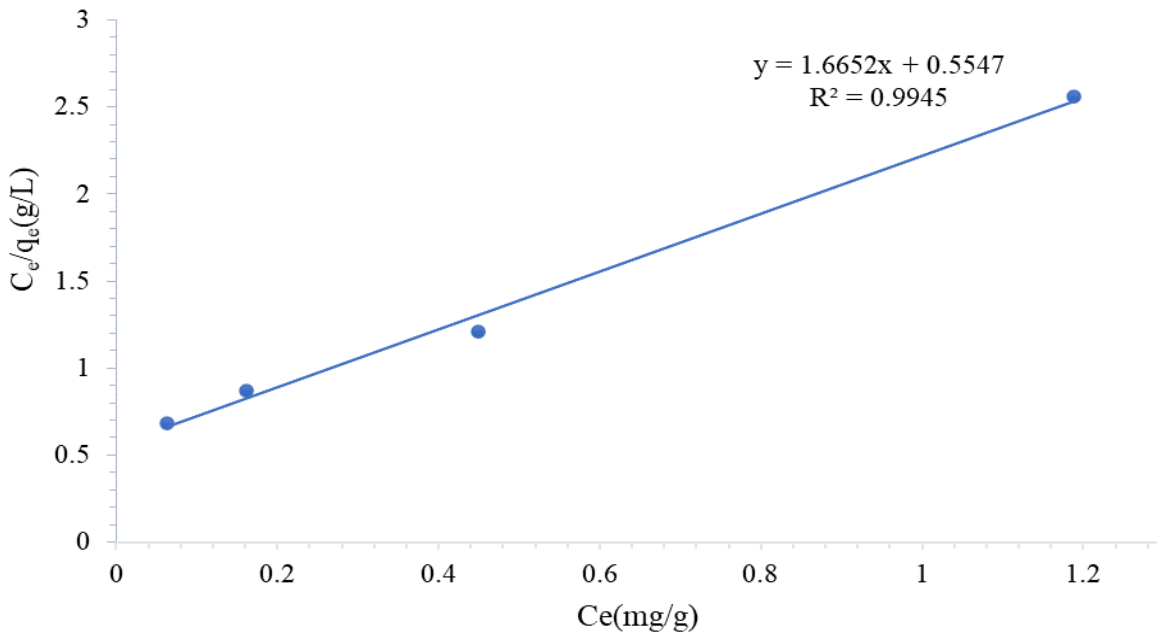
Figure 4.35: Langmuir Isotherm for MG Adsorption onto *R. mucronata* stem-bark.

$$y = 1.88x + 3.1727$$
$$R^2 = 0.9765$$
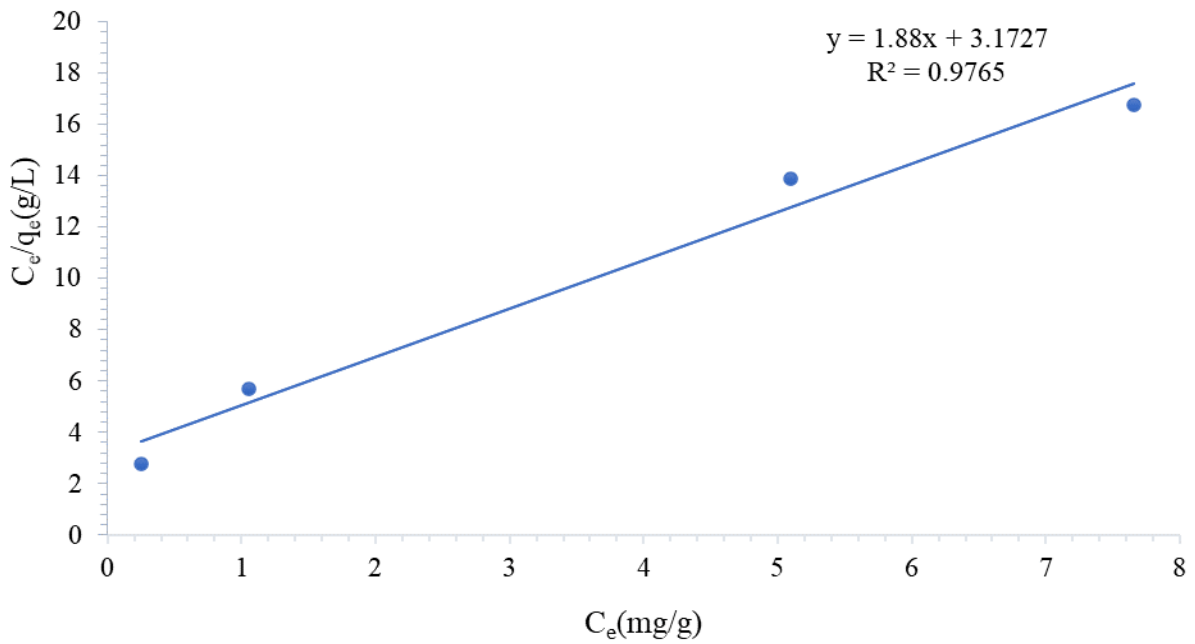
Figure 4.36: Langmuir Isotherm for MG Adsorption onto *R. mucronata* stem.

The results of Langmuir' plots are shown in the Table 4.1;

Table 4.1: Langmuir Isotherm Parameters for CV and MG dyes.

| Adsorbent | Langmuir Isotherm | | | | | | | |
| | CV Dye | | | | MG Dye | | | |
	q_m (mg/g)	K_L	R^2	R_L	q_m (mg/g)	K_L	R^2	R_L
R. mucronata stem-bark	1.1809	1.8978	0.8783	0.4462	1.6652	0.5547	0.9945	1.0826
R. mucronata stem	5.0089	2.1902	0.9741	0.0912	1.8800	3.1727	0.9765	0.1677
X. moluccensis stem-bark	1.1327	3.3402	0.9912	0.2643	0.8728	5.0878	0.8054	0.2252
X. moluccensis stem	2.5558	2.1957	0.8193	0.1782	0.9499	8.0830	0.8181	0.1302

The correlation coefficient, R^2, values determines the isotherm model best fitting the equilibrium data. The R^2 values for the adsorption of CV dye onto *R. mucronata* stem and stem-bark are 0.9741 and 0.8783 respectively; 0.9912 and 0.8193 for *X. moluccensis* respective stem and stem-bark. The R^2 values for the adsorption of MG dye onto *R. mucronata* stem and stem-bark are 0.9765 and 0.9945 respectively; 0.8181 and 0.8054 for *X. moluccensis* respective stem and stem-bark. The data R^2 values are all significantly large ($R^2 \geq 0.8054$) thus the adsorption of CV and MG dyes follows the Langmuir isotherm model. For the dimensionless parameter R_L, the adsorption of CV dye is favoured by both stem and stem-bark for the two species with R_L values of 0.0912 and 0.4462 for *R. mucronata* stem and stem-bark respectively, 0.1782 and 0.2643 for *X. moluccensis* stem and stem-bark respectively. This evidence is supported by reasonable Q_{max} (mg/g), values which are 5.0089 and 1.1809 for CV dye onto *R. mucronata* stem and stem-bark respectively, 2.5558 and 1.1327 for CV dye onto *X. moluccensis* stem and stem-bark respectively, 1.8800 and 1.6652 for MG dye onto *R. mucronata* stem and stem-bark respectively, and finally 0.9499 and 0.8728 for MG dye onto *X. moluccensis* stem and stem-bark respectively. In addition, as observed in Table 4.1; the significantly good Langmuir energy constant K_L values suggests that both the adsorption of CV dye and MG dye onto the stem and stem-bark parts of the species are favoured under the described conditions with the sorption of MG dye giving better

values of K_L as 0.5547 and 3.1727 for *R. mucronata* stem and stem-bark respectively; 8.0830 and 5.0878 for *X. moluccensis* stem and stem-bark, respectively. This observation can be attributed to the variation of molecular structure of the two dyes with CV dye having an extra amine centre (Figure 2.6) compared to that of MG dye (Figure 2.7) which could have dictated the adsorption properties noted.

4.5.2 Freundlich Isotherm on CV and MG Adsorption

A plot of $log_{10}q_e$ against $log_{10}C_e$ is linear with K_f and η obtained from the intercepts and the slope respectively as given in equation 4. The plots in Figures 4.37 to 4.44 illustrates the linear form of Freundlich isotherm model.
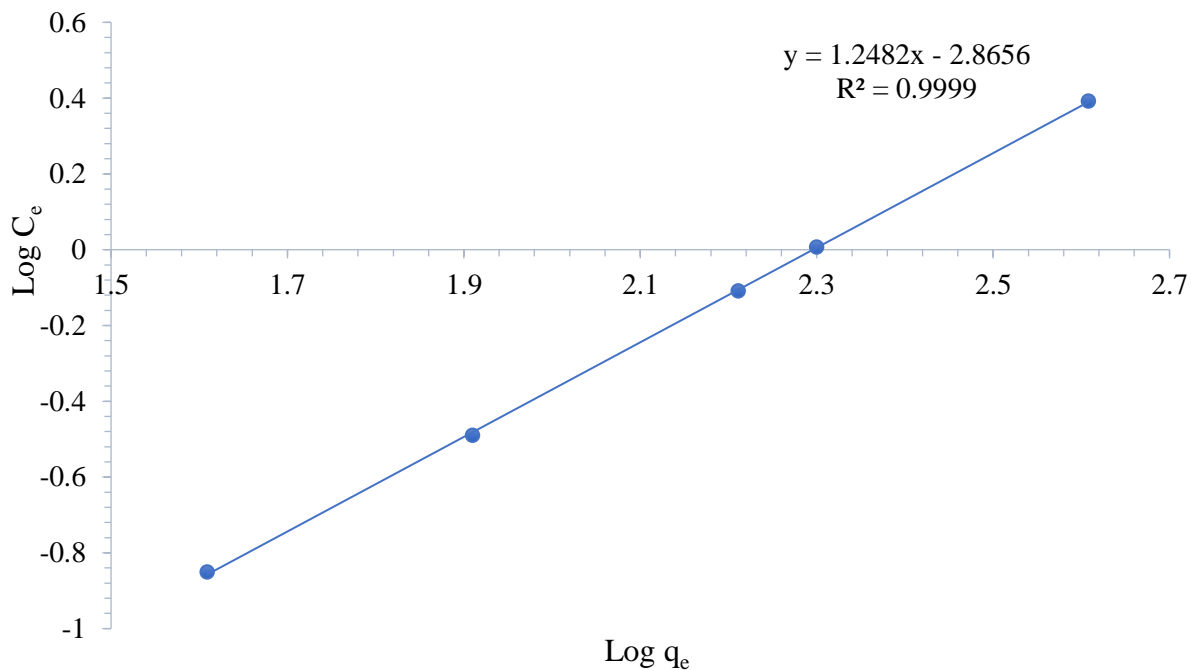
Figure 4.37: Freundlich Isotherm for CV adsorption onto *X. moluccensis* stem-bark.
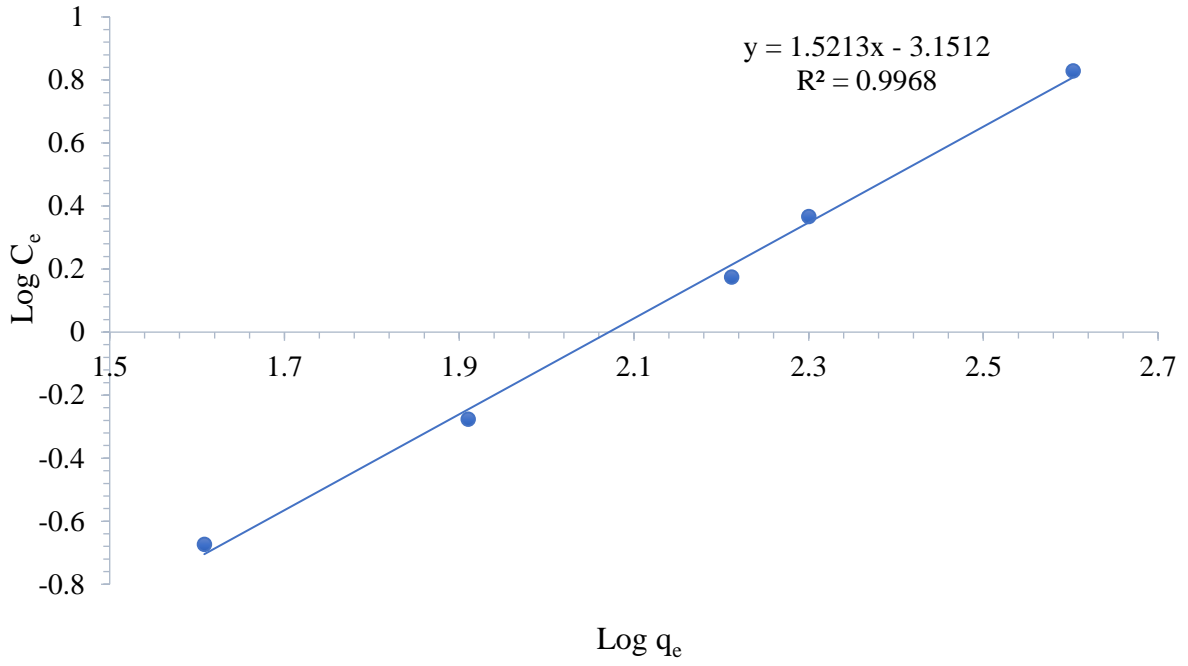
Figure 4.38: Freundlich Isotherm for CV adsorption onto *X. moluccensis* stem.
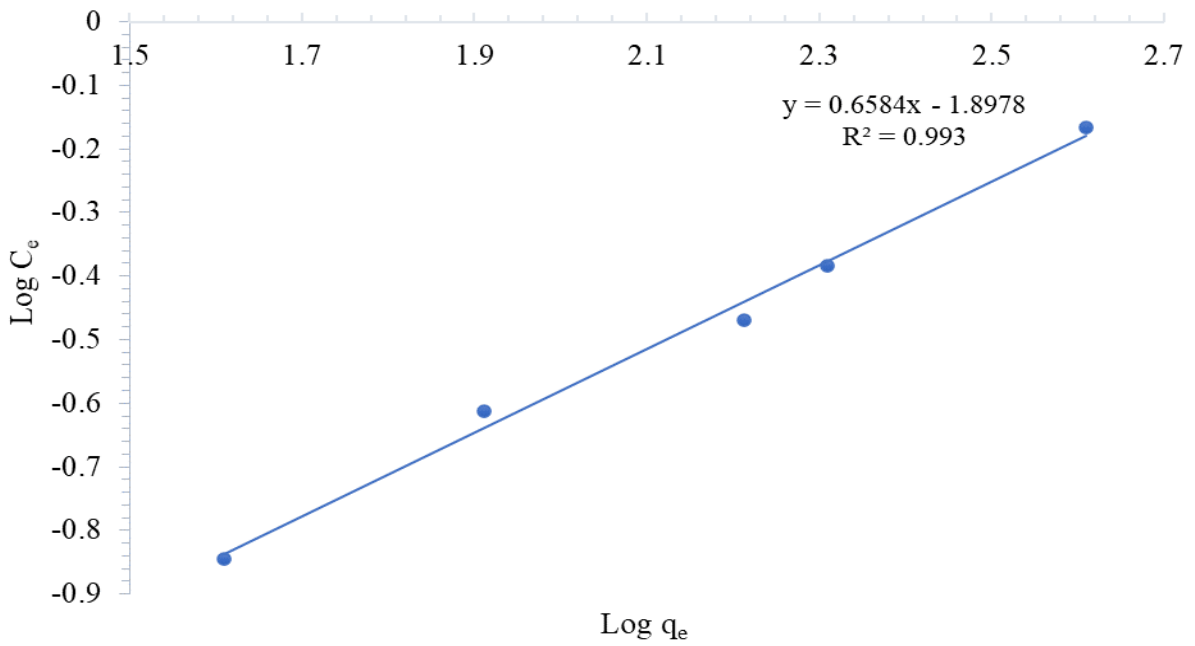
Figure 4.39: Freundlich Isotherm for CV adsorption onto *R. mucronata stem*-bark.
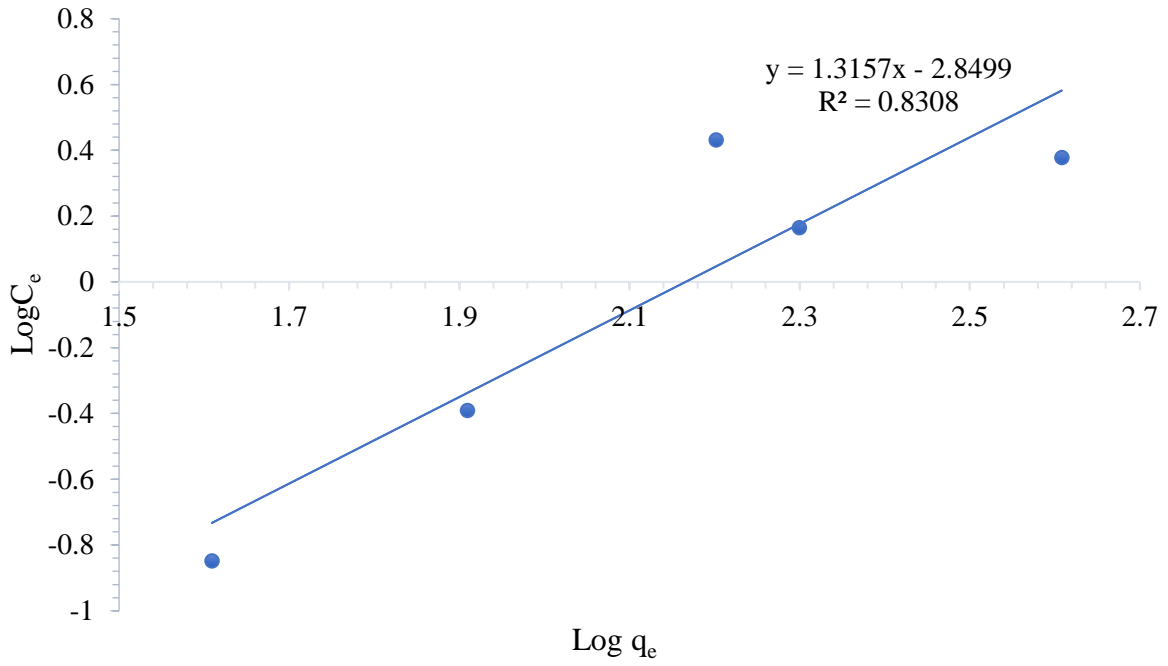
Figure 4.40: Freundlich Isotherm for CV adsorption onto *R. mucronata* stem.
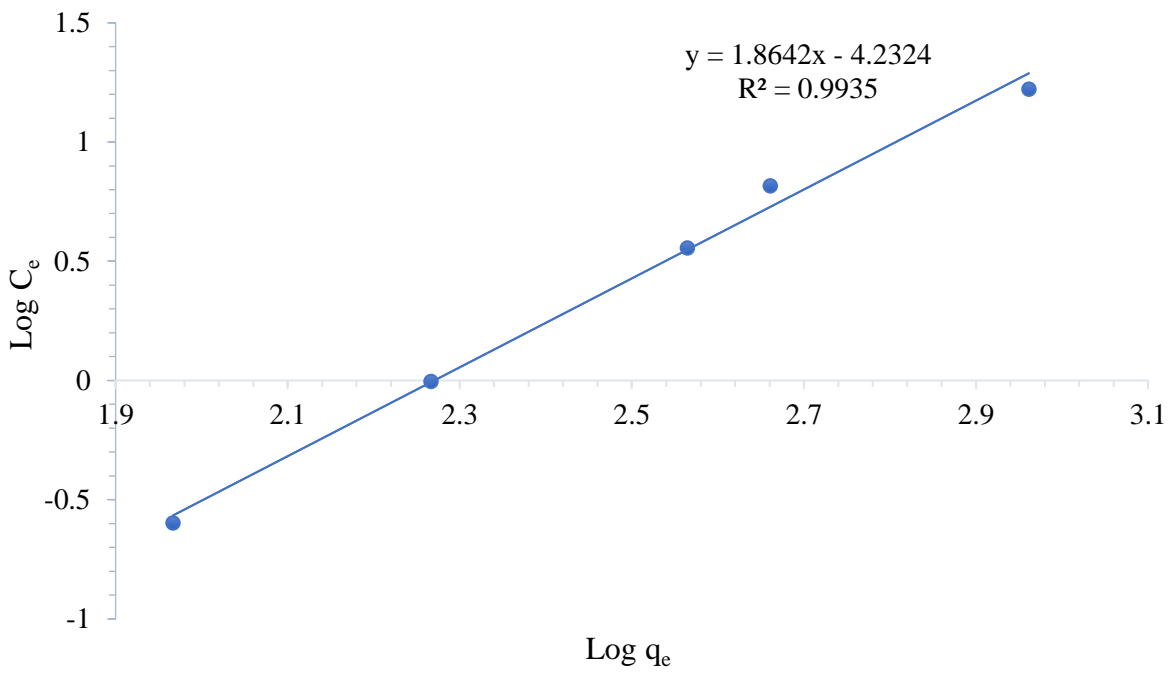
Figure 4.41: Freundlich Isotherm for MG adsorption onto *X. moluccensis* stem-bark.
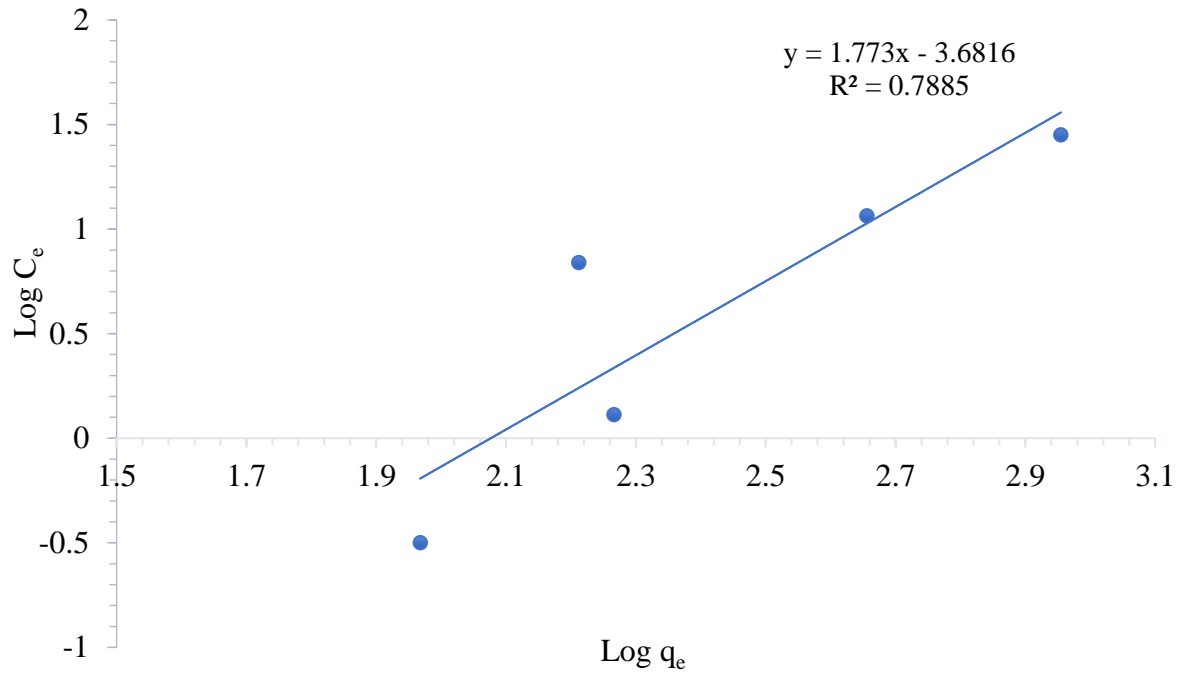
Figure 4.42: Freundlich Isotherm for MG adsorption onto *X. moluccensis* stem.
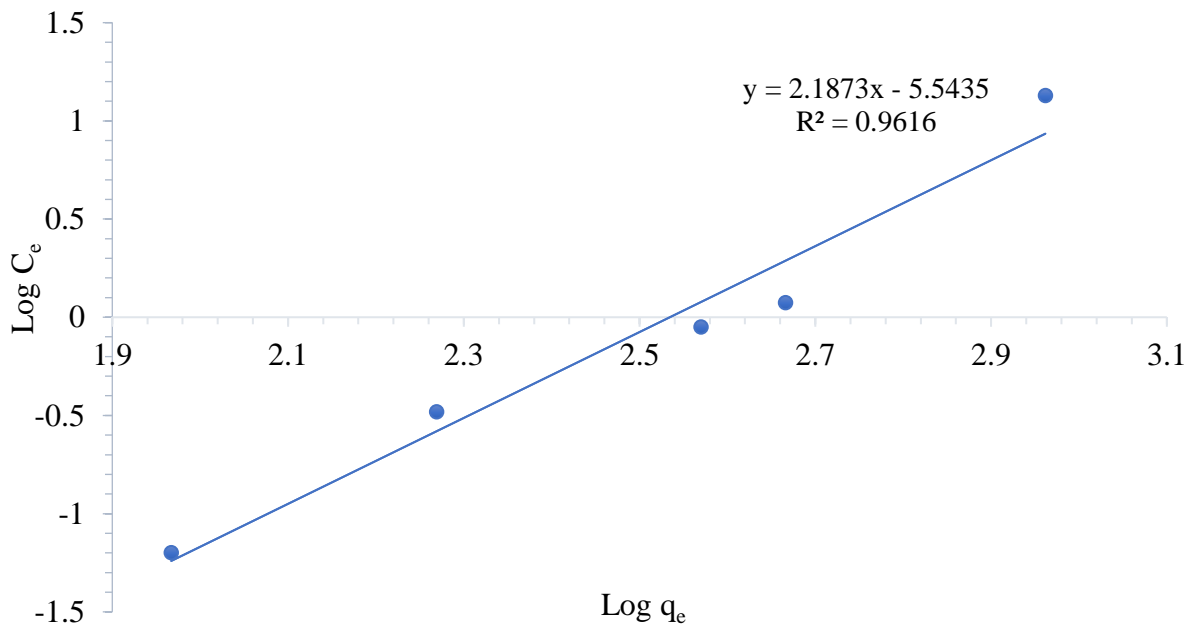
Figure 4.43: Freundlich Isotherm for MG adsorption onto *R. mucronata* stem-bark.
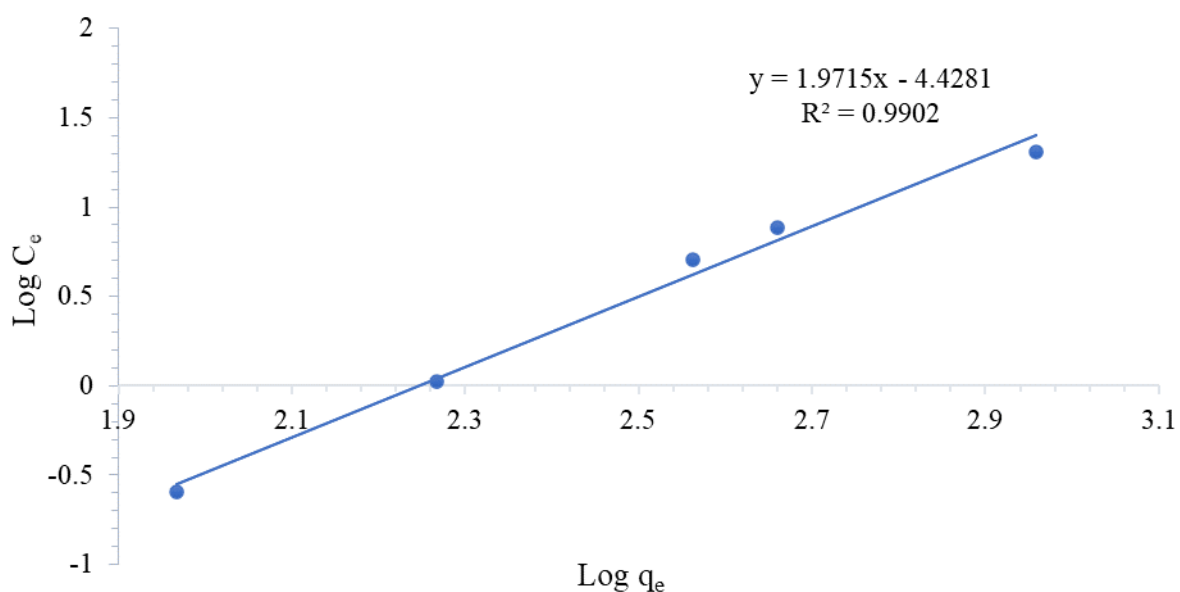
Figure 4.44: Freundlich Isotherm for MG adsorption onto *R. mucronata* stem.

Table 4.2 summarises the Freundlich isotherm parameters.

Table 4.2: Freundlich Isotherm Parameters for CV and MG dyes.

Adsorbent	CV Dye			MG Dye		
	K_f (mg/g)	n (g/L)	R^2	K_f (mg/g)	n (g/L)	R^2
R. mucronata stem-bark	0.6584	-0.5269	0.9930	2.1873	-0.1804	0.9616
R. mucronata stem	1.3157	-0.3508	0.8308	1.9715	-0.2258	0.9902
X. moluccensis stem-bark	1.2482	-0.3490	0.9999	1.8642	-0.2363	0.9935
X. moluccensis stem	1.5213	-0.3173	0.9968	1.7730	-0.2716	0.7885

The Freundlich constant , K_f, gives the extent of adsorption and the intensity factor, n , gives an estimate of the adsorption intensity while R^2 indicates whether the adsorption process positively fits the model (Mittal *et al*., 2007). Despite higher R^2 values indicating a favourable adsorption process, the data reported gives very low K_f Values in the range of 1.5213; hence Freundlich Isotherm model and its assumptions does not significantly influence the process. The negative values of the intensity coefficient n show an inverse relationship between Q_e and the nth root of C_e as defined in equation (3).

4.6 Kinetics for Crystal Violet Adsorption

4.6.1 Pseudo-First Order Kinetics on CV and MG Adsorption

Appendix A and B gives the raw data used to work out the equilibrium kinetics of the adsorption process. The pseudo-first order kinetics (equation 5, page 15) was modelled for CV and MG adsorption onto aerial parts of the two species and the results were as illustrated in figure 4.45 to 4.52.
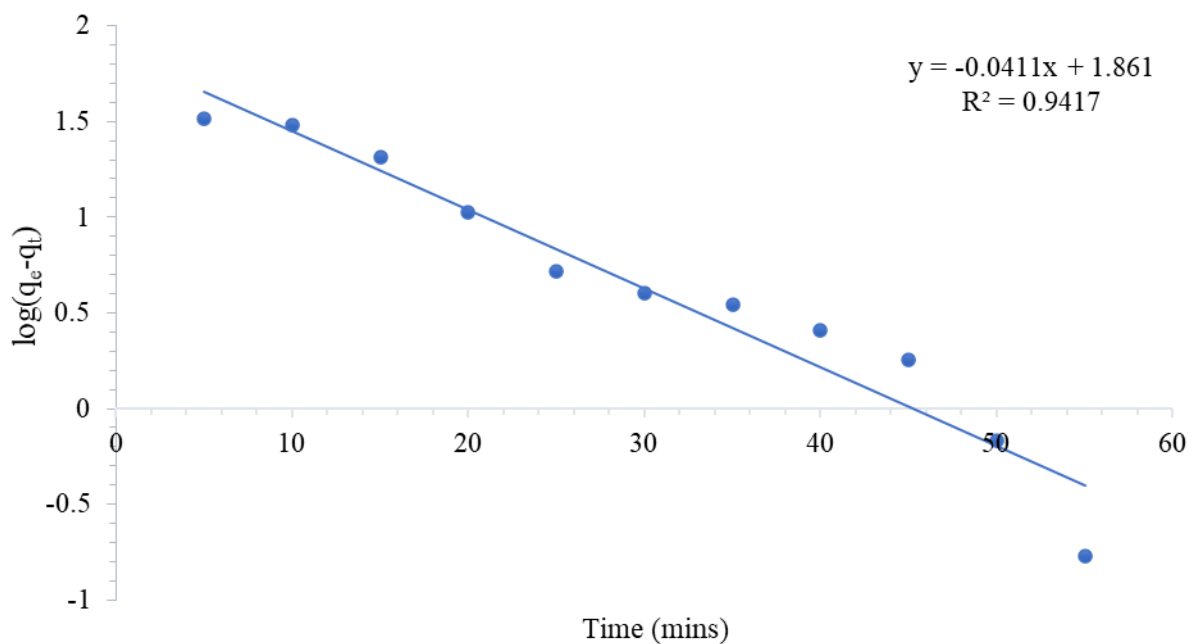
Figure 4.45: Pseudo-First Order Kinetics for CV adsorption onto *X. moluccensis* stem-bark.
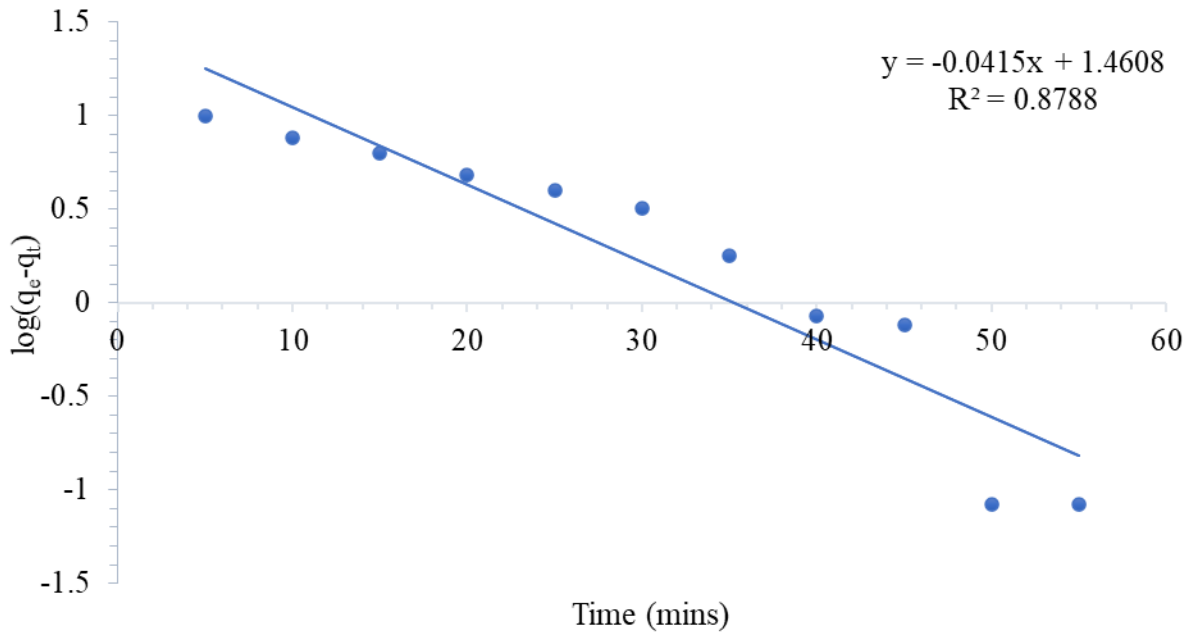
Figure 4.46: Pseudo-First Order Kinetics for CV adsorption onto *X. moluccensis* stem.
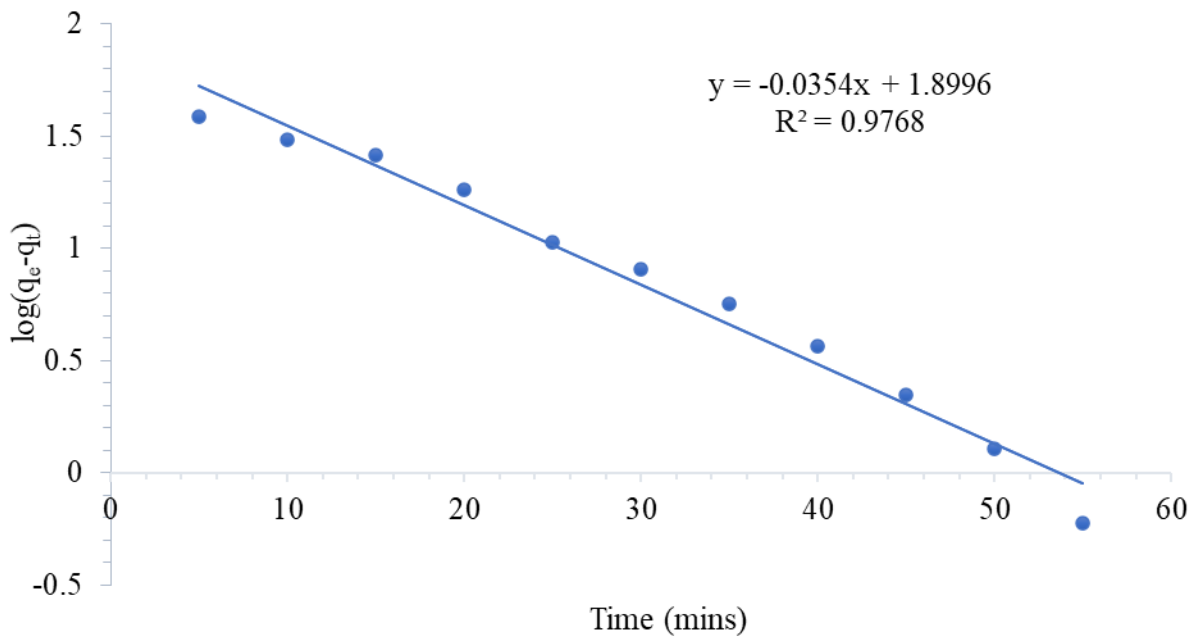
Figure 4.47: Pseudo-First Order Kinetics for CV adsorption onto *R. mucronata* stem-bark.
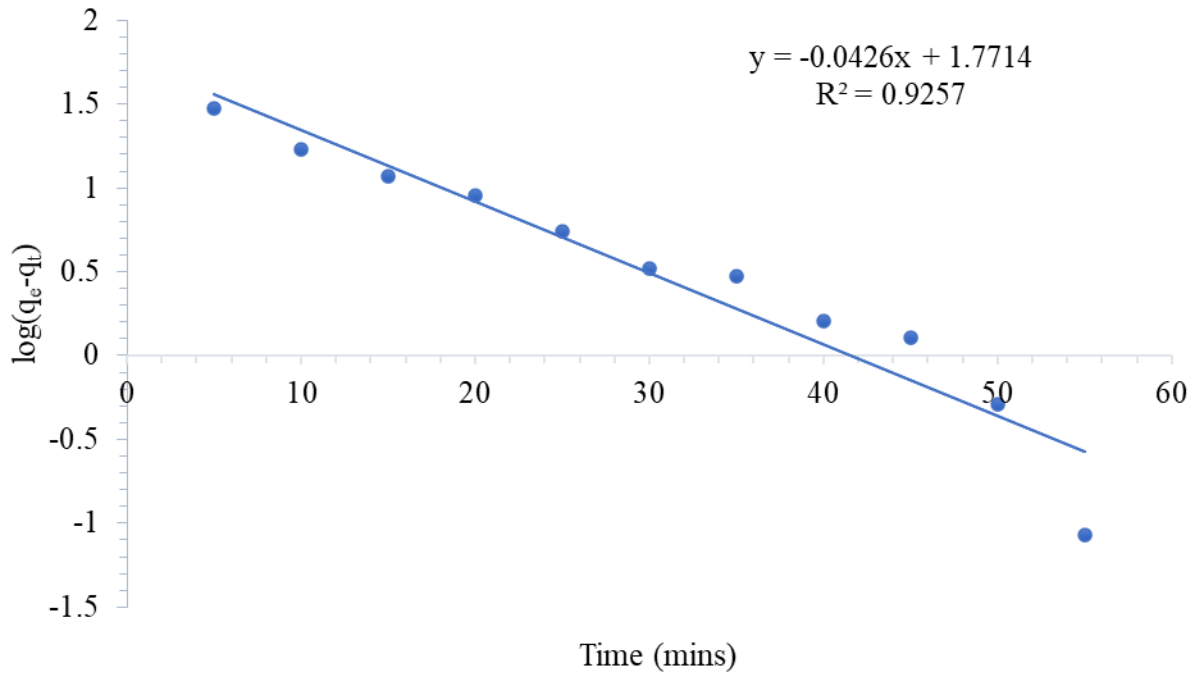
Figure 4.48: Pseudo-First Order Kinetics for CV adsorption onto *R. mucronata* stem.
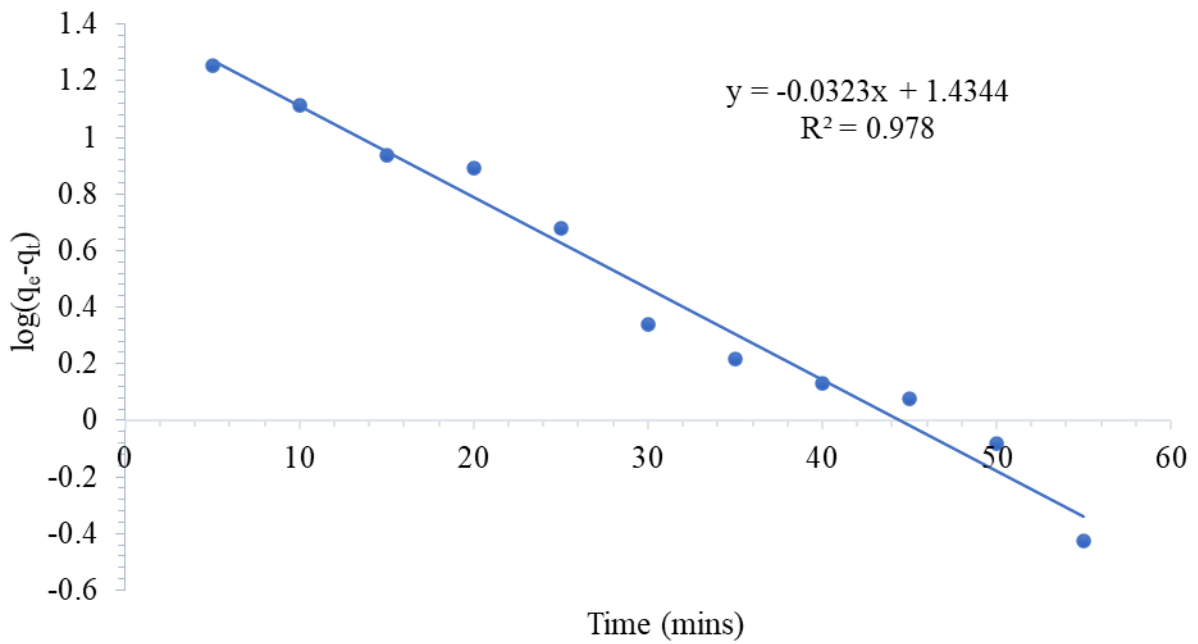
Figure 4.49: Pseudo-First Order Kinetics for MG adsorption onto *X. moluccensis* stem-bark.
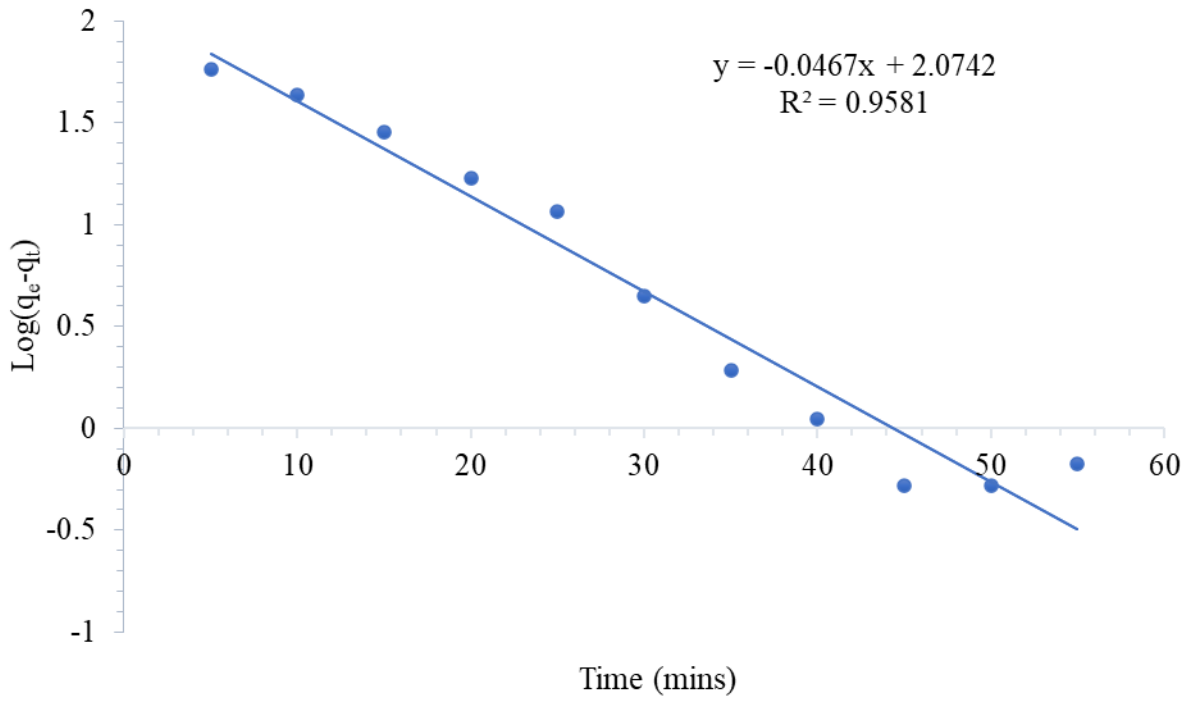
Figure 4.50: Pseudo-First Order Kinetics for MG adsorption onto *X. moluccensis* stem.
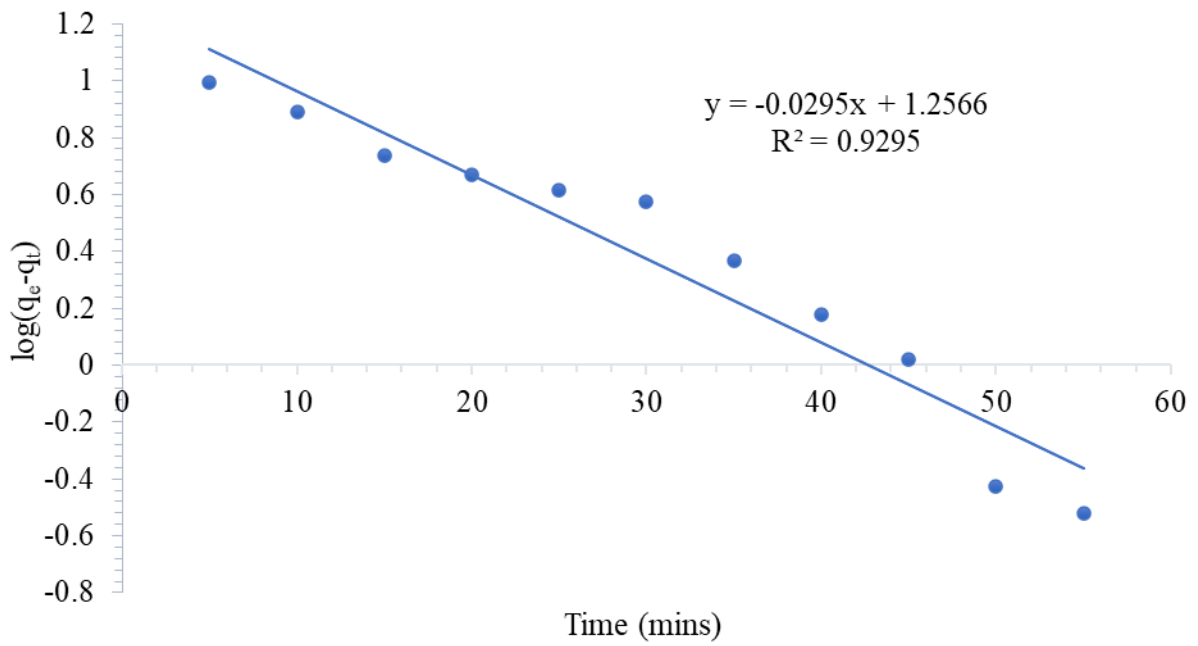
Figure 4.51: Pseudo-First Order Kinetics for MG adsorption onto *R. mucronata* stem-bark.
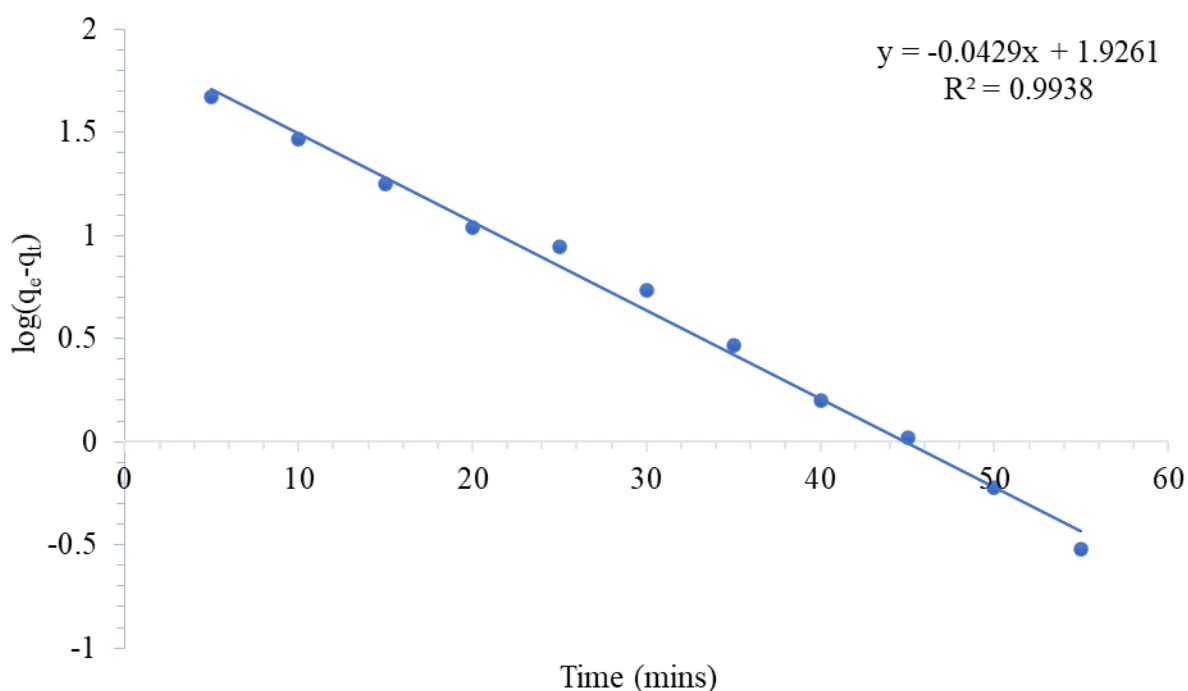
Figure 4.52: Pseudo-First Order Kinetics for MG adsorption onto *R. mucronata* stem.

The results are as summarised in tables 4.3 and 4.4.

Table 4.3: Pseudo-First Order Kinetics Parameters for CV dye Adsorption.

CV Dye Adsorption				
Adsorbent	**Parameters**			
	$q_{e,exp}$ **(mg/g)**	$q_{e,cal}$ **(mg/g)**	K_1 **(min^{-1})**	R^2
X. moluccensis **stem-bark**	405.5100	478.1206	0.0947	0.9417
X. moluccensis **stem**	401.0820	429.9755	0.0956	0.8788
R. mucronata **stem-bark**	407.2990	486.6587	0.0815	0.9768
R. mucronata **stem**	405.594	464.6685	0.0981	0.9257

Table 4.4: Pseudo-First Order Kinetics Parameters for MG dye Adsorption.

MG Dye Adsorption				
Adsorbent	**Parameters**			
	$q_{e,exp}$ **(mg/g)**	$q_{e,cal}$ **(mg/g)**	K_1 **(min^{-1})**	R^2
X. *moluccensis* **stem-bark**	366.8910	394.0804	0.0744	0.9780
X. moluccensis **stem**	364.6880	483.3229	0.1076	0.9581
R. mucronata **stem-bark**	371.3120	389.3671	0.0679	0.9295
R. mucronata **stem**	365.1690	449.5219	0.0988	0.9938

As shown in tables 4.3 and 4.4, the experimental equilibrium adsorption capacity, q_e,exp (mg/g) values differ by a large margin to the calculated equilibrium adsorption capacity, q_e,cal (mg/g) values and the pseudo-first order adsorption rate constant K_l (min^{-1}), values are very low. Hence the adsorption of CV and MG dyes sorption onto the species stem and stem-bark generally does not infinitely follows Pseudo-First Order kinetics.

4.6.2 Pseudo-Second Order Kinetics on CV and MG Adsorption

The pseudo-second order kinetics (equation 6, page 15) was also tested for CV and MG adsorption onto stem and stem-bark of the two species as presented in figures 4.53 to 4.60.
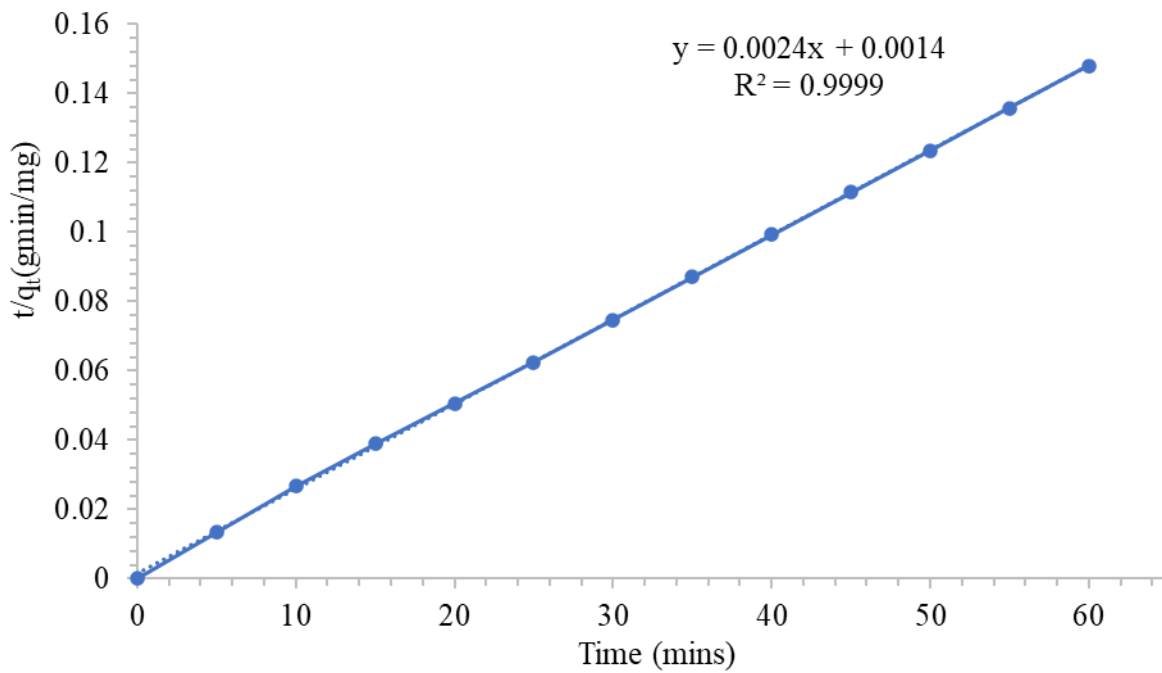
Figure 4.53: Pseudo-Second Order Kinetics for CV adsorption onto *X. moluccensis* stem-bark.
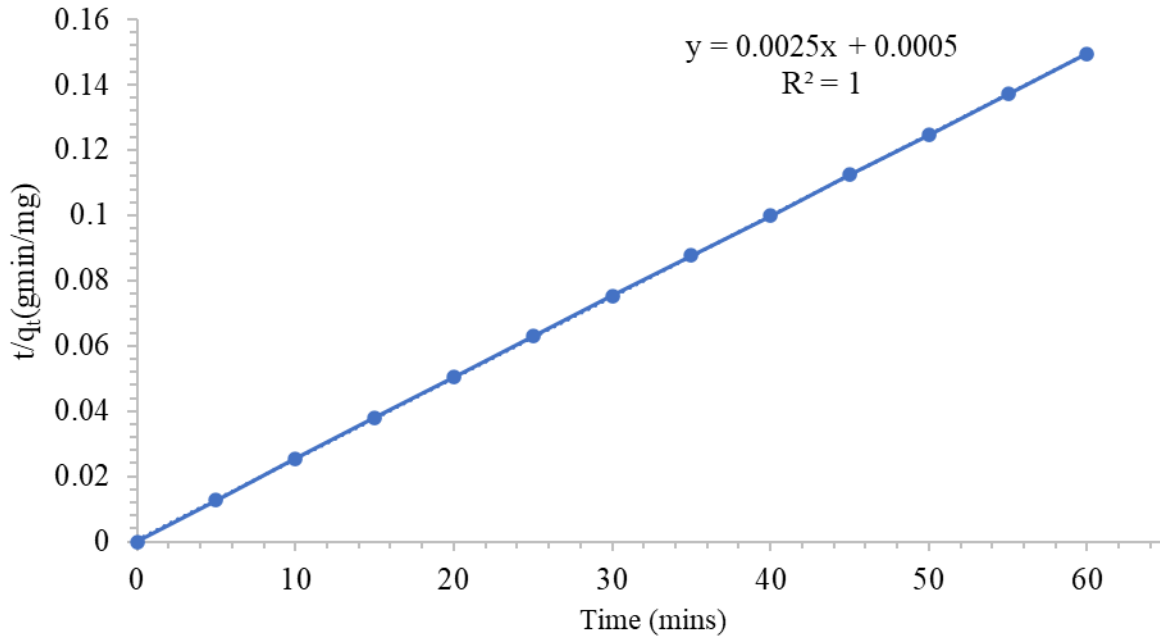
Figure 4.54: Pseudo-Second Order Kinetics for CV adsorption onto *X. moluccensis* stem.
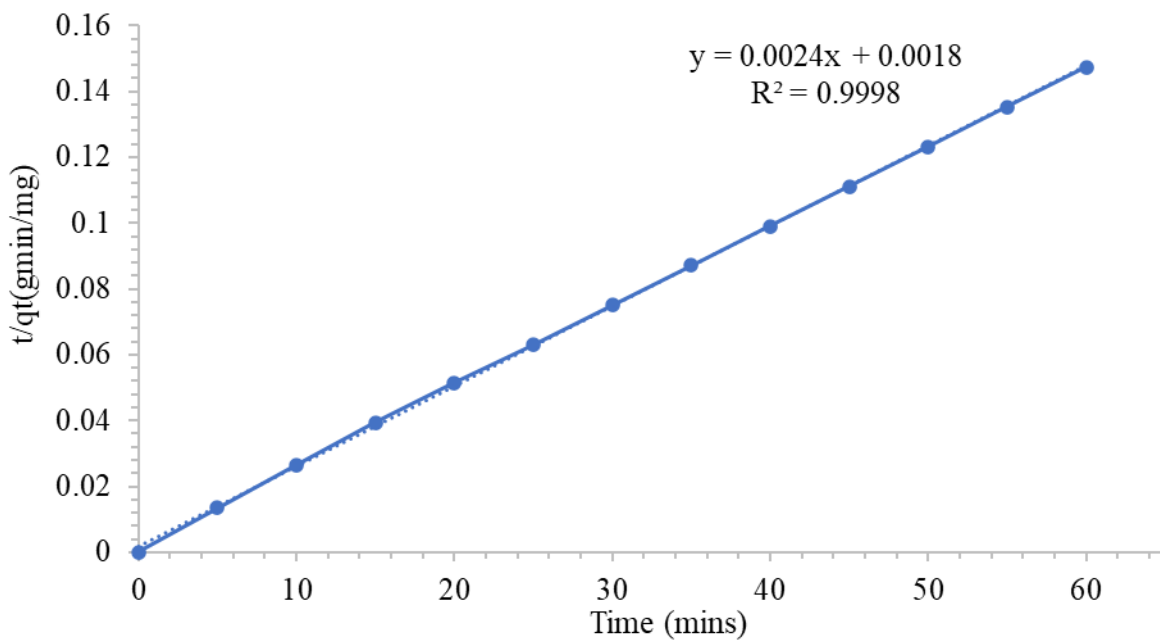
Figure 4.55: Pseudo-Second Kinetics for CV adsorption onto *R. mucronata* stem-bark.
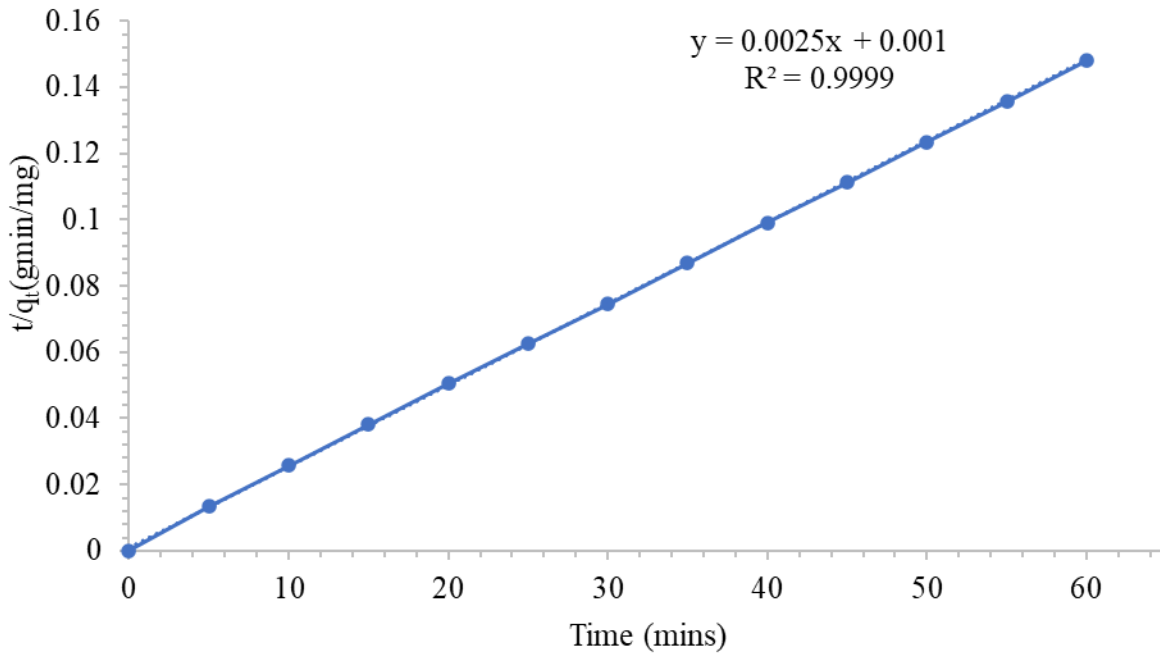
Figure 4.56: Pseudo-Second Kinetics for CV adsorption onto *R. mucronata* stem.
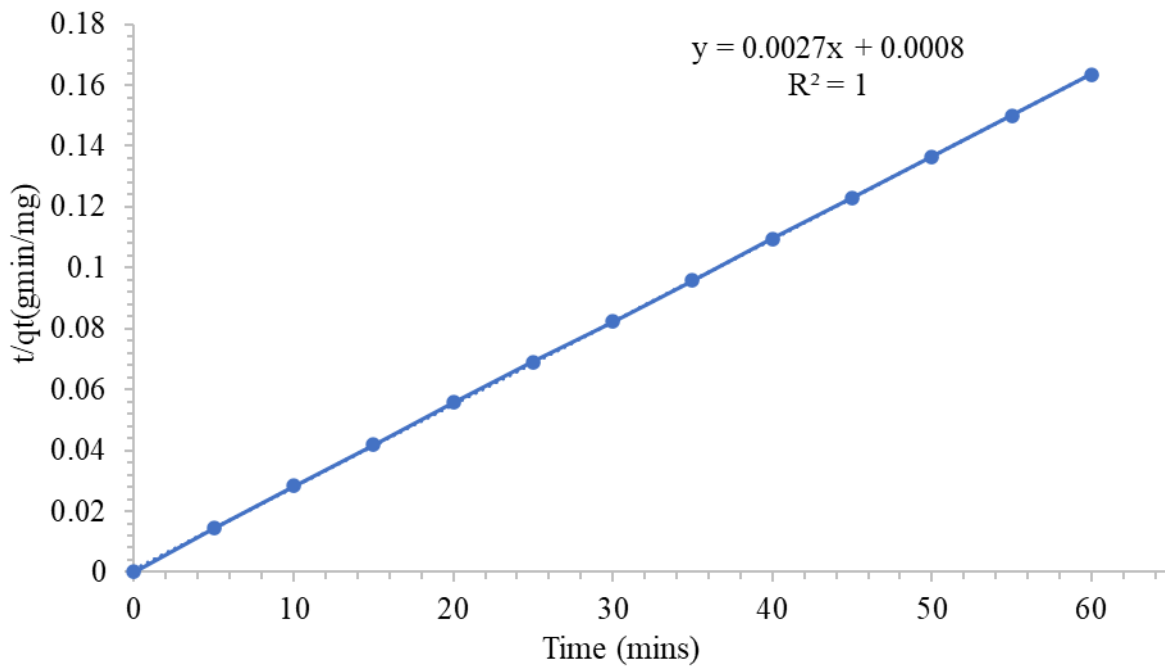
Figure 4.57: Pseudo-Second Order Kinetics for MG adsorption onto *X. moluccensis* stem-bark.
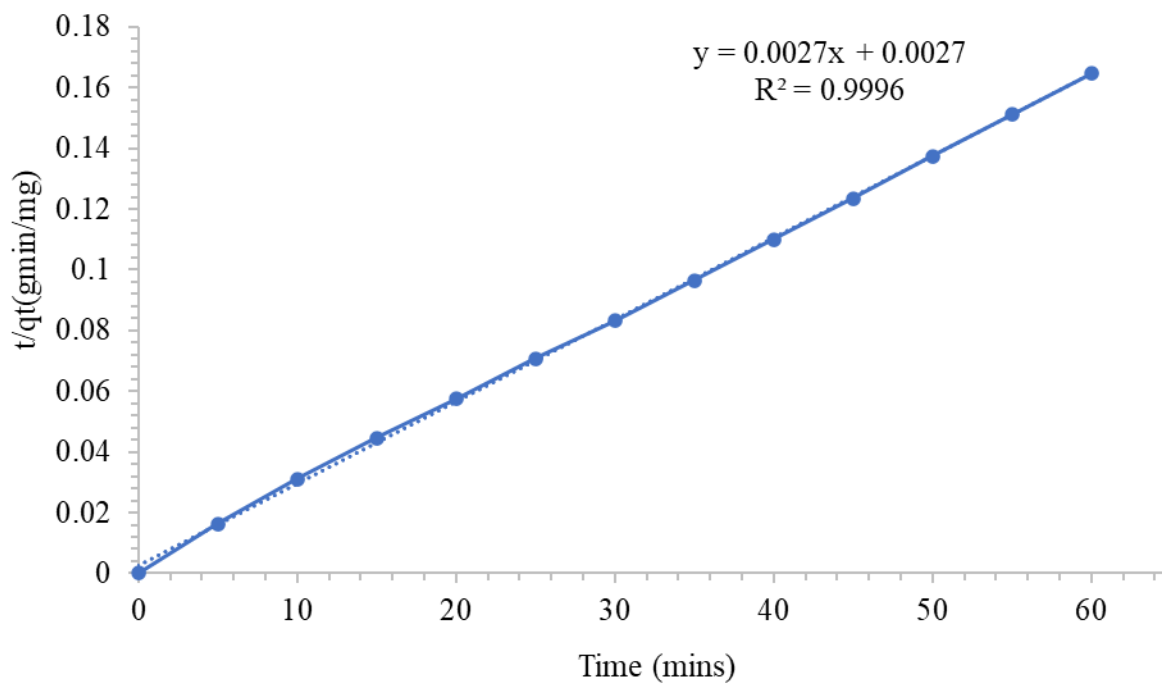
Figure 4.58: Pseudo-Second Order Kinetics for MG adsorption onto *X. moluccensis* stem.
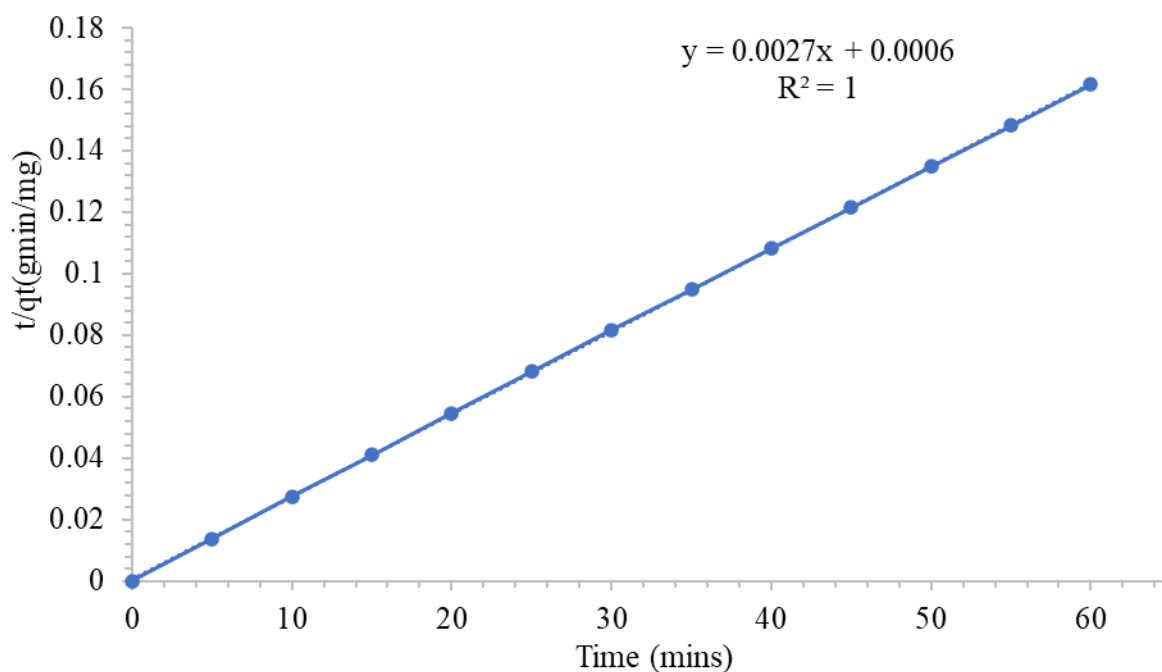
Figure 4.59: Pseudo-Second Order Kinetics for MG adsorption onto *X. moluccensis* stem-bark.
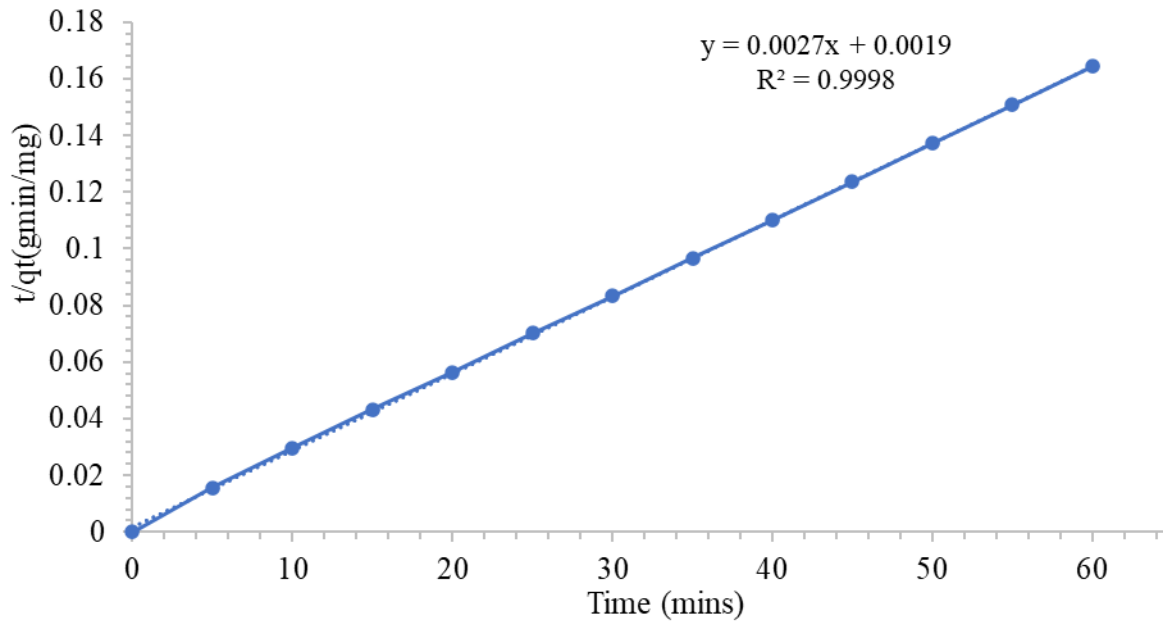
Figure 4.60: Pseudo-Second Order Kinetics for MG adsorption onto *X. moluccensis* stem.

The Pseudo-Second Order Kinetics parameters for CV and MG dyes adsorption onto the two

species adsorbent materials are shown in the tables 4.5 and 4.6.

Table 4.5: Pseudo-Second Order Kinetics Parameters for CV Adsorption.

Crystal Violet (CV) Dye Adsorption				
Adsorbent	**Parameters**			
	$q_{e,exp}$ **(mg/g)**	$q_{e,cal}$ **(mg/g)**	K_2 **(min^{-1})**	R^2
X. moluccensis stem-bark	405.5100	416.6667	0.0043	0.9999
X. moluccensis stem	401.0820	400.0000	0.0124	1.0000
R. mucronata stem-bark	407.2990	416.6667	0.0033	0.9998
R. mucronata stem	405.594	400.0000	0.0061	0.9999

Table 4.6: Pseudo-Second Order Kinetics Parameters for MG Adsorption.

Malachite Green (MG) Dye Adsorption				
Adsorbent	Parameters			
	$q_{e,exp}$ (mg/g)	$q_{e,cal}$ (mg/g)	K_2 (min^{-1})	R^2
X. moluccensis stem-bark	366.8910	370.3704	0.0093	1.0000
X. moluccensis stem	364.6880	370.3704	0.0028	0.9996
R. mucronata stem-bark	371.3120	370.3704	0.0121	1.0000
R. mucronata stem	365.1690	370.3704	0.0039	0.9998

Assessment of the results in Tables 4.5 and 4.6 shows that $q_{e,exp}$ and $q_{e,cal}$ (mg/g), are very much in agreement with large values for the correlation coefficient R^2. This clearly indicates that CV and MG dyes adsorption purely follow Pseudo-Second Order Kinetics, an observation that was also made by Chakraborty *et al*., (2012).

4.7 Intraparticle Diffusion for CV and MG onto *X. moluccensis* and *R. mucronata* Species

Below are plots of q_t against $\sqrt{t}$ (equation 7) for the dye adsorption process by the two species as derived from values as given in Appendix A and B. A line of best fit has been constructed for each graph as a measure of the rate limiting step as illustrated in Figures 4.61 to 4.68.
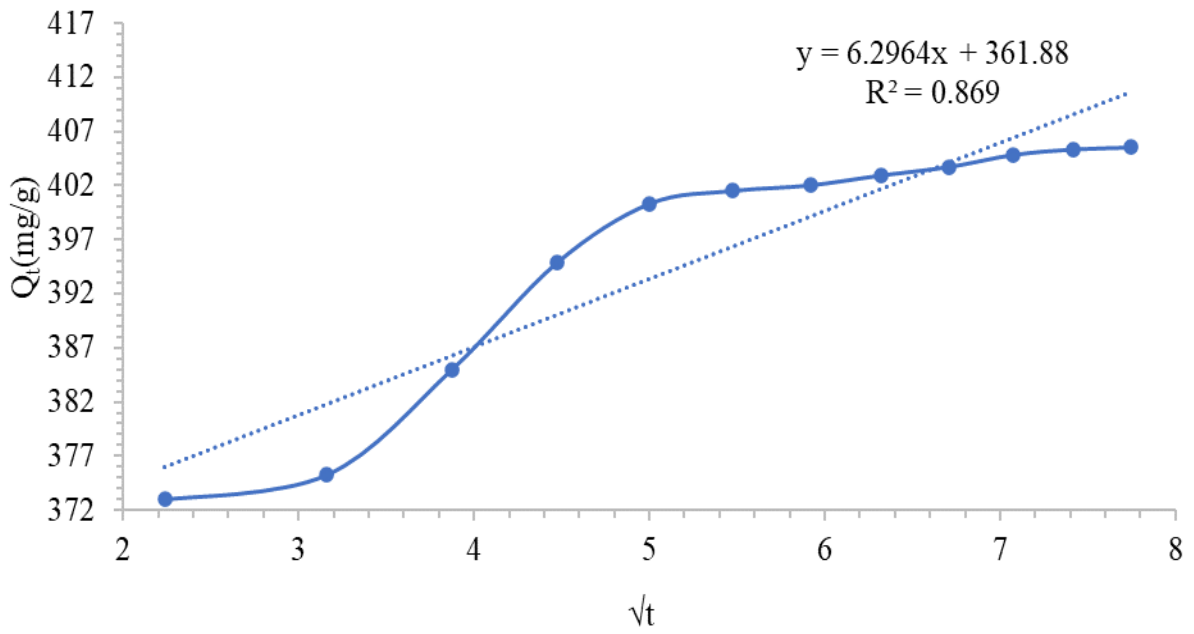
Figure 4.61: Intraparticle Diffusion for CV onto *X. moluccensis* stem-bark.

$y = 6.2964x + 361.88$
$R^2 = 0.869$
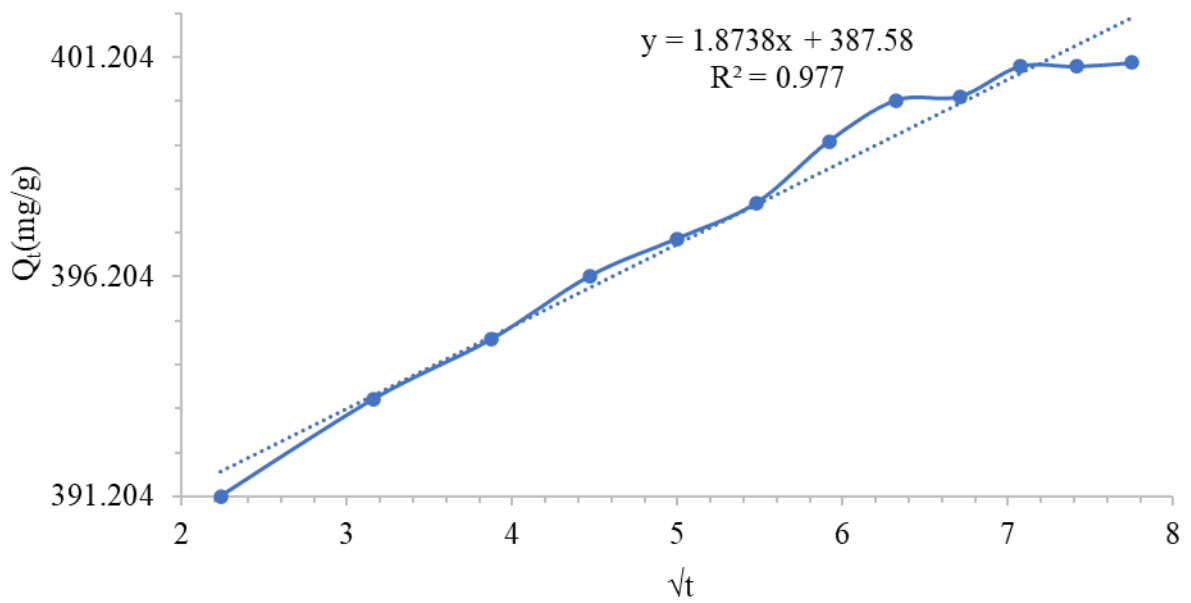
Figure 4.62: Intraparticle Diffusion for CV onto *X. moluccensis* stem.

$y = 1.8738x + 387.58$
$R^2 = 0.977$
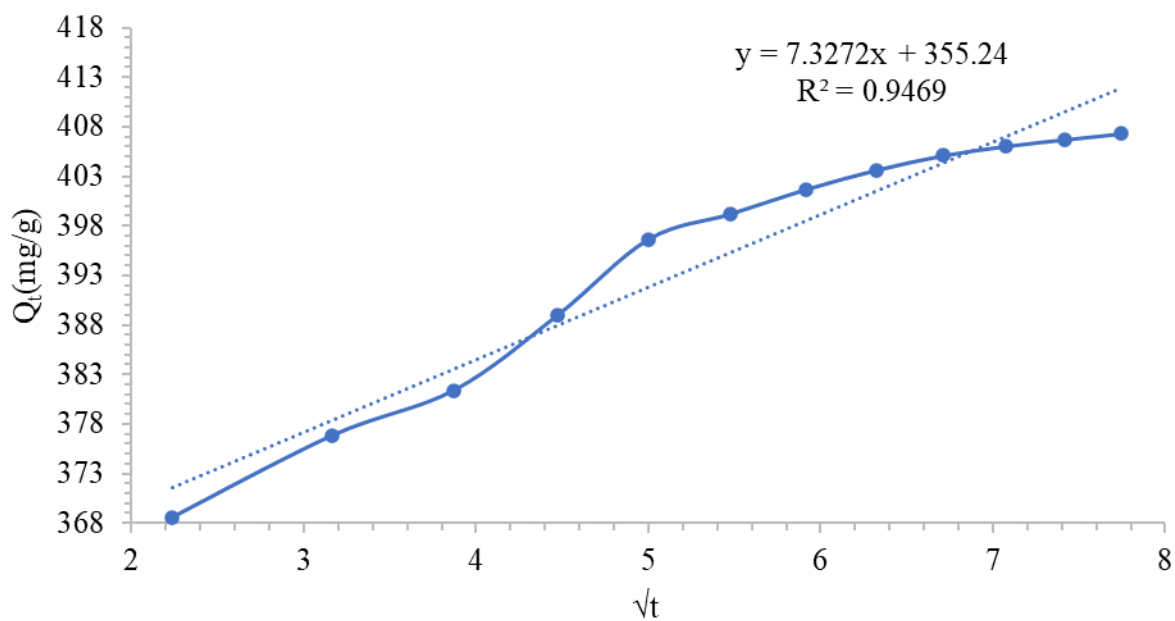
Figure 4.63: Intraparticle Diffusion for CV onto *R. mucronata* stem-bark.
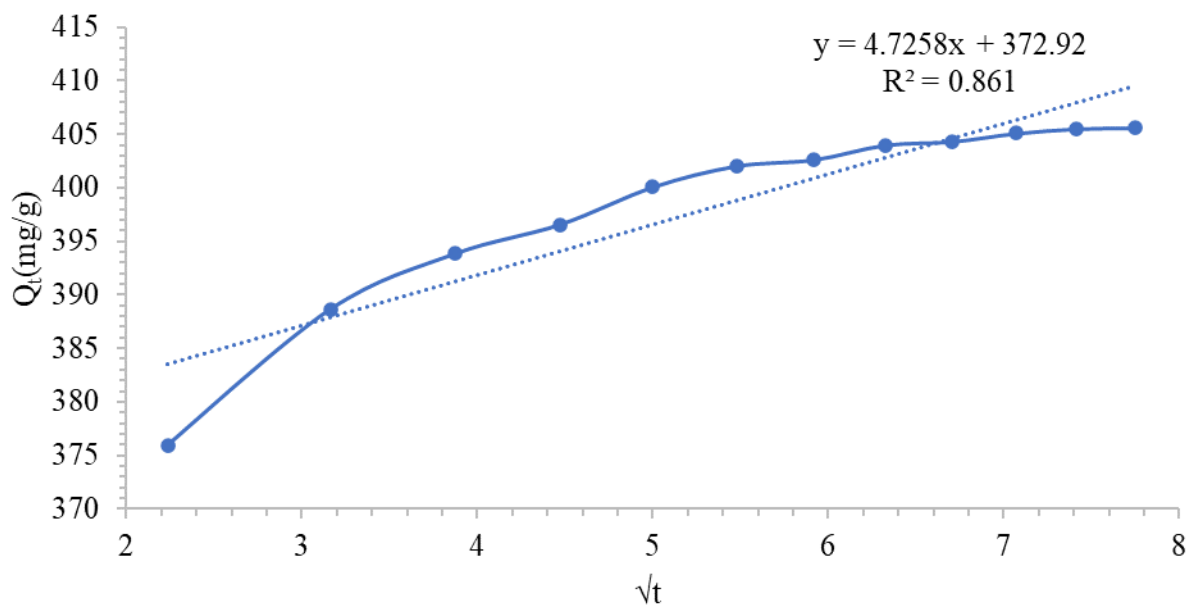
Figure 4.64: Intraparticle Diffusion for CV onto *R. mucronata* stem.
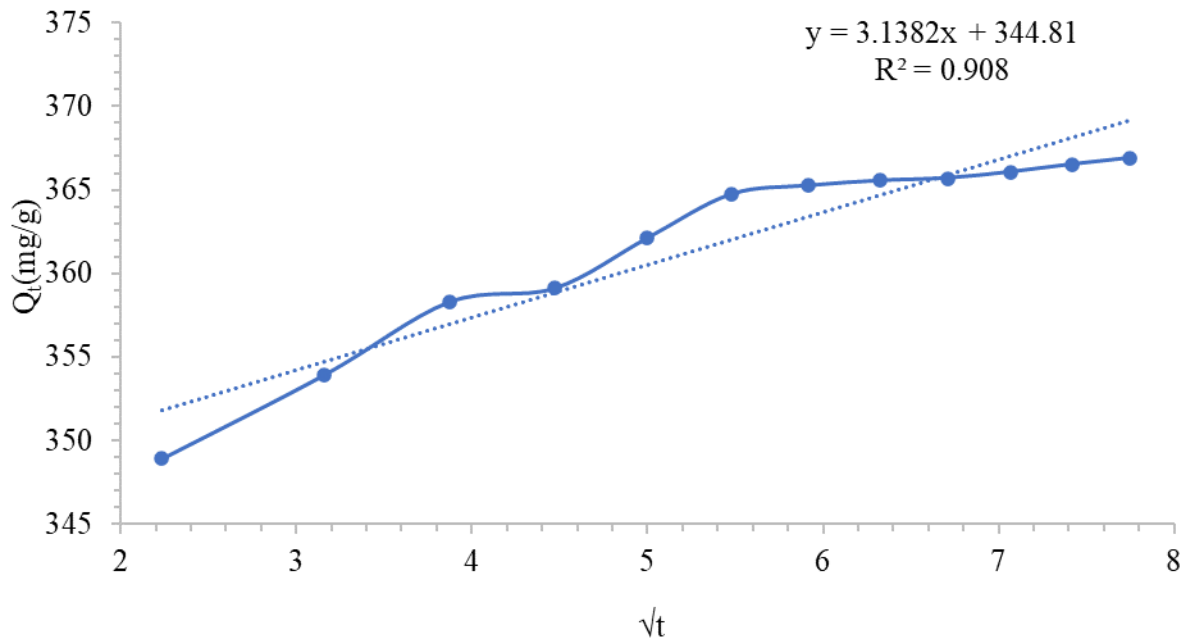
Figure 4.65: Intraparticle Diffusion for MG onto *X. moluccensis* stem-bark.
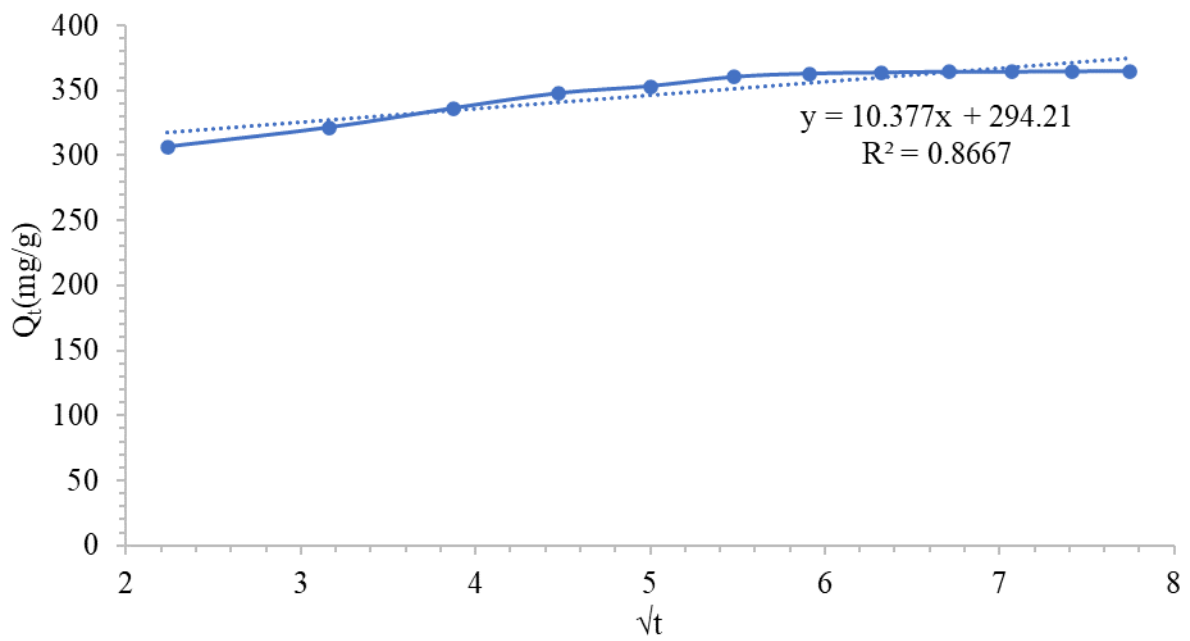
Figure 4.66: Intraparticle Diffusion for MG onto *X. moluccensis* stem.
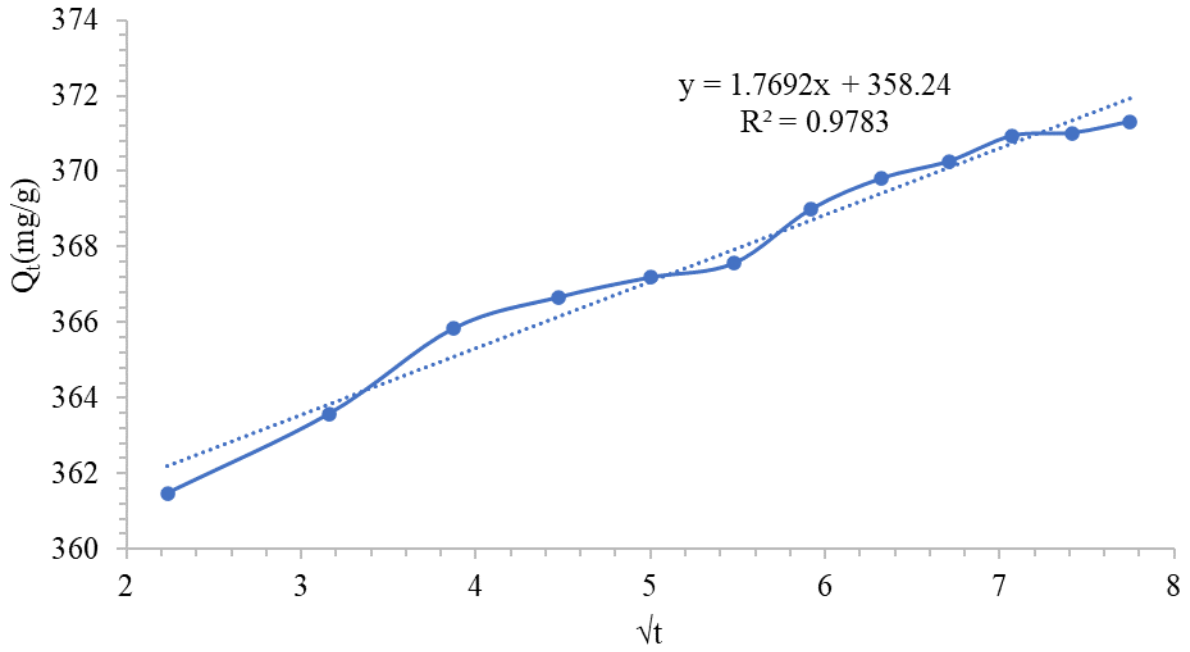
Figure 4.67: Intraparticle Diffusion for MG onto *R. mucronata* stem-bark.
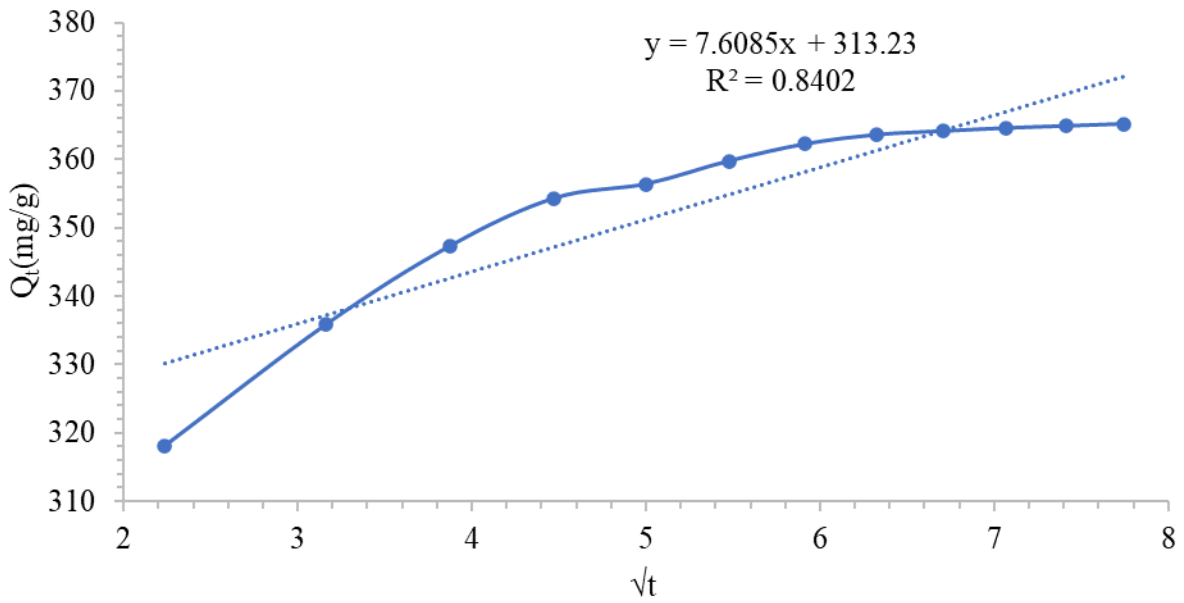
Figure 4.68: Intraparticle Diffusion for MG onto *R. mucronata* stem.

The intraparticle diffusion parameters derived from the graphs are summarised in the Table 4.7.

Table 4.7: Intraparticle Diffusion Parameters for CV and MG dyes Adsorption.

Adsorbent	CV Dye			MG Dye		
	K_{diff} (mg/g)	C (g/L)	R^2	K_{diff} (mg/g)	C (g/L)	R^2
R. mucronata stem-bark	7.3272	355.24	0.9469	1.7692	358.24	0.9783
R. mucronata stem	4.7258	372.92	0.8610	7.6085	313.23	0.8402
X. moluccensis stem-bark	6.2964	361.88	0.8690	3.1382	344.81	0.9080
X. moluccensis stem	1.8738	387.58	0.9770	10.377	294.21	0.8667

The rate of diffusion of adsorbate molecules towards adsorbent surfaces is determined by the intraparticle diffusion rate constant, $K_{diff,}$ (mg g^{-1}min^{-1}). The K_{diff} values in Table 4.7 are all significant positive numbers showing a positive rate constant but the curves in Figures 4.61 to 4.68 shows that intraparticle distance is not the only factor that is controlling the dye adsorption process. The large boundary layer thickness as given by values for C, g/L, as shown in Table 4.7, for species stem and stem-bark above indicates that adsorption of both dyes is majorly a process controlled by intraparticle diffusion.

4.8 Surface Characterisation

4.8.1 *X. moluccensis* Surface Characterisation

 Figures 4.69 to 4.74 shows the FT-IR spectrums of the stem and stem-bark of before and after adsorption of the dyes. Surface studies was done using a Shimadzu FT-IR Affinity-IF spectrometer with a scanning range of $4000 - 600\text{cm}^{-1}$.
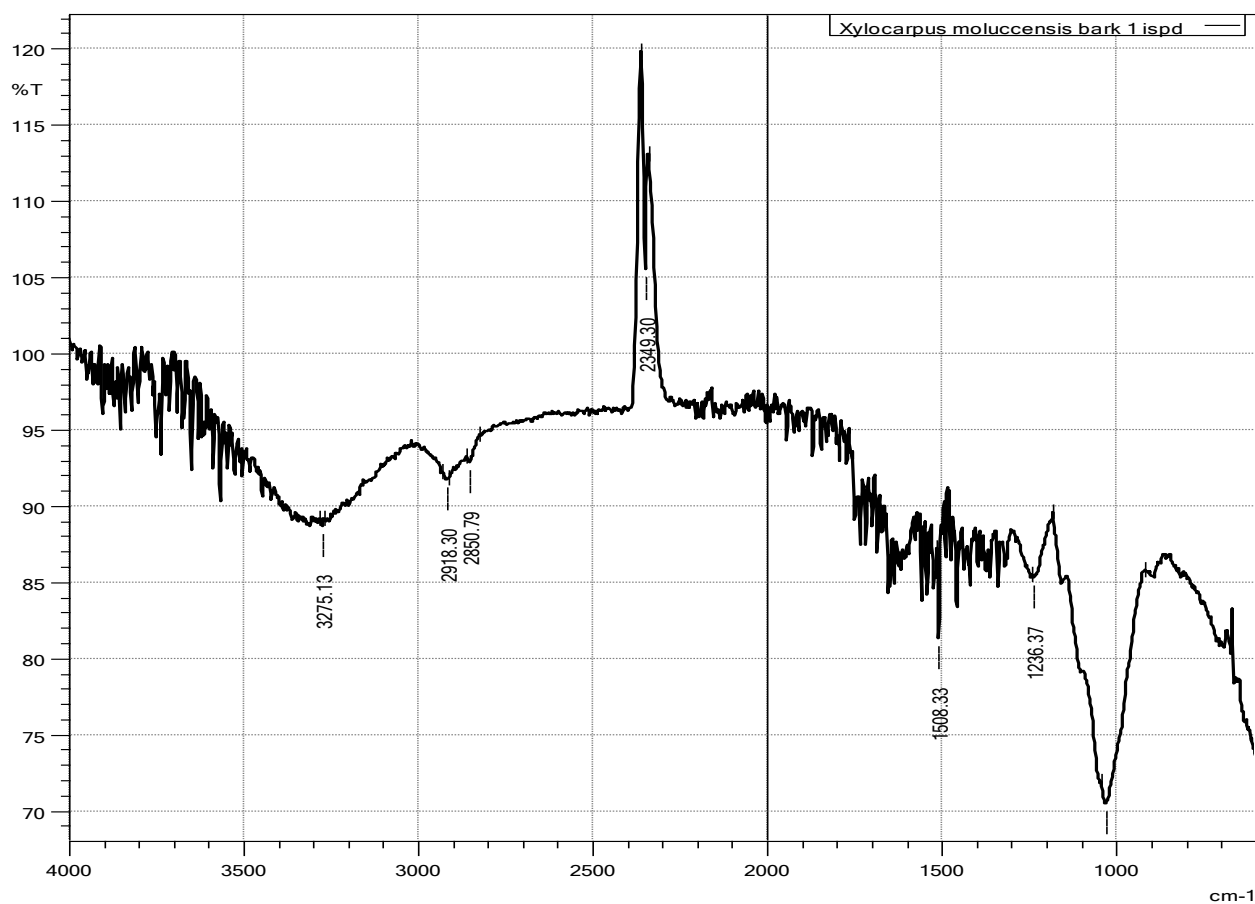
Figure 4.69: FT-IR spectrum of *X. moluccensis* stem-bark before adsorption.
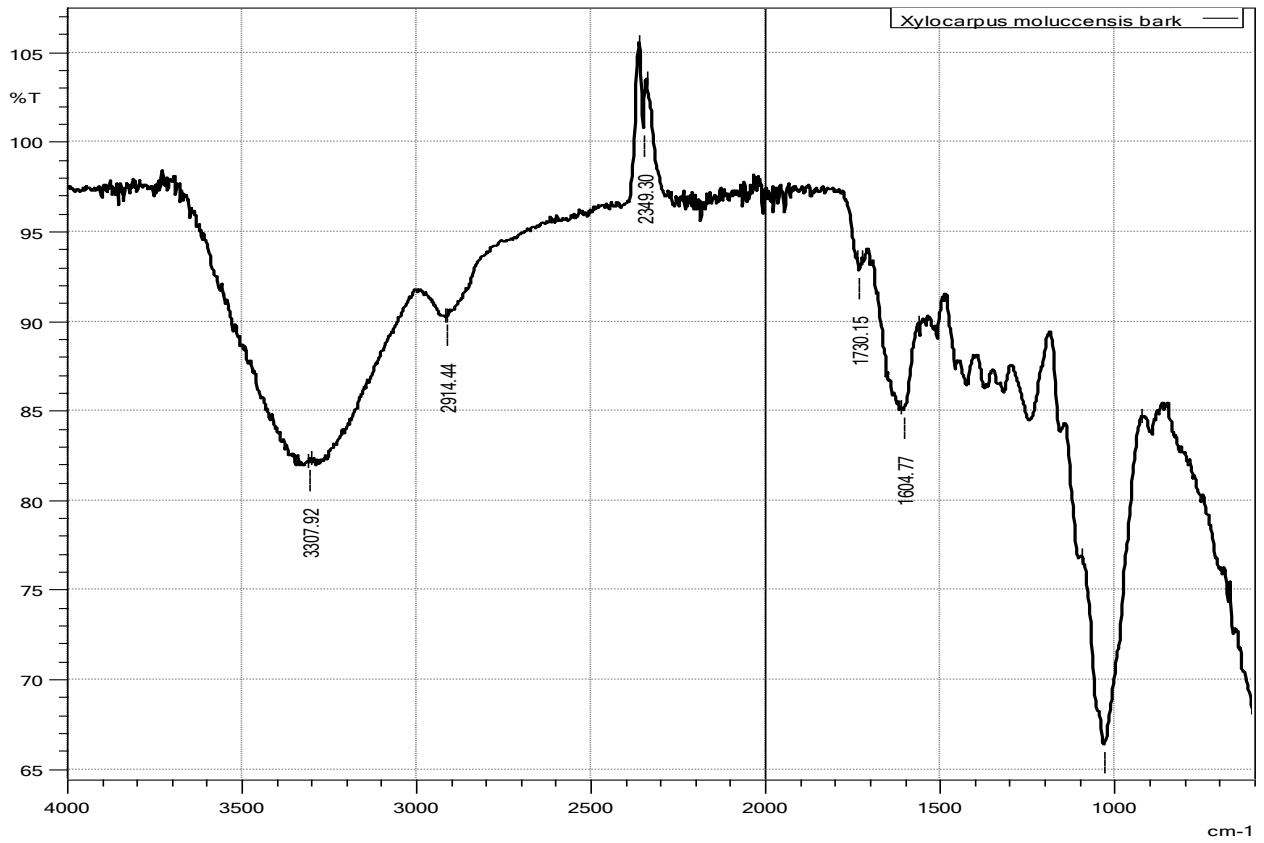
Figure 4.70: FT-IR spectrum of *X. moluccensis* stem-bark after adsorption of CV.
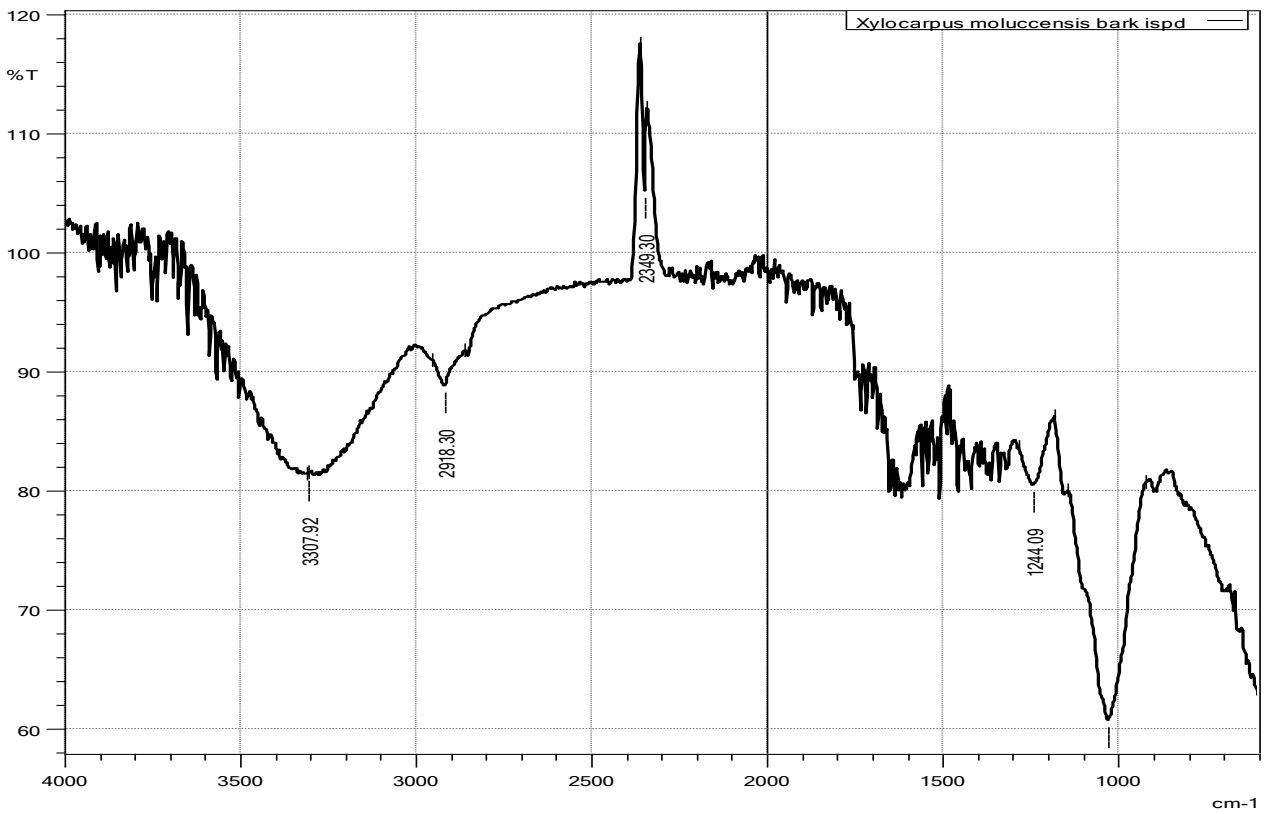
Figure 4.71: FT-IR spectrum of *X. moluccensis* stem-bark after adsorption of MG.

Table 4.8 compares a summary of the major peaks in the vibrational spectra from Figures 4.69 to 4.71, for the adsorption of CV and MG onto *X. moluccensis* stem-bark.

Table 4.8: Observed Frequencies in the FT-IR spectra for the Adsorption of CV and MG onto *X. moluccensis* stem-bark.

Nature of the Sample	Vibrational frequency (cm^{-1})		
	Raw (Fig. 4.69)	**Used CV (Fig. 4.70)**	**Used MG (Fig. 4.71)**
	3275.13	3307.92	3307.92
	2918.30	2914.44	2918.30
	2850.79		
	2349.30	2349.30	2349.30
		1730.15	1717.15
	1508.33		
		1604.77	1601.89
	1236.37		
	1031.92	1031.92	1031.92

The displayed results show some similarity in terms of the main functional groups to those in figures 4.69 to 4.71 except, some bonds disappeared and others appeared after adsorption. Peaks that disappeared were those at 2850.79 cm^{-1}, 1508.33 cm^{-1} and 1236.37 cm^{-1} while peaks that appeared after adsorption included those at 1730.15 cm^{-1} and 1604.77 cm^{-1}. The disappearance or appearance of some peaks can be associated to shielding effect and formation of new bonds respectively, from the adsorbed dye molecules. Similarity is witnessed in the consistency of the strong broad peak at 3307.92 cm^{-1} representing the -O-H bond stretch; the peak at 2918.30 cm^{-1} for an alkane C – H stretch and that at 1031.92 cm^{-1} representing C – O – O$^-$ bend. The adsorption can further be associated to the shifting of the peaks as for 3275.13 cm^{-1} which shifted to 3307.92 cm^{-1} after adsorption of both dyes due to formation of dispersion forces as an interactive property of the adsorption process.

Figures 4.72 to 4.74 gives the FT-IR spectrums of the stem of *R. mucronata* and *X. moluccensis* before and after adsorption of the CV and MG dyes.
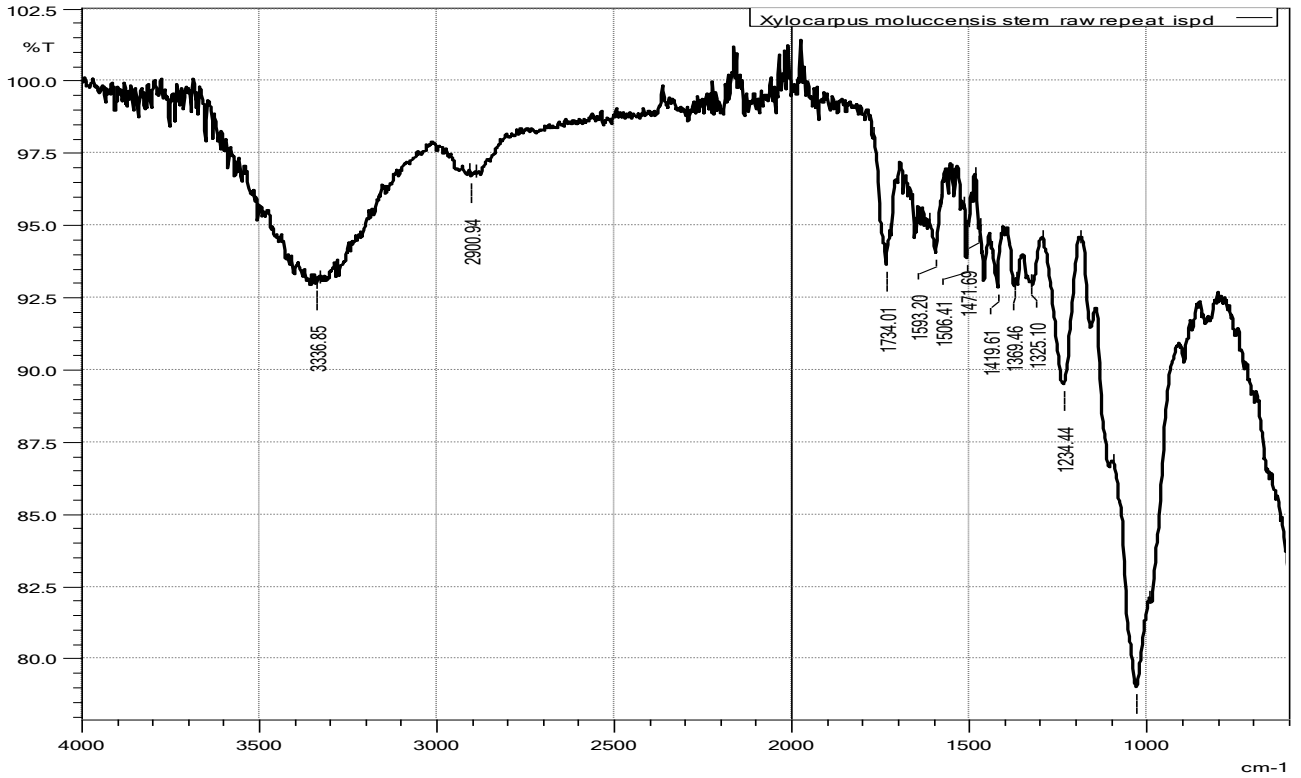
Figure 4.72:FT-IR spectrum of *X. moluccensis* stem before adsorption.
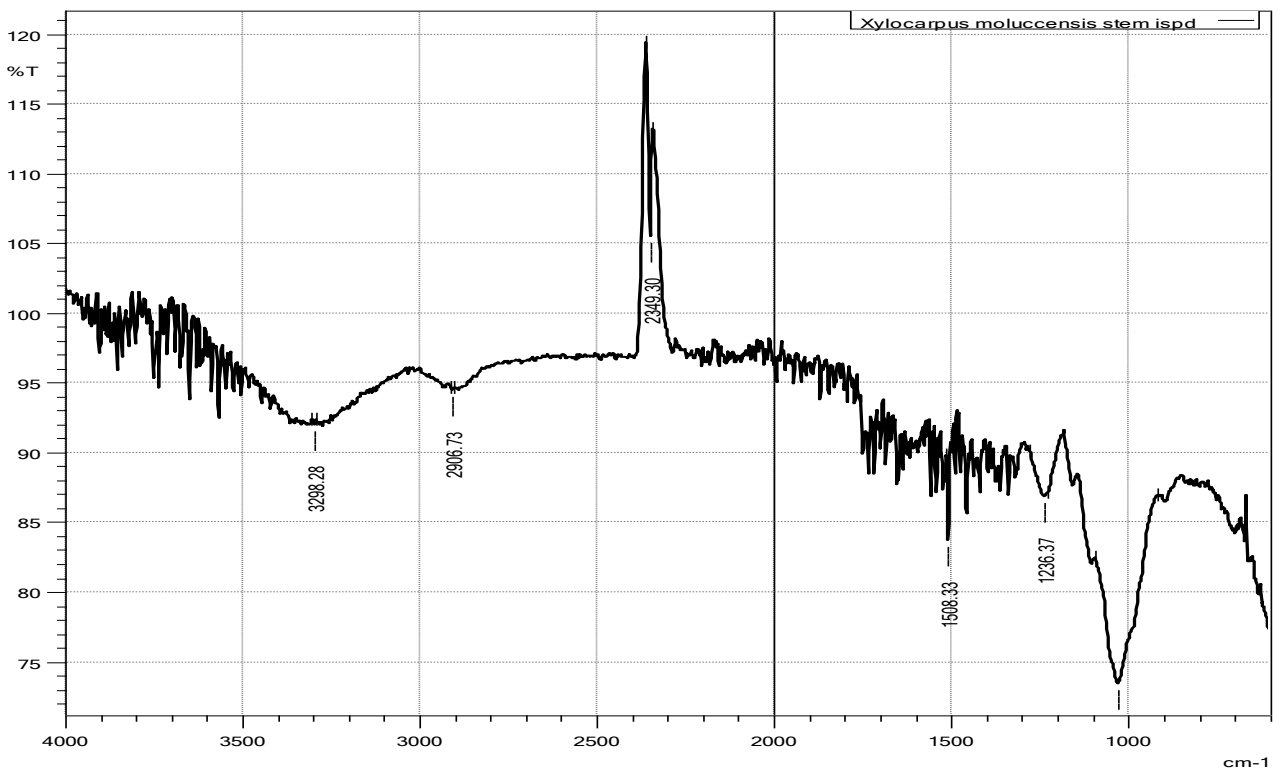
Figure 4.73: FT-IR spectrum of *X. moluccensis* stem after adsorption of CV.

75
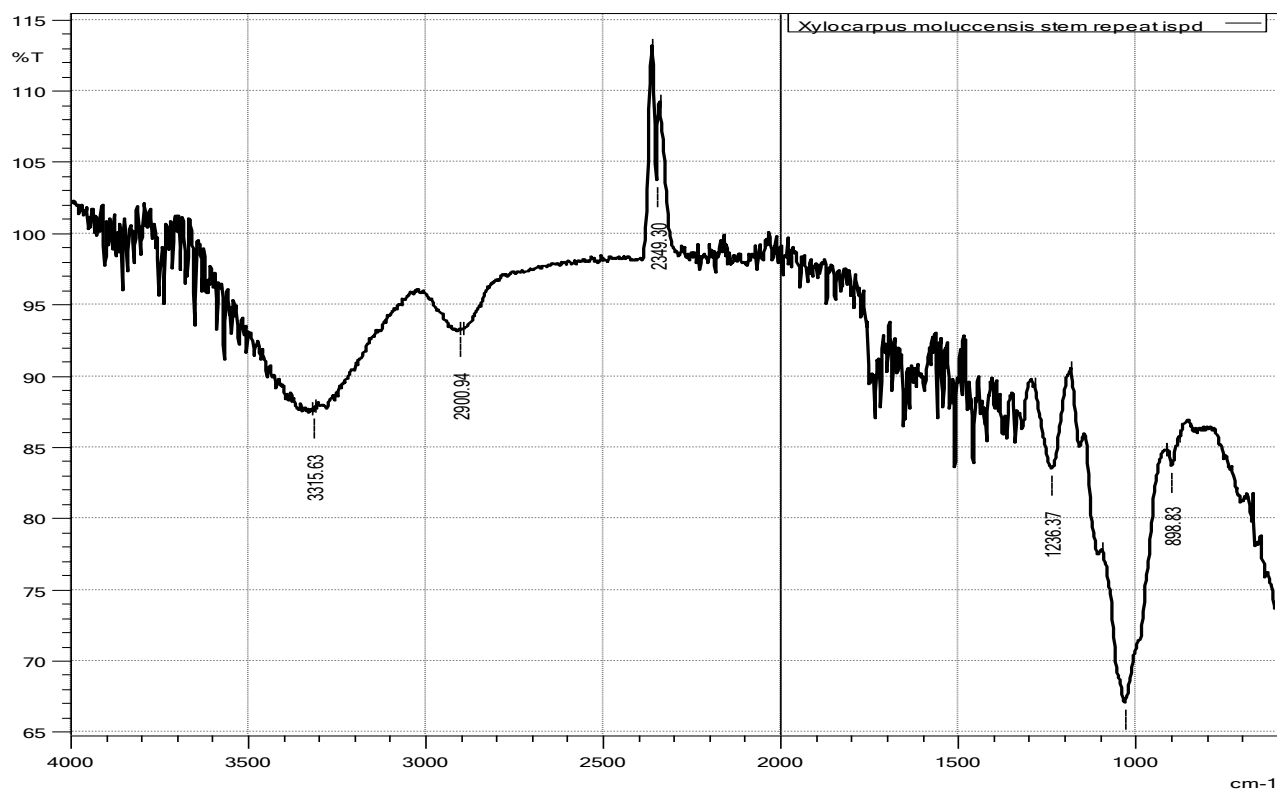
Figure 4.74: FT-IR spectrum of *X. moluccensis* stem after adsorption of MG.

Table 4.9, compares a summary of the major peaks in the vibrational spectra from figures 4.72

to 4.74, for the adsorption of CV and MG onto *X. moluccensis* stem.

Table 4.9: Observed Frequencies in the FT-IR Spectra for the Adsorption of CV and MG onto
X. moluccensis stem.

	Vibrational frequency (cm^{-1})		
Nature of the Sample	**Raw (Fig. 4.72)**	**Used CV (Fig. 4.73)**	**Used MG (Fig. 4.74)**
	3336.85	3298.28	3315.63
	2900.94	2906.73	2900.94
		2349.30	2349.30
	1734.01		
	1593.20		
	1506.41	1508.33	1500.00
	1471.69		
	1419.61		
	1369.46		
	1325.10		
		1236.37	1236.37
	1028.06		

It is observed that quite a number of peaks which were present before process have disappeared. Then adsorption being a surface activity may have resulted to overlapping of dye molecules onto the stem matrix creating a strong shield hence the disappearance. Some peaks such as 898.83 cm^{-1} appeared after, and further proves that adsorption occurred.

4.8.2 *R. mucronata* surface characterisation.

The stem-bark of *R. mucronata* FT-IR spectra are shown in figures 4.75 to 4.80 taken before and after adsorption of the dyes. The FT-IR surface studies was done using a Shimadzu FT-IR Affinity-IF spectrometer with a scanning range of 4000 – 600cm^{-1}.
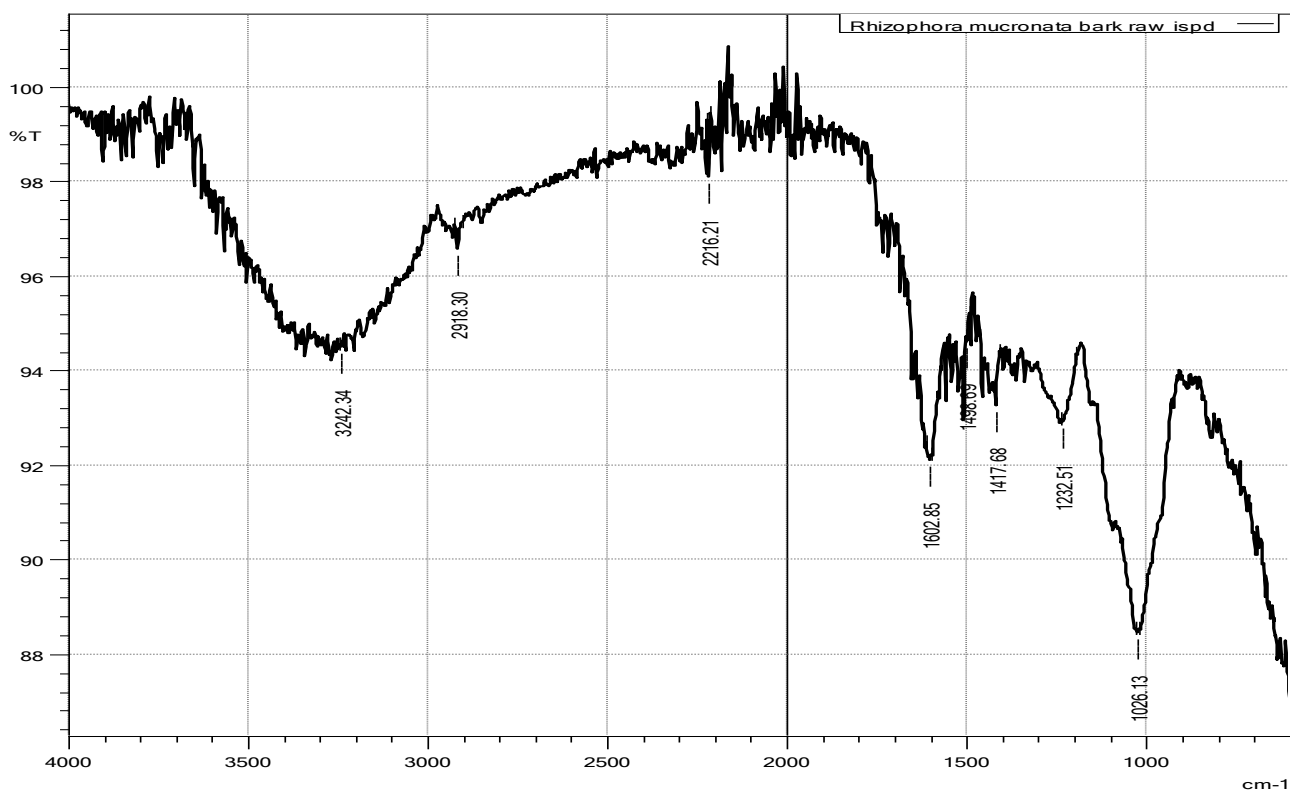
Figure 4.75: FT-IR spectrum of *R. mucronata* stem-bark before adsorption.
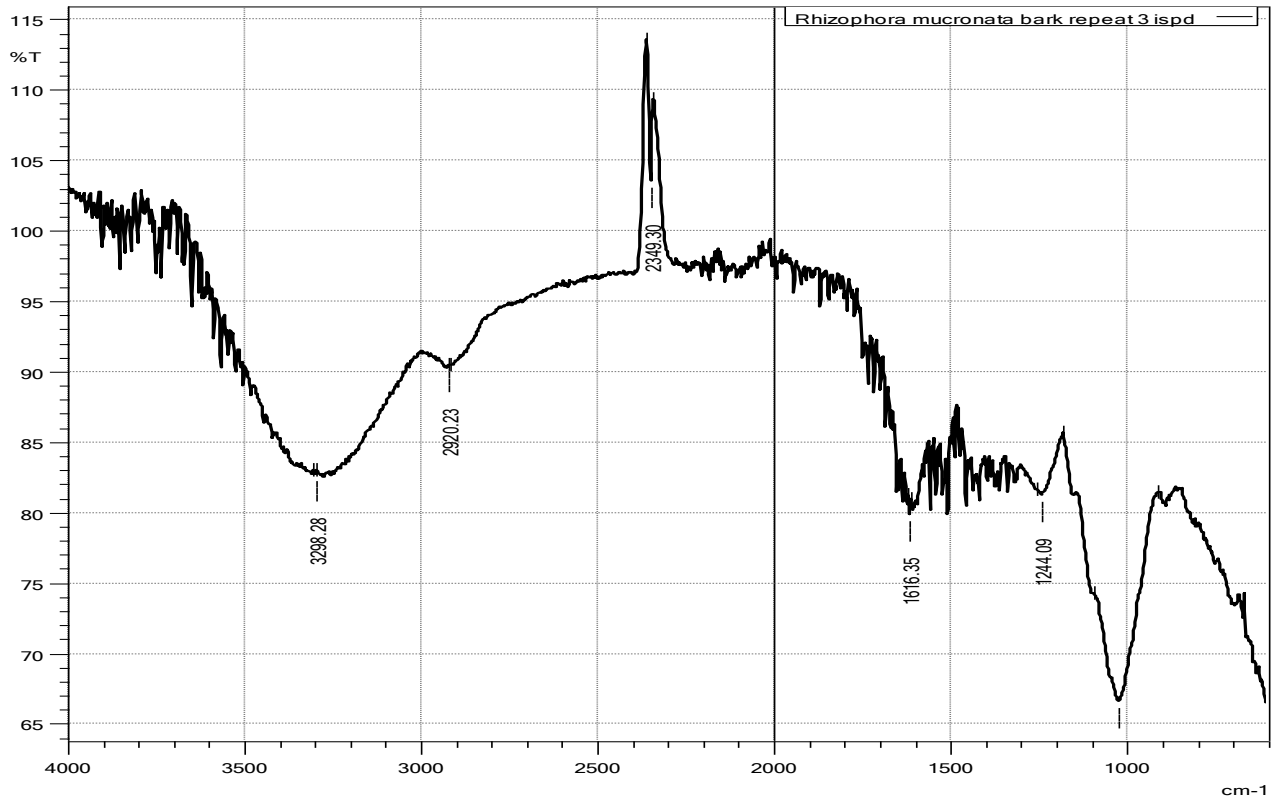
Figure 4.76: FT-IR spectrum of *R. mucronata* stem-bark after adsorption of CV.
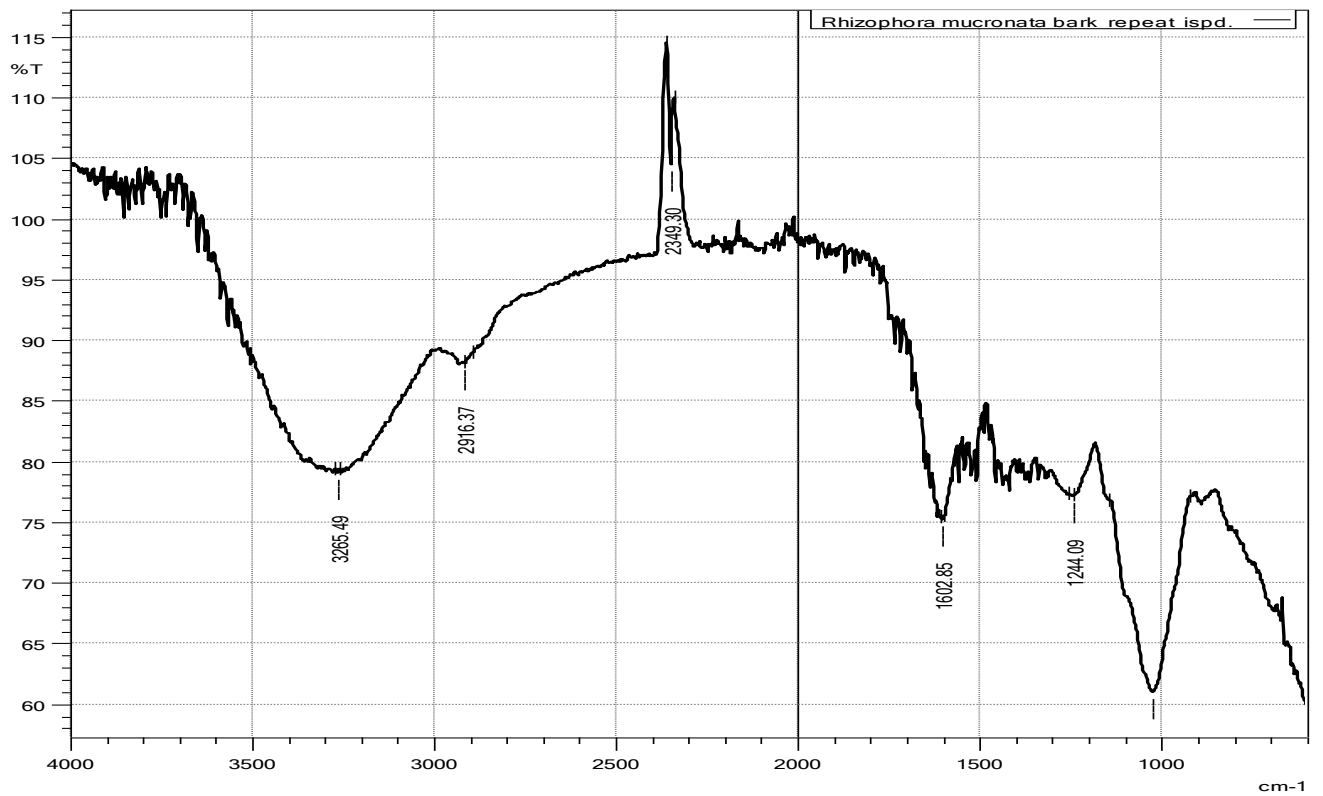
Figure 4.77: FT-IR spectrum of *R. mucronata* stem-bark after adsorption of MG.

Table 4.10 compares a summary of the major peaks in the vibrational spectra from figures 4.75 to 4.80 for the adsorption of CV and MG onto *R. mucronata* stem-bark.

Table 4.10: Observed Frequencies in the FT-IR Spectra for the Adsorption of CV and MG onto *R. mucronata* stem-bark.

Nature of the Sample	Vibrational frequency (cm^{-1})		
	Raw (Fig. 4.75)	Used CV (Fig. 4.76)	Used MG (Fig. 4.77)
	3242.34	3298.28	3265.49
	2918.30	2920.23	2916.37
	2216.21	2349.30	2349.30
	1602.85	1616.35	1602.85
	1417.68	1730.15	1717.15
	1508.33	1417.68	1417.68
	1232.51	1244.09	1244.09
	1026.31	1024.13	1024.20

The broad peak at 3242.34 cm^{-1} stretch indicates the presence of an – OH group from a phenol or an alcohol. The peak observed at 2918.30 is due to an alkyl C – H stretch while the peak at 1602.85 cm^{-1} is characteristic of aromatic C=C bending and the strong peak at 1026.13 cm^{-1} is due to C-O bending (Muinde *et al*., 2017). After adsorption, the peaks broaden and a new peak is observed at 2349.30 cm^{-1}. The presence of –OH group and the carbonyl indicate a possible carboxylic group. Adsorption was also shown by shifting of peaks for example, the peaks at 2216.21cm^{-1} shifted to 2349.30 cm^{-1} in CV and 2349.30 cm^{-1} in MG. This not only shows that a new bond has been created but also predicts the major functional groups on the adsorbent and compares cationic nature of the dyes.

Figures 4.78 to 4.80 shows the FT-IR spectra of the stem of *R. mucronata* and *X. moluccensis* before and after adsorption of the CV and MG dyes. The scanning range was from 4000 - 600cm^{-1}.
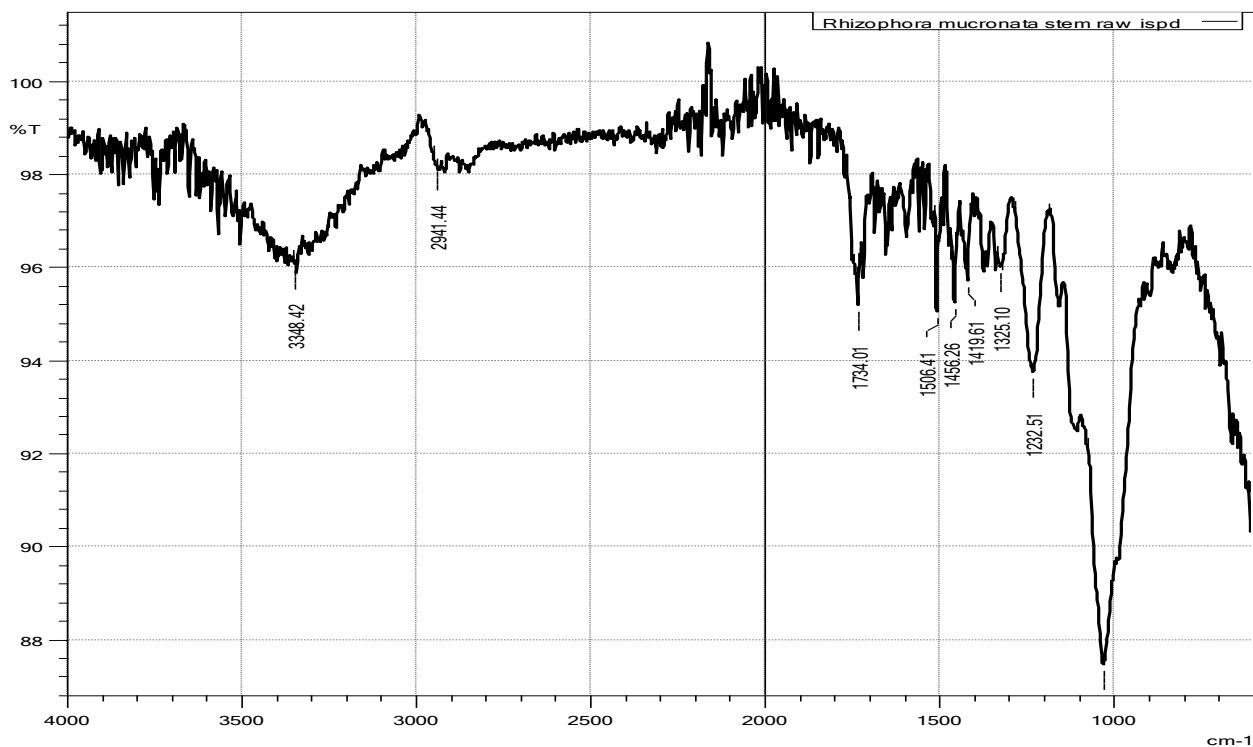
Figure 4.78 : FT-IR spectrum of *R. mucronata* stem before adsorption.
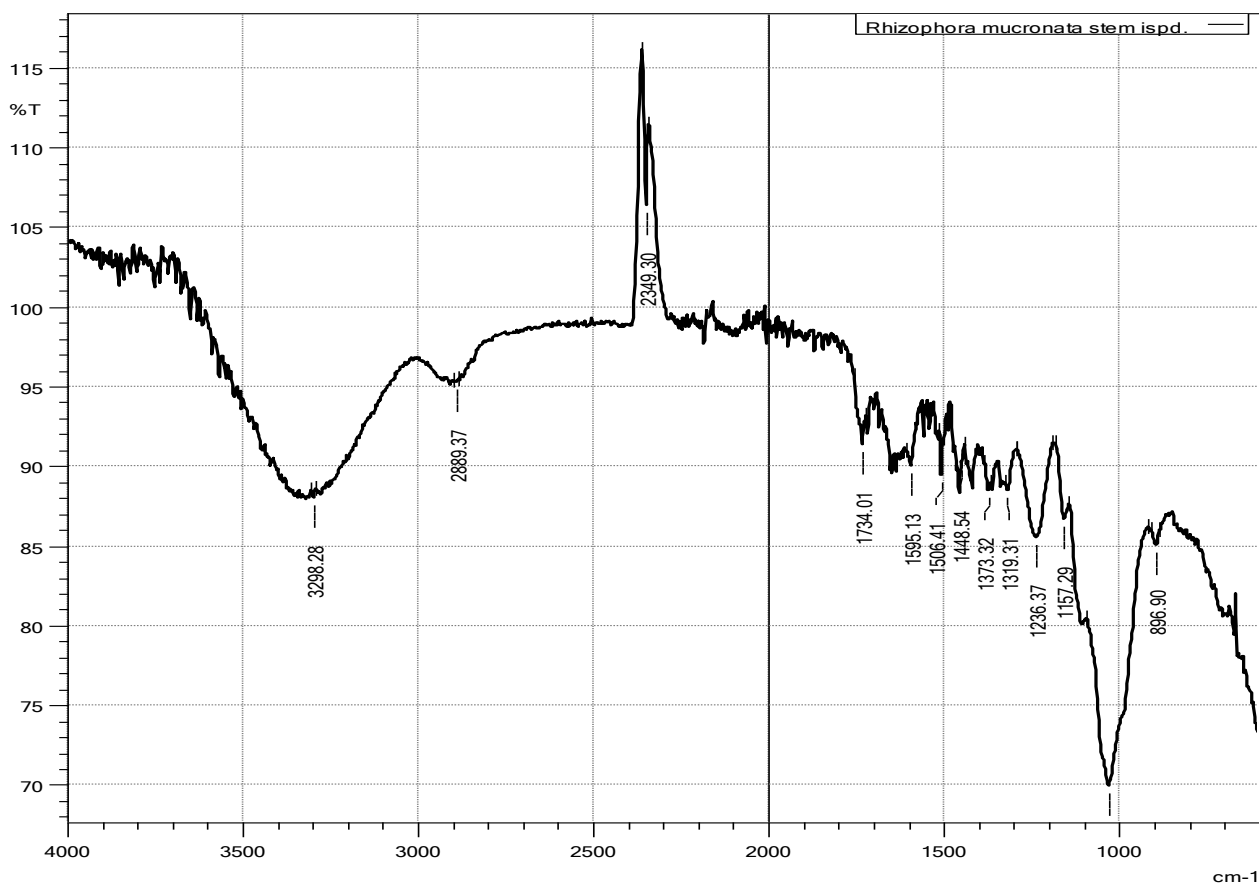
Figure 4.79: FT-IR spectrum of *R. mucronata* stem after adsorption of CV.
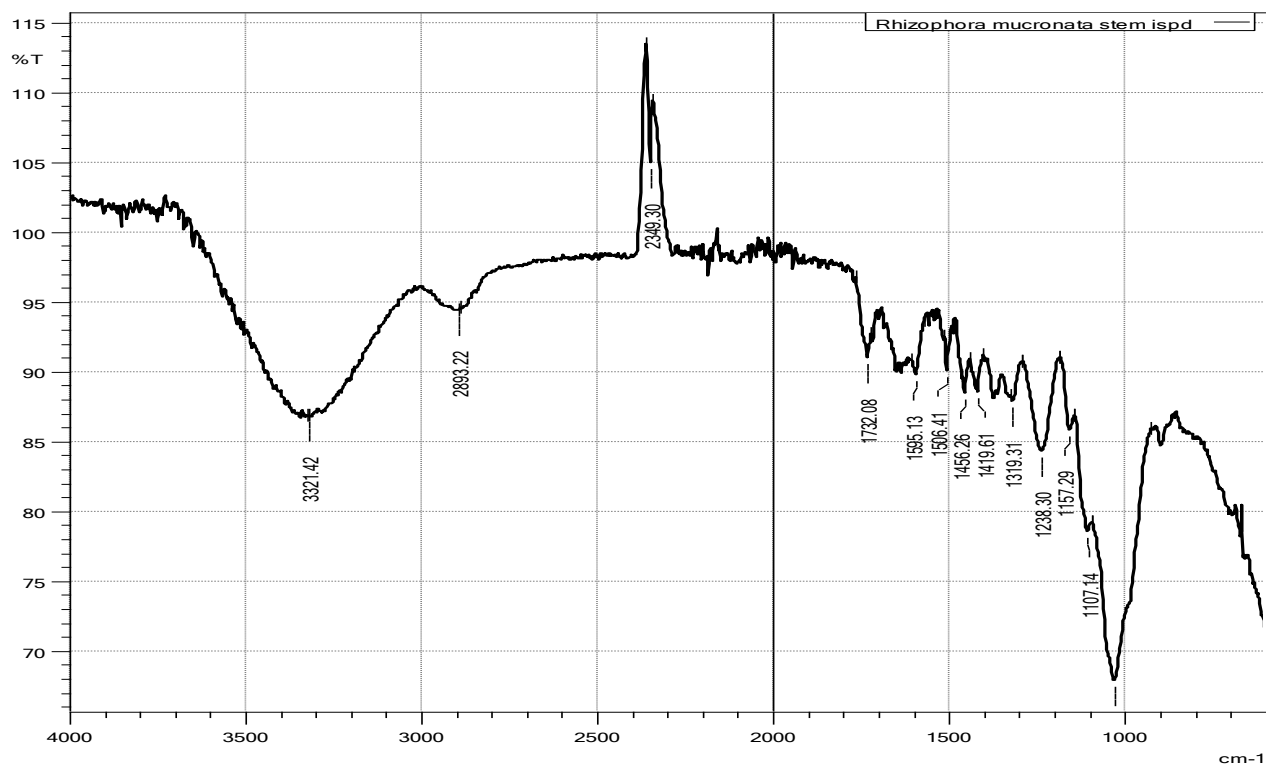
Figure 4.80: FT-IR spectrum of *R. mucronata* stem after adsorption of MG.

Table 4.11 below compares the major peaks in the vibrational spectra from figures 4.78 to 4.80

for the CV and MG sorption onto R. mucronata stem.

Table 4.11: Observed Frequencies in the FT-IR Spectra for the Adsorption of CV and MG onto *R. mucronata* stem.

Nature of the Sample	Vibrational frequency (cm⁻¹)		
	Raw (Fig. 4.78)	Used CV (Fig. 4.79)	Used MG (Fig. 4.80)
	3348.42	3298.28	3321.42
	2941.44	2889.37	2893.22
		2349.30	2349.30
	1734.01	1734.01	1732.08
		1595.13	1595.13
	1506.41	1506.41	1506.41
	1456.26	1448.54	1456.26
	1419.26	1373.32	1419.61
	1325.10	1319.31	1319.31
	1232.51	1236.37	1238.30
	1031.92	1157.29	1157.29
		1107.14	1107.14
		1031.92	1031.92
		896.90	

The results displayed in the table clearly shows that there was presence of the following characteristic groups; -O-H representing the strong broad peak stretching at 3348.42cm^{-1}. This gives a possible alcoholic intermolecular bond within the structure. This peak also shifted to 3298.28 cm^{-1} and 3321.42 cm^{-1} on adsorption of CV and MG dyes respectively indicating intermolecular interactions between adsorptive sites in the adsorbent and dye molecules. A stretching C – H bond of alkane at 2941.44 cm^{-1} and another C – H bending of a methyl group at 1456.26 cm^{-1}. New bonds created were at 2349.30cm^{-1}, 1595.13 cm^{-1}, 1107.14 cm^{-1}, 1031.92 cm^{-1} and 896.90 corresponding to a C=O stretch, C=C stretch, C – O stretch, C – O – O $^-$ and a C=C bending respectively. These are electron rich regions and since the adsorbate are cationic in nature this further indicates a possible adsorption process proceeded as shown by other parameters. Bonds that remained unchanged after adsorption include; C=O stretching at 1734.01 cm^{-1}; an N-O bond stretching at 1506.41cm^{-1}; a C – H stretching at 1456.26 cm^{-1}; and a strong C – N bond of an aromatic amine stretching at 1325.10 cm^{-1}.

CHAPTER FIVE

5.0 CONCLUSION AND RECOMMENDATIONS

5.1 Conclusions

This study has shown the potential of *X. moluccensis* and *R. mucronata* stem and stem-bark as eco-friendly materials for treatment of wastewaters containing dyes. The stem-bark was the best sorbent material followed by the stem for *R. mucronata* and *X. moluccensis* species in that order. The respective equilibrium adsorption capacities for CV dye are as follows: *X. moluccensis* stem and stem-bark, 401.082 mg/g and 405.510 mg/g; *R. mucronata* stem and stem-bark, 405.594 mg/g and 407.725 mg/g respectively. The respective MG dye equilibrium adsorption capacities using the species stem and stem-bark are as follows: *X. moluccensis* stem and stem-bark, 364.688 mg/g and 366.414 mg/g respectively; 365.169 mg/g and 371.312 mg/g for *R. mucronata* stem and stem-bark respectively.

The adsorption capacity for both CV and MG dyes increased with an increase in initial dye concentration, contact time, adsorbent dose and decreased with particle sizes of adsorbents. The rate of dye adsorption becomes almost constant at equilibrium and notably smaller adsorbent particle sizes reached equilibrium time earlier than larger particle sizes.

Adsorption process was found to be electrostatic due to its dependence on pH and ionic strength An increase in ionic strength decreases the adsorption of both CV and MG dyes; at high Ionic Strength of 10ml of 1.0M NaCl concentration, *R. mucronata* stem and stem-bark performed best at 286.6 ± 1.06 mg/g; 294.4 ± 0.37 mg/g and 248.6 ± 0.20 mg/g; 272.3 ± 0.22 mg/g against *X, moluccensis* stem and stem bark at 285.5 ± 0.27 mg/g; 290.3 ± 0.36 mg/g and 252.0 ± 0.88 mg/g; 273.6 ± 0.13 mg/g equilibrium adsorption capacities for CV and MG dyes respectively showing the superior nature of *R. mucronata* over *X. moluccensis* species due to its higher adaptation to numerous stress conditions such as water logging, high salinity, low nutrition condition, light

stress and low oxygen condition, normally found in abundant along the Worlds' coastal regions. CV adsorption onto *X. moluccensis* and *R. mucronata* stem and stem-bark was attained at pH (7.2 to 8.3) while MG adsorption for both species reached its maximum at a neutral pH 7.0. The species *R. mucronata* is dominant on muddy or waterlogged soils found near the water edge inundated by frequent high tides and is therefore more adapted to the hash saline conditions as compared to *X. moluccensis* which is a rare species commonly found in inland areas.

Large correlation coefficient, R^2, values in the range of 0.8054 to 0.9945 shows that the equilibrium data for MB fits well to the Langmuir isotherm model. Hence the adsorption of CV and MG onto *X. moluccensis* and *R. mucronata* stem and stem-bark occurs through monolayer formation on the adsorbent.

The adsorption of CV and MG dyes follows pseudo-second order kinetics implying a chemisorption rate controlling step while intraparticle diffusion was not the only rate determining step. Hence CV and MG dyes adsorption is a multi-process activity and the rate of dye removal from aqueous solution was dependent on electrostatic interactions between dye molecules and adsorbent surface functional groups.

5.2 Recommendations

1. The surface morphology of *X. moluccensis* and *R. mucronata* species should be studied to enable description of the adsorption mechanisms controlling the process.
2. Further studies to be undertaken to investigate the mechanism of CV and MG dye sorption and desorption process.

REFERENCES

Alawam, K. (2014). Application of Proteomics in Diagnosis of ADHD, Schizophrenia, Major Depression, and Suicidal Behaviour. In R. Donev (Ed.), *Advances in Protein Chemistry and Structural Biology* **95**, 283–315.

Ali, S., Onyari, J. M., & Wabomba, J. N. (2014). Comparative Adsorption of Methylene Blue and Congo Red Dyes onto Coconut Husks, Mangrove and Polylactide Blended Films. *Thesis: Master of Science in Chemistry, University of Nairobi,* 1–130.

Aljeboree, A. M. (2016). Adsorption of Crystal Violet Dye by Fugas Sawdust from Aqueous Solution. *International Journal of ChemTech Research* **9**, 412–423.

Alshabanat, M., Alsenani, G., & Almufarij, R. (2013). Removal of Crystal Violet Dye from Aqueous Solutions onto Date Palm Fibre by Adsorption Technique. *Journal of Chemistry* **12**, 1–7.

Andersson, K., & Stockholm Environment Institute. (2016). Sanitation, Wastewater Management and Sustainability: from Waste Disposal to Resource Recovery. *United Nations Environment Programme and Stockholm Environment Institute* **1**, 1-70.

Anirudhan, T. S., & Sreekumari, S. S. (2011). Adsorptive Removal of Heavy Metal Ions from Industrial Effluents using Activated Carbon Derived from Waste Coconut Buttons. *Journal of Environmental Sciences* **23**, 1989–1998.

Arivoli, S., Hema, M., & Prasath, P. M. D. (2009). Adsorption of Malachite Green onto Carbon prepared from Borassus Bark. *The Arabian Journal for Science and Engineering*, **34**(2a).

Astuti, W., Hermawan, R. A., Mukti, H., & Sugiyono, N. R. (2017). Preparation of Activated Carbon from Mangrove Propagule Waste by H_3PO_4 Activation for Pb^{2+} Adsorption. *American Institute of Physics* **4,** 201-216.

Ayawei, N., Ebelegi, A. N., & Wankasi, D. (2017). Modelling and Interpretation of Adsorption Isotherms. *Journal of Chemistry* **5**, 57-96.

Baek, M. H., Ijagbemi, C. O., Se-Jin, O., & Kim, D. S. (2010). Removal of Malachite Green from Aqueous Solution using Degreased Coffee Bean. *Journal of Hazardous Materials* **176**, 820–828.

Bajpai, S. K., & Jain, A. (2012). Equilibrium and Thermodynamic Studies for Adsorption of Crystal Violet onto Spent Tea Leaves (STL). *Water* **4**, 52–71.

Basyuni M., Agustinna L., & Putri P. (2017). Growth and Biomass in Response to Salinity and Subsequent Fresh Water in Mangrove Seedlings of *Avicennia marina* and *Rhizophora stylosa*. *IOSR Journal of Applied Chemistry* **20**, 1-9.

Bertolini, T. C. R., Izidoro, J. C., Magdalena, C. P., & Fungaro, D. A. (2013). Adsorption of Crystal Violet Dye from Aqueous Solution onto Zeolites from Coal Fly and Bottom Ashes. *Orbital-The Electronic Journal of Chemistry* **5**, 179–191.

Boukhemkhem, A., & Rida, K. (2017). Improvement Adsorption Capacity of Methylene Blue onto Modified Tamazert Kaolin. *Adsorption Science & Technology* **35**, 753–773.

Bulut, E., Özacar, M., & Şengil, İ. A. (2008). Adsorption of Malachite Green onto Bentonite: Equilibrium and Kinetic Studies and Process Design. *Microporous and Mesoporous Materials* **115**, 234–246.

Carmen, Z., & Daniela, S. (2014). Textile Organic Dyes – Characteristics, Polluting Effects and Separation/Elimination Procedures from Industrial Effluents – A Critical Overview. *Intech Open, Gheorghe Asachi' Technical University of Iasi, Romania* **1**, 34.

Chakraborty, S., Chowdhury, S., & Saha, P. D. (2012). Insight into Biosorption Equilibrium, Kinetics and Thermodynamics of Crystal Violet onto *Ananas comosus* (Pineapple) Leaf Powder. *Applied Water Science* **2**, 135–141.

Chanzu, H. A., Onyari, J. M., & Shiundu, P. M. (2012). Biosorption of Malachite Green from Aqueous Solutions onto Polylactide/Spent Brewery Grains Films: Kinetic and Equilibrium Studies. *Journal of Polymers and the Environment* **20**, 60–72.

Chen, F., Fang, P., Gao, Y., Liu, Z., Liu, Y., & Dai, Y. (2012). Effective Removal of High-Chroma Crystal Violet over TiO_2-Based Nanosheet by Adsorption–Photocatalytic Degradation. *Chemical Engineering Journal* **204**, 107–113.

Chequer, F. M. D., Oliveira, G. A. R. de, Ferraz, E. R. A., Cardoso, J. C., Zanoni, M. V. B., & Oliveira, D. P. (2013). Textile Dyes: Dyeing Process and Environmental Impact. *Eco-Friendly Textile Dyeing and Finishing* **6**, 21-236.

Chieng, H. I., Lim, L. B., Priyantha, N., & Tennakoon, D. T. B. (2013). Sorption characteristics of Peat of Brunei Darussalam III: Equilibrium and Kinetics Studies on Adsorption of Crystal Violet (CV). *International Journal of Earth Sciences Engineering* **6**, 791–801.

Chowdhury, S., Chakraborty, S., & Saha, P. D. (2013). Response Surface Optimization of a Dynamic Dye Adsorption Process: A Case Study of Crystal Violet Adsorption onto NaOH-Modified Rice Husk. *Environmental Science and Pollution Research* **20**, 1698–1705.

Coates, J. (2000). Interpretation of Infrared Spectra, A Practical Approach. *Encyclopaedia of Analytical Chemistry* **4**, 1211-1282.

Crini, G., Peindy, H. N., Gimbert, F., & Robert, C. (2007). Removal of CI Basic Green 4 (Malachite Green) from Aqueous Solutions by Adsorption using Cyclodextrin-Based Adsorbent: Kinetic and equilibrium studies. *Separation and Purification Technology* **53**, 97–110.

El-Sayed, G. O. (2011). Removal of Methylene Blue and Crystal Violet from Aqueous Solutions by Palm Kernel Fibre. *Desalination* **272**, 225–232.

Eren, [5 0] E., Cubuk, O., Ciftci, H., Eren, B., & Caglar, B. (2010). Adsorption of Basic Dye from aqueous solutions by Modified Sepiolite: Equilibrium, Kinetics and Thermodynamics Study. *Desalination*, **252**, 88–96.

Hameed, B. H., & El-Khaiary, M. I. (2008). Malachite Green Adsorption by Rattan Sawdust: Isotherm, Kinetic and Mechanism Modelling. *Journal of Hazardous Materials* **159**, 574–579.

Hendy, I. W., Michie, L., & Taylor, B. W. (2014). Habitat Creation and Biodiversity Maintenance in Mangrove Forests: Teredinid Bivalves as Ecosystem Engineers. *Peer Journal* **2**, 9-31.

Ho, Y. S., & McKay, G. (1998). A Comparison of Chemisorption Kinetic Models Applied to Pollutant Removal on Various Sorbents. *Process Safety and Environmental Protection* **76**, 332–340.

Ho, Y.-S., & McKay, G. (1999). Pseudo-Second Order Model for Sorption Processes. *Process Biochemistry* **34**, 451–465.

Jain, S., & Jayaram, R. V. (2010). Removal of Basic Dyes from Aqueous Solution by Low-Cost Adsorbent: Wood Apple Shell (*Feronia acidissima*). *Desalination* **250**, 921–927.

Jebrail, A., Arash, & fatah. (2016). *Wastewater treatment process. Thesis: Häme University of Applied Sciences Press, Hämeenlinna, Finland*, 1-39.

Jedynak, K., & Repelewicz, M. (2017). Adsorption of Methylene Blue and Malachite Green on Micro-Mesoporous Carbon Materials. *Adsorption Science & Technology* **35**, 499–506.

Joseph, F., Agrawal, Y. K., & Rawtani, D. (2013). Behaviour of Malachite Green with Different Adsorption Matrices. *Frontiers in Life Science* **7**, 99–111.

Kharub, M. (2012). Use of Various Technologies, Methods and Adsorbents for the Removal of Dyes. *Journal of Environmental Research and Development* **6**(3a), 879–883.

Kim, K., Seo, E., Chang, S.-K., Park, T. J., & Lee, S. J. (2016). Novel Water Filtration of Saline Water in the Outermost Layer of Mangrove Roots. *Scientific Reports* **6**, 2-26.

Kumar, P. S., & Gayathri, R. (2009). Adsorption of Pb^{2+} ions from aqueous solutions onto Bael Tree Leaf Powder: Isotherms, kinetics and thermodynamics study. *Journal of Engineering Sciences Technology* **4**, 381–399.

Kushwaha, A. K., Gupta, N., & Chattopadhyaya, M. C. (2014). Removal of Cationic Methylene Blue and Malachite Green Dyes from Aqueous Solution by Waste Materials of *Daucus carota*. *Journal of Saudi Chemical Society* **18**, 200–207.

Lang'at, J. K., & Kairo, J. G. (2008). Conservation and Management of Mangrove Forests in Kenya. *Kenya Marine and Fisheries Research Institute, Mombasa, Kenya,* **4**, 1- 7.

Lim, L. B., Priyantha, N., & Mansor, N. H. M. (2015). *Artocarpus altilis* (breadfruit) Skin as a Potential Low-Cost Bio-sorbent for the Removal of Crystal Violet Dye: Equilibrium, Thermodynamics and Kinetics Studies. *Environmental Earth Sciences* **73**, 3239–3247.

Mittal, A., Kurup, L., & Mittal, J. (2007). Freundlich and Langmuir Adsorption Isotherms and Kinetics for the Removal of Tartrazine from Aqueous Solutions using Hen Feathers. *Journal of Hazardous Materials* **146**, 243–248.

Mohammed, M. A., Shitu, A., & Ibrahim, A. (2014). Removal of Methylene Blue using Low Cost Adsorbent: A review. *Research Journal of Chemical Sciences* **2231**, 606X.

Muinde, V. M., Onyari, J. M., Wamalwa, B., Wabomba, J., & Nthumbi, R. M. (2017). Adsorption of Malachite Green from Aqueous Solutions onto Rice Husks: Kinetic and Equilibrium Studies. *Journal of Environmental Protection* **8**, 3–25.

Nandi, B. K., Goswami, A., & Purkait, M. K. (2009). Removal of Cationic Dyes from Aqueous Solutions by Kaolin: Kinetic and Equilibrium Studies. *Applied Clay Science* **42**, 583–590.

Ngugi, F., Onyari, J. M., & Wabomba, J. N. (2016). Efficacy of Mangrove (*Rhizophora mucronata*) Roots Powder in Adsorption of Lead (II) Ions from Aqueous Solutions: Equilibrium and Kinetics Studies. *IOSR Journal of Applied Chemistry* **9**, 21–43.

Oladipo, A. A., & Gazi, M. (2014). Enhanced Removal of Crystal Violet by Low Cost Alginate/Acid Activated Bentonite Composite Beads: Optimization and Modelling using Non-Linear Regression Technique. *Journal of Water Process Engineering* **2**, 43–52.

Önal, Y., Akmil-Başar, C., & Sarıcı-Özdemir, Ç. (2007). Investigation Kinetics Mechanisms of Adsorption Malachite Green onto Activated Carbon. *Journal of Hazardous Materials* **146**, 194–203.

Pavan, F. A., Camacho, E. S., Lima, E. C., Dotto, G. L., Branco, V. T., & Dias, S. L. (2014). Formosa Papaya Seed Powder (FPSP): Preparation, Characterization and Application as an Alternative Adsorbent for the Removal of Crystal Violet from Aqueous Phase. *Journal of Environmental Chemical Engineering* **2**, 230–238.

Raval, N. P., Shah, P. U., & Shah, N. K. (2017). Malachite Green "A Cationic Dye" and Its Removal from Aqueous Solution by Adsorption. *Applied Water Science* **7**, 3407–3445.

Romañach, S. S., DeAngelis, D. L., Koh, H. L., Li, Y., Teh, S. Y., Raja Barizan, R. S., & Zhai, L. (2018). Conservation and Restoration of Mangroves: Global Status, Perspectives, And Prognosis. *Ocean & Coastal Management* **154**, 72–82.

Ruwa, R. K. (1993). Zonation and Distribution of Creek and Fringe Mangroves in the Semi-Arid Kenyan Coast. In H. Lieth & A. A. Al Masoom (Eds.), *Towards the rational use of high salinity tolerant plants* **27**, 97–105.

Saeed, A., Sharif, M., & Iqbal, M. (2010). Application Potential of Grapefruit Peel as Dye Sorbent: Kinetics, Equilibrium and Mechanism of Crystal Violet Adsorption. *Journal of Hazardous Materials* **179**, 564–572.

Salahshoor, Z., & Shahbazi, A. (2014). Review of the use of Mesoporous Silicas for Removing Dye from Textile Wastewater. *European Journal of Environmental Sciences* **4**, 116–130.

Salleh, M. A. M., Mahmoud, D. K., Karim, W. A. W. A., & Idris, A. (2011). Cationic and Anionic Dye Adsorption by Agricultural Solid Wastes: A Comprehensive Review. *Desalination* **280**, 1–13.

Samiey, B., & Toosi, A. R. (2010). Adsorption of Malachite Green on Silica Gel: Effects of Nacl, pH and 2-propanol. *Journal of Hazardous Materials* **184**, 739–745.

Santhi, T., Manonmani, S., & Smitha, T. (2010). Removal of Malachite Green from Aqueous Solution by Activated Carbon Prepared from the Epicarp of *Ricinus communis* by Adsorption. *Journal of Hazardous Materials* **179**, 178–186.

Sun, W., Han, J.Y., Li, Q.J., & Jiao, K. (2007). Spectrophotometric and Voltammetric Studies on the Interaction of Heparin with Crystal Violet and its Analytical Application. *South African Journal of Chemistry* **14**, 1–5.

Tan, P., M., Kassim. (2012). Reactive Black 5 Dye Removal from Water Using Electrocoagulation Method. *International Journal of Pure and Applied Sciences and Technology* **1**, 1-46.

Upadhye, G. C., Renge, A. S., Singh, V. H., & Mandal, N. K. (2018). Batch Adsorption Studies on Removal of Dye using Agro-Waste. *Engineering Technology* **6**, 1–6.

Veetil Nidheesh, P., Gandhimathi, R., Thanga Ramesh, S., & Anantha Singh, T. S. (2012). Adsorption and Desorption Characteristics of Crystal Violet in Bottom Ash Column. *Journal of Urban and Environmental Engineering* **6**, 221–233.

Wanyonyi, W. C., Onyari, J. M., & Shiundu, P. M. (2014). Adsorption of Congo Red Dye from Aqueous Solutions using Roots of *Eichhornia crassipes*: Kinetic and Equilibrium Studies. *Energy Procedia* **50**, 2–9.

Weber, W. J., & Morris, J. C. (1963). Kinetics of Adsorption on Carbon from Solution. *Journal of the Sanitary Engineering Division*, **89**, 31–60.

Zhang, J. X., & Ou, L. L. (2013). Kinetic, Isotherm and Thermodynamic Studies of The Adsorption of Crystal Violet by Activated Carbon from Peanut Shells. *Water Science and Technology* **67**, 737–744.

Zolgharnein, J., Bagtash, M., & Shariatmanesh, T. (2015). Simultaneous Removal of Binary Mixture of Brilliant Green and Crystal Violet using Derivative Spectrophotometric Determination, Multivariate Optimization and Adsorption Characterization of Dyes on Surfactant Modified Nano-Γ-Alumina. *Spectrochimica Acta Part A: Molecular and Biomolecular Spectroscopy* **137**, 1016–1028.

ONLINE REFERENCES

https://www.researchgate.net/figure/245691228/Retrieved on Friday 2nd August 2016 at 3.00 p.m.

http://mbgnet.mobot.org/salt/mudflat/mangrove.htm. Retrieved on Friday 26th August 2016 at 6:05 pm.

https://www.conservationtraining.org/mod/scorm/Retrieved on Friday 26th August 2016 at 7:15pm.

http://indiabiodiversity.org/observation/show/Retrieved on Sunday 28th August 2016 at 3.00 p.m.

https://www.sciencedirect.com/topics/engineering/langmuir-adsorption. Retrieved on Monday July 30, 2018 at 9.20 a.m.

http://www.unenvironment.org/news-and-stories/story/mangrove-conservation-kenyan-style. Retrieved on Monday 30th July, 2018 at 10.20 a.m.

https://textilelearner.blogspot.com/2011/04/problems-of-textile-dyes-inenvironment_4787.html on Friday 1st May 2020 at 8.22pm.

APPENDICES

Appendix A

Raw Data Used to Evaluate Equilibrium Characteristics of CV adsorption

X. moluccensis stem-bark

Time (mins)		0	5	10	15	20	25	30
Abs	A	1.597	0.199	0.133	0.095	0.054	0.034	0.026
	B	1.597	0.186	0.126	0.089	0.052	0.03	0.025
	C	1.597	0.169	0.125	0.086	0.048	0.026	0.025
Abs Average		1.597	0.311	0.126	0.088	0.053	0.032	0.025
S.D			0.0016	0.0005	0.0015	0.001	0.002	0.0005
% S.D			0.1633	0.0500	0.1500	0.1000	0.2000	0.0471
% Abs			80.526	92.142	94.521	96.681	97.996	98.414
Dye conc. (mg/g)		407.980	79.450	32.061	22.353	13.540	8.175	6.472
Dye Adsorbed			328.530	375.919	385.627	394.440	399.805	401.508
Dye Adsorbed, q_e-q_t (mg/g)			76.980	29.591	19.883	11.070	5.705	4.002
log q_e-q_t			1.8864	1.4712	1.2985	1.0441	0.7563	0.6023
t/q_t (gmin/mg)			0.0152	0.0266	0.0389	0.0507	0.0625	0.0747
$t^{1/2}$			2.2361	3.1623	3.873	4.4721	5.0000	5.4772

35	40	45	50	55	60
0.024	0.021	0.018	0.014	0.012	0.012
0.024	0.02	0.017	0.012	0.010	0.009
0.022	0.018	0.015	0.011	0.009	0.008
0.023	0.021	0.018	0.012	0.010	0.009
0.0009	0.0005	0.0005	0.0005	0.0005	0.0005
0.0943	0.0500	0.0500	0.0500	0.0500	0.0500
98.539	98.716	98.904	99.280	99.405	99.468
5.961	5.237	4.471	2.938	2.427	2.171
402.019	402.743	403.509	405.042	405.553	405.809
3.491	2.767	2.001	0.468	-0.043	-0.299
0.5429	0.4420	0.3012	-0.3299	0.0000	0.0000
0.0871	0.0993	0.1115	0.1234	0.1356	0.1479
5.9161	6.3246	6.7082	7.0711	7.4162	7.7460

X. moluccensis **stem**

Time (mins)		0	5	10	15	20	25	30	35	40	45	50	55	60
Abs	A	1.597	0.385	0.059	0.054	0.047	0.044	0.039	0.024	0.021	0.018	0.014	0.012	0.012
	B	1.597	0.382	0.057	0.052	0.046	0.043	0.038	0.024	0.02	0.017	0.012	0.01	0.009
	C	1.597	0.389	0.055	0.049	0.045	0.041	0.037	0.022	0.018	0.015	0.011	0.009	0.008
Abs Average		1.597	0.386	0.057	0.053	0.046	0.044	0.038	0.023	0.021	0.018	0.012	0.010	0.009
S.D			0.0035	0.0016	0.001	0.0008	0.0005	0.0005	0.0009	0.0005	0.0005	0.0005	0.0005	0.0005
% S.D			0.3500	0.1633	0.1000	0.0817	0.0500	0.0500	0.0943	0.0500	0.0500	0.0500	0.0500	0.0500
% Abs			75.861	96.431	96.681	97.120	97.276	97.652	98.539	98.716	98.904	99.280	99.405	99.468
Dye conc. (mg/g)		407.980	16.777	14.562	13.200	11.752	10.901	9.113	5.961	5.237	4.471	2.938	2.427	2.171
Dye Adsorbed			391.204	393.418	394.780	396.229	397.079	397.888	402.019	402.743	403.509	405.042	405.553	405.809
Dye Adsorbed, q_e-q_t (mg/g)			9.879	7.664	6.302	4.854	4.003	3.195	3.491	2.767	2.001	0.468	-0.043	-0.299
log q_e-q_t			0.9947	0.8844	0.7995	0.6861	0.6024	0.5044	0.5429	0.4420	0.3012	-0.3299	0.0000	0.0000
t/q_t (gmin/mg)			0.0128	0.0254	0.0380	0.0505	0.0630	0.0754	0.0871	0.0993	0.1115	0.1234	0.1356	0.1479
$t^{1/2}$			2.2361	3.1622	3.8730	4.4721	5.0000	5.4772	5.9161	6.3246	6.7082	7.0711	7.4162	7.7460

R. mucronata stem-bark

Time (mins)		0	5	10	15	20	25	30
Abs	A	1.597	0.150	0.087	0.098	0.075	0.041	0.030
	B	1.597	0.160	0.13	0.108	0.074	0.045	0.031
	C	1.597	0.153	0.149	0.106	0.074	0.047	0.042
Abs Average		1.597	0.237	0.140	0.104	0.074	0.046	0.031
S.D			0.0047	0.0095	0.001	0.0005	0.001	0.0005
% S.D			0.4714	0.9500	0.1000	0.0471	0.1000	0.0500
% Abs			85.181	91.265	93.488	95.345	97.120	98.090
Dye conc. (mg/g)		407.980	60.460	35.638	26.569	18.990	11.751	7.792
Dye Adsorbed			347.520	372.342	381.412	388.990	396.229	400.188
Dye Adsorbed, q_e-q_t (mg/g)			59.779	34.957	25.888	18.309	11.070	7.111
log q_e-q_t			1.7766	1.5435	1.4131	1.2627	0.852	0.852
t/q_t (gmin/mg)			0.0144	0.0269	0.0393	0.0514	0.0631	0.0750
$t^{1/2}$			2.2361	3.1623	3.8730	4.4721	5.0000	5.4772

	35	40	45	50	55	60
	0.023	0.018	0.014	0.008	0.005	0.002
	0.024	0.019	0.010	0.008	0.006	0.003
	0.027	0.014	0.010	0.007	0.004	0.003
	0.024	0.019	0.010	0.008	0.005	0.003
	0.0005	0.0005	0.0000	0.0005	0.0008	0.0005
	0.0500	0.0500	0.0000	0.0471	0.0817	0.0471
	98.529	98.842	99.374	99.520	99.687	99.833
	6.003	4.726	2.555	1.959	1.277	0.681
	401.977	403.254	405.425	406.021	406.703	407.299
	5.322	4.045	1.874	1.278	0.596	0.000
	0.726	0.607	0.273	0.106	-0.225	0.000
	0.0871	0.0992	0.1110	0.1231	0.1352	0.1473
	5.9161	6.3246	6.7082	7.0711	7.4162	7.7460

R. mucronata stem

Time (mins)		0	5	10	15	20	25	30
Abs	A	1.597	0.078	0.074	0.062	0.050	0.047	0.023
	B	1.596	0.136	0.074	0.052	0.044	0.024	0.024
	C	1.594	0.162	0.079	0.052	0.040	0.022	0.020
Abs Average		1.596	0.125	0.076	0.055	0.045	0.031	0.022
S.D		0.0012	0.0016	0.0000	0.0000	0.0020	0.0000	0.0005
% S.D		0.1247	0.1633	0.0000	0.0000	0.2000	0.0000	0.0500
% Abs			85.209	95.362	96.741	97.368	98.496	98.527
Dye conc. (mg/g)		407.980	60.340	18.920	13.295	10.739	6.136	6.008
Dye Adsorbed			347.640	389.060	394.685	397.241	401.844	401.972
Dye Adsorbed, q_e-q_t (mg/g)			57.954	16.534	10.909	8.353	3.750	3.622
log q_e-q_t			1.763	1.218	1.038	0.922	0.574	0.559
t/q_t (gmin/mg)			0.0144	0.0257	0.0380	0.0503	0.0622	0.0746
$t^{1/2}$			2.2361	3.1623	3.8730	4.4721	5.0000	5.4772

35	40	45	50	55	60
0.02	0.016	0.015	0.013	0.009	0.010
0.021	0.017	0.014	0.011	0.010	0.010
0.022	0.014	0.014	0.011	0.010	0.008
0.021	0.017	0.014	0.011	0.001	0.010
0.0008	0.0005	0.0005	0.0000	0.0005	0.0000
0.0817	0.0500	0.0471	0.0000	0.0471	0.0000
98.684	98.966	99.102	99.311	99.394	99.373
5.369	4.219	3.665	2.812	2.472	2.557
402.610	403.761	404.315	405.168	405.508	405.423
2.983	1.833	1.279	0.426	0.086	0.171
0.475	0.263	0.107	-0.370	-1.068	-0.768
0.0869	0.0991	0.1113	0.1234	0.1356	0.1480
5.9161	6.3246	6.7082	7.0711	7.4162	7.7460

Appendix B

Raw Data used to Evaluate Equilibrium Characteristics of MG Adsorption

Xylocarpus moluccensis **stem-bark**

Time (mins)		0	5	10	15	20	25	30
Abs	A	1.651	0.104	0.078	0.073	0.071	0.059	0.034
	B	1.654	0.116	0.106	0.068	0.063	0.034	0.028
	C	1.654	0.083	0.052	0.037	0.033	0.034	0.030
Abs Average		1.653	0.101	0.079	0.059	0.056	0.042	0.029
S.D		0.0014	0.0057	0.0221	0.0159	0.0040	0.0000	0.0010
% S.D		0.1414	0.5735	2.2050	1.5923	0.4000	0.0000	0.1000
% Abs			87.900	95.241	95.735	95.947	97.943	98.246
Dye conc. (mg/g)		371.612	44.962	17.685	15.849	15.062	7.644	6.5195
Dye Adsorbed			326.650	353.927	355.763	356.550	363.968	365.093
Dye Adsorbed, q_e-q_t (mg/g)			40.241	12.964	11.128	10.341	2.923	1.799
log q_e-q_t			1.6047	1.1127	1.0464	1.0146	0.4658	0.2549
t/q_t (gmin/mg)			0.0153	0.0283	0.0422	0.0561	0.0687	0.0822
$t^{1/2}$			2.2360	3.1623	3.8730	4.4721	5.0000	5.4772

35	40	45	50	55	60
0.029	0.030	0.029	0.024	0.022	0.020
0.030	0.026	0.025	0.025	0.024	0.022
0.026	0.025	0.025	0.025	0.022	0.021
0.030	0.026	0.025	0.025	0.023	0.021
0.0005	0.0005	0.0000	0.0005	0.0009	0.0008
0.0500	0.0500	0.0000	0.0471	0.0943	0.0817
98.215	98.457	98.487	98.508	98.629	98.730
6.632	5.733	5.620	5.545	5.096	4.721
364.980	365.879	365.992	366.067	366.516	366.891
1.911	1.012	0.899	0.824	0.375	0.000
0.2812	0.0050	-0.0461	-0.0839	-0.4263	0.0000
0.0959	0.1093	0.1230	0.1366	0.1501	0.1635
5.9161	6.3246	6.7082	7.0711	7.4162	7.7460

X. moluccensis stem

Time (mins)		0	5	10	15	20	25	30
Abs	A	1.664	0.408	0.232	0.180	0.118	0.084	0.072
	B	1.664	0.409	0.226	0.160	0.108	0.083	0.06
	C	1.663	0.407	0.215	0.135	0.095	0.081	0.021
Abs Average		1.664	0.408	0.224	0.170	0.107	0.084	0.066
S.D			0.0008	0.0070	0.0100	0.0094	0.0005	0.0060
% S.D			0.0817	0.7040	1.0000	0.9416	0.0500	0.6000
% Abs			75.476	86.516	89.782	93.568	94.981	96.033
Dye conc. (mg/g)		371.612	91.135	50.109	37.973	23.901	18.651	14.742
Dye Adsorbed			280.477	321.503	333.639	347.712	352.961	356.870
Dye Adsorbed, q_e-q_t (mg/g)			84.210	43.185	31.049	16.977	11.727	7.818
log q_e-q_t			1.925	1.635	1.492	1.230	1.069	0.893
t/q_t (gmin/mg)			0.0178	0.0311	0.0450	0.0575	0.0708	0.0841
$t^{1/2}$			2.2361	3.1623	3.8730	4.4721	5.0000	5.4772

	35	40	45	50	55	60
	0.039	0.036	0.032	0.032	0.032	0.031
	0.040	0.036	0.034	0.034	0.033	0.032
	0.040	0.036	0.034	0.034	0.032	0.030
	0.040	0.036	0.033	0.033	0.032	0.031
	0.0005	0.0000	0.0009	0.0009	0.0005	0.0008
	0.04714	0.0000	0.0943	0.0943	0.0471	0.0817
	97.616	97.836	97.996	97.996	98.057	98.137
	8.860	8.041	7.446	7.446	7.222	6.924
	362.752	363.571	364.166	364.166	364.390	364.688
	1.936	1.117	0.522	0.522	0.298	0.000
	0.2870	0.0482	-0.2826	-0.2826	-0.5254	-3.3508
	0.0965	0.1100	0.1236	0.1373	0.1509	0.1645
	5.9160	6.3246	6.7082	7.0711	7.4162	7.7460

R. mucronata stem-bark

Time (mins)		0	5	10	15	20	25	30
Abs	A	1.649	0.043	0.040	0.029	0.022	0.022	0.018
	B	1.651	0.056	0.036	0.026	0.024	0.022	0.020
	C	1.650	0.036	0.031	0.022	0.020	0.015	0.016
Abs Average		1.650	0.045	0.036	0.026	0.022	0.020	0.018
S.D			0.0008	0.0037	0.0015	0.0000	0.0000	0.0016
% S.D			0.0817	0.3682	0.1500	0.0000	0.0000	0.1633
% Abs			97.273	97.838	98.444	98.667	98.808	98.909
Dye conc. (mg/g)		371.612	36.260	8.033	6.194	4.730	4.429	4.054
Dye Adsorbed		0	335.352	363.579	365.419	366.882	367.183	367.558
Dye Adsorbed, q_e-q_t (mg/g)			35.960	7.732825	5.894	4.430	4.129	3.754
log q_e-q_t			1.556	0.888	0.770	0.646	0.616	0.574
t/q_t (gmin/mg)			0.0149	0.0275	0.0410	0.0545	0.0681	0.0816
$t^{1/2}$			2.2361	3.1623	3.8730	4.4721	5.0000	5.4772

	35	40	45	50	55	60
	0.013	0.008	0.006	0.003	0.001	0.001
	0.014	0.010	0.009	0.005	0.005	0.002
	0.008	0.006	0.003	0.001	0.002	0.001
	0.012	0.008	0.006	0.003	0.003	0.001
	99.293	99.515	99.636	99.818	99.838	99.919
	0.0005	0.0016	0.0024	0.0016	0.0005	0.0005
	0.0500	0.1633	0.2449	0.1633	0.0500	0.0471
	3.040	1.802	1.689	0.676	0.338	0.300
	368.572	369.810	369.923	370.936	371.274	371.312
	2.740	1.502	1.389	0.376	0.038	0.000
	0.4378	0.1765	0.1427	-0.4252	-1.4221	0.0000
	0.0950	0.1082	0.1216	0.1348	0.1481	0.1616
	5.9160	6.3246	6.7082	7.0711	7.4162	7.7460

***R. mucronata* stem**

Time (mins)		0	5	10	15	20	25	30
Abs	A	1.653	0.091	0.209	0.113	0.083	0.067	0.055
	B	1.654	0.311	0.148	0.106	0.080	0.067	0.051
	C	1.653	0.312	0.120	0.105	0.068	0.069	0.052
Abs Average		1.653	0.238	0.159	0.108	0.077	0.067	0.053
S.D			0.0005	0.0140	0.0005	0.0065	0.0009	0.0005
% S.D			0.0471	1.4000	0.0500	0.6481	0.0943	0.0500
% Abs			85.605	90.383	93.468	95.343	95.907	96.815
Dye conc. (mg/g)		371.612	72.225	30.119	23.713	18.318	15.209	11.575
Dye Adsorbed			299.387	341.493	347.899	353.294	356.403	360.037
Dye Adsorbed, q_e-q_t (mg/g)			65.782	23.676	17.270	11.875	8.766	5.132
log q_e-q_t			1.8181	1.3743	1.2373	1.0746	0.9428	0.7103
t/q_t (gmin/mg)			0.0167	0.0292	0.0431	0.0566	0.0701	0.0833
$t^{1/2}$			2.2361	3.1623	3.8730	4.4721	5.0000	5.4772

35	40	45	50	55	60
0.045	0.034	0.034	0.031	0.032	0.028
0.042	0.033	0.030	0.029	0.028	0.028
0.038	0.040	0.036	0.034	0.030	0.030
0.042	0.036	0.033	0.031	0.030	0.029
0.0029	0.0005	0.0010	0.0021	0.0016	0.0009
0.2867	0.0500	0.1000	0.2055	0.1633	0.0943
97.480	97.843	97.984	98.105	98.185	98.267
9.365	7.530	6.968	6.743	6.743	6.443
362.247	364.082	364.644	364.869	364.869	365.169
2.922	1.087	0.525	0.300	0.300	0.000
0.4657	0.0361	-0.2801	-0.5229	-0.5229	-3.5645
0.0966	0.1099	0.1234	0.1370	0.1507	0.1643
5.9160	6.3246	6.7082	7.0711	7.4162	7.7460